MECHANICS, DYNAMICS AND OPTIMIZATION OF SPECIAL END MILLS

by

Recep Koca

Submitted to the Graduate School of Engineering and Natural Sciences

in partial fulfillment of the requirements for the degree of

Master of Science

Sabancı University

August, 2012

MECHANICS, DYNAMICS AND OPTIMIZATION OF SPECIAL END MILLS

Approved By:

Prof.Dr.Erhan Budak (Thesis Advisor)...

Assoc.Prof.Dr.Bahattin Koç...

Assoc.Prof.Dr.Tonguç Ünlüyurt...
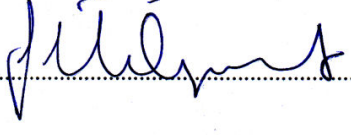
Assoc.Prof.Dr.Ali Koşar...

Assoc.Prof.Dr. Meriç Özcan...

Date of Approval

07.08.2012

To my family

MECHANICS, DYNAMICS AND OPTIMIZATION OF SPECIAL END MILLS

Recep Koca

Industrial Engineering, MSc. Thesis, 2012

Thesis Supervisor: Prof. Dr. Erhan Budak

Abstract

Machining, especially milling, is still one of the most commonly employed manufacturing operations in industry because of its flexibility and potential to produce high quality parts. Milling performance can be increased significantly using special milling tools, such as variable pitch and helix or serrated end mills. The literature on these special tools is mostly limited to prediction of milling forces and chatter stability. Although there are very few studies on optimal design of variable pitch and helix tools, no work has been reported on selection or optimization of serrated end mills. In this thesis, mechanics and dynamics of these tools are investigated in detail. Furthermore, methods and their results on optimization of these tools for minimized milling forces and increased stability are also presented. Optimal variable pitch tools are designed for a given milling system and a desired spindle speed, using different pitch patterns. Their performances are compared and some important and practical results are found. The effects of serration waveform geometry on cutting forces and chatter stability are also investigated in detail. According to the optimization results, guidelines for selection and design of these tools are proposed.

ÖZEL FREZELEME TAKIMLARININ MEKANİĞİ, DİNAMİĞİ VE ENİYİLENMESİ

Recep Koca

Endüstri Mühendisliği, Yüksek Lisans Tezi, 2012

Tez Danışmanı: Prof. Dr. Erhan Budak

Anahtar Kelimeler: Özel Frezeleme Takımları, Kaba Frezeleme Takımları, Değişken Adım Aralıklı Frezeleme Takımları, Yüksek Performans için Eniyileme, Frezeleme Mekaniği ve Dinamiği, Yarı – Ayrıklaştırma Metodu.

Talaşlı imalat, özellikle frezeleme operasyonları yüksek kalitede parça üretme potansiyeli ve esnekliği sayesinde endüstride en sık kullanılan imalat yöntemlerinden birisidir. Frezeleme performansı değişken aralıklı, değişken helisli veya kaba frezeleme takımları gibi özel frezeleme takımları kullanılarak belirgin bir şekilde arttırılabilmektedir. Bu takımlar hakkında yapılmış yayınlar genellikle frezeleme kuvvetlerinin ve frezeleme kararlılığının modellenmesi ve tahmin edilmesi ile sınırlıdır. Değişken aralıklı ve değişken helisli takımların eniyilenmesi üzerine birkaç yayın bulunmasına rağmen, kaba frezeleme takımlarının seçimi veya eniyilenmesi üzerine herhangi bir yayın bulunmamaktadır. Bu tezde, bahsi geçen frezeleme takımlarının mekaniği ve dinamiği detaylı bir şekilde incelenmiştir. Ayrıca bu takımlarla yüksek kararlılık ve düşük frezeleme kuvvetleri elde edilmesi için eniyileme yöntemleri ve sonuçları sunulmuştur. Verilen bir frezeleme sistemi ve istenilen bir iş mili devri için farklı aralık açısı kalıpları kullanılarak değişken aralıklı freze takımları tasarlanmıştır. Tasarlanan değişken aralıklı freze takımlarının performansları incelenmiş, önemli ve pratik sonuçlar bulunmuştur. Kaba frezeleme takımlarının dalga geometrilerinin frezeleme kuvvetleri ve süreç kararlılığı üzerindeki etkileri detaylı bir şekilde incelenmiştir. Eniyileme sonuçlarına göre bu takımların seçimi ve tasarımı için yollar sunulmuştur.

Acknowledgement

TABLE OF CONTENTS

List of Figures

xii

CHAPTER 1

INTRODUCTION

Machining is a manufacturing process which is based on removing material from a bulk or a near net shape part in the form of chips using shearing mechanism involving high strains and strain rates. Machining processes, especially milling, is still one of the most commonly employed manufacturing operations in industry because of its high flexibility, versatility and effectiveness. Manufacturing industry today increasingly demands shorter lead times, competitive prices and higher product quality. In order to fulfill these requirements a milling operation should achieve high productivity with increased MRRs (Material Removal Rate) and tight dimensional, form and surface tolerances under stable cutting conditions. Reduced cutting forces and increased chatter stability can increase productivity and part quality substantially. Special milling tools can be very effective for reduced cutting forces and increased stability when they are designed or selected properly.

There are several special milling tools. These tools can be classified in three main groups:

- End mills having cutting teeth with variable pitch, variable helix and combination of these. (Figure 1.1)
- End mills having cutting teeth with undulations on their flank faces. Undulations can have different waveforms such as sinusoidal, circular and trapezoidal. This type of tools are called serrated end mills or roughing end mills. (Figure 1.2)
- End mills having cutting teeth with harmonically varying helix angles. This type of tools have undulations on their rake faces in contrast to serrated end mills. (Figure 1.3)

1

In Figure 1.1 a), bottom view of a variable pitch end mill can be seen. Cutting teeth of these tools are placed on the tool circumference with different pitch angles. In Figure 1 b), front view of a variable helix end mill can be seen. Cutting teeth have different helix angles in contrast to regular end mills. Also these type of variable pitch and variable helix angles can be combined.

a)   b)
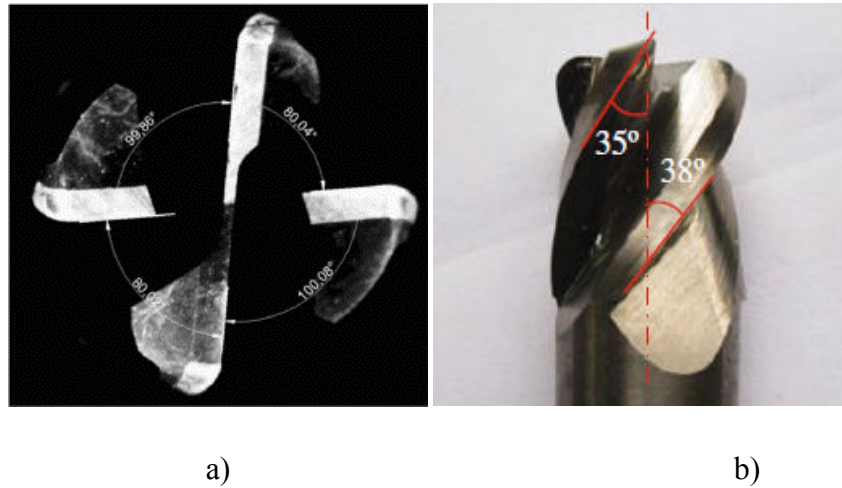
Figure 1.1. End mills with cutting teeth having a) variable pitch angles [37] b) variable helix angles [38]
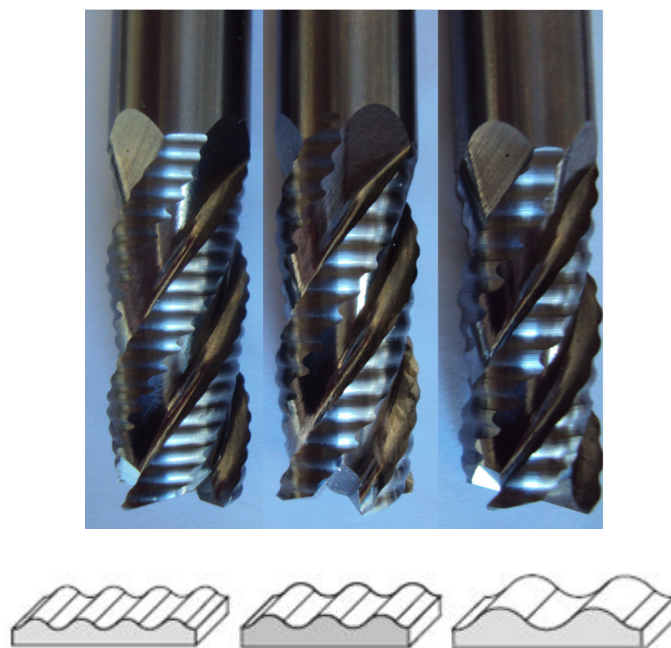
Figure 1.2. Standard serrated end mills with different serration form parameters (Circular serration form)

In Figure 1.2 three serrated end mills with different serration parameters can be seen. Circular serration form is defined with two tangent arcs. The leftmost tool has smaller amplitude and wavelength dimensions while the rightmost one has bigger amplitude and wavelength values. Because of the differences among the serration forms, milling forces and chatter stability behavior of these tools vary.
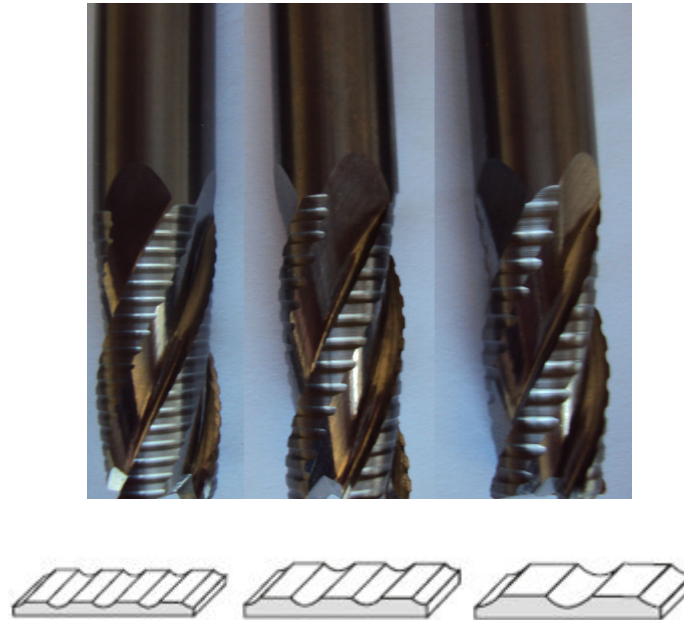
Figure 1.3. Standard serrated end mills with different serration form parameters (trapezoidal serration)

In Figure 1.3 another type of serration form can be seen. This type of serration forms can be employed in finishing operations. They do not leave any material on the cut surface because of the tool geometry if they are specifically designed for finishing operations.

Figure 1.4. End mills with harmonically varying helix angles

3

Harmonically varying helix angles in figure 1.4 introduce a distribution of delays into the milling system. Variable helix angles (Figure 1.1 b) also have the same effect however harmonically varying helix angles introduce more delays into the system even for small axial depths of cut because of their geometry.

Special milling tools increase productivity and milling performance by exploiting different mechanisms. End mills that have variable pitch teeth, variable helix teeth, or their combination, alter the phase difference between the undulations on consecutively machined surfaces to suppress regeneration of waviness and consequently self-excited chatter type vibrations. On the other hand, serrated cutting teeth engage with the workpiece only at certain axial heights, resulting in a decreased total tool-workpiece contact length. As a result, edge force components and effective axial depth of cut decrease which reduces milling forces and increase stability against chatter. This situation also introduces variable time delays into the system.

Design of special end mills are mostly based on try-error methods or experience. In the literature, the publications about these tools are based on force and stability analysis. These predictive methods are useful for analyzing the performance of a given special milling tool. However, a more important problem is the optimal design or selection of a special tool for a given application. There are only two studies in the literature in which methods for design and optimization for variable pitch and variable helix tools are presented. In [19, 20] an analytical design method for variable pitch and mills was proposed. In another study [35] variable pitch and variable helix angles are optimized by using a heuristic method, namely Differential Evolution Method. These two studies are the only ones attempting to find optimal pitch or helix variations for a given application.

Similar to the case of the variable geometry tool, there isn't any study on the selection or optimization of serrated end mills in the literature. Serrated end mills may have different waveforms on their cutting teeth and these waveforms may have different dimensions. These geometrical properties of the waveforms have strong effect on both milling forces and chatter stability. If they are not designed properly and employed with appropriate process parameters, the improvement will be very small or even worse comparing to regular end mills.

The main motivation behind this study is to provide useful information and guidelines about the use and design of special end mills and fill the gaps in the literature in this regard. Main contribution will be in design and optimization of serrated end mills. Guidelines for design and application of serrated end mills will be presented in different chapters of the thesis.

In this study mechanics and dynamics of milling operations with special end mills are investigated. Milling forces are modeled for variable helix, variable pitch and serrated end mills. Serration waveforms such as sinusoidal, circular and trapezoidal waves are modeled parametrically. Local radius, local chip thickness definitions are proposed for these waveforms.

For the first time in the literature, serration wave geometries are optimized for minimization of milling forces. Optimization is carried out for various milling cases with Differential Evolution algorithm and the force model. The objective function is selected as the maximum resultant force in X-Y plane occurring in one tool revolution. It's found out that serration form parameters have a great influence on milling forces and chatter stability. Resulting optimal geometries showed that milling forces can further be decreased compared to both regular end mills and standard serrated end mills available on the market. Another improvement is achieved in chatter stability. Optimal serrated geometries showed superior chatter stability behavior comparing with both regular and standard serrated end mills.

Stability of special tools is analyzed with First Order Semi-Discretization Method including multiple delays. Cutting tests are carried out in order to validate force and stability models for standard and custom milling tools with optimal geometry.

1.1. Organization of the thesis

The thesis organized as follows;

- In chapter 2, milling forces are modeled for variable helix and variable pitch end mills. Stability of variable helix and variable pitch end mills is modeled with First Order Semi - Discretization Method including multiple delays. Stability results are compared with previously published results from the literature. Also

variable pitch angles are optimized for a desired spindle speed using the method proposed by Budak in [19, 20]. Optimal pitch angle difference is found. Using the variable pitch patterns (linear, alternating and sinusoidal), optimal tools are designed. Chatter stability of variable pitch tools having different pitch variation patterns are compared against each other.

- In chapter 3, milling forces are modeled for serrated end mills. Different serration forms such as sinusoidal, circular and trapezoidal geometries are modeled parametrically. Using chip thickness predictions and serration geometry, milling forces are modeled for these three different serrated end mill types. Milling forces are measured in various milling experiments with serrated end mills having different serration forms and the results are compared with the predicted ones.

- In chapter 4, three different serration forms are optimized with Differential Evolution Algorithm for minimized milling forces. Optimized serration geometries are compared to standard regular end mills and standard serrated end mills. Custom made serrated end mills having the optimal serration forms are tested in milling operations.

- In chapter 5, stability model presented in chapter 2 is applied to serrated end mills with necessary changes. Obtained results are verified with chatter tests using the optimized serrated end mills and compared with standard serrated end mills.

- In chapter 6, conclusions obtained from this study are presented. Some possible improvements for future works are proposed.

1.2. Literature Survey

Although serrated, variable helix and variable pitch end mills are often used in industry, the publications on these cutting tools are limited. However, in the last few years with the introduction of alternative stability prediction methods like Semi-Discretization and Full-Discretization Methods which allow the multiple delay phenomenon to be taken into account easily, the studies about stability of special end mills gained acceleration.

In the literature there are many stability prediction methods for milling operations, however they are the variants of three main methods: Frequency Domain Solutions (i.e. Zero-Order Solution, Multifrequency Solution) [1], discrete time methods (i.e. Semi-Discretization Method, Full Discretization Method) [2] and time-domain solutions.

Budak and Altıntas [1] proposed an analytical stability prediction method for regular end mills. The method uses the transfer function of the system at the cutter-workpiece contact area. The excitation terms are approximated by Fourier series components of the time varying directional force coefficients. The stability lobes for the milling system are constructed with analytical expressions in frequency domain. This method is applied to many different milling problems for stability analysis throughout the years with necessary changes [3-5].

Altıntas et al. [3] applied the analytical stability prediction method proposed in [1] to the stability of ball-end milling. Later Altıntas used the analytical method for three-dimensional chatter stability in milling [4]. Altıntas et al. [5] adopted the analytical chatter stability mode in the case of variable pitch cutters.

Insperger and Stépán [2] proposed a stability prediction method for linear dynamic systems with time delays. This method is used for stability analysis of delay differential equations with time periodic coefficients. Milling operation can be expressed with delay differential equations with time periodic coefficients. In milling operations, cutting teeth leave a wavy surface because of the vibrations of the system. Cutting teeth remove the material from the wavy surface left from previously in cut tooth. Because of this situation stability of milling operation strongly depends on this delay effect. Proposed method is called Semi-Discretization method which only discretizes the delayed terms in the equations. Principle period of the system is divided into N number of discrete time steps. Time dependent coefficient matrices are approximated with their average values for these discrete time intervals. Infinite dimensional monodromy matrix of the system is approximated with a finite matrix. Stability of the system is analyzed with the eigenvalues of the monodromy matrix according to Floquet theory. They also proposed another method which discretises both delayed terms and the terms at the current time, and called this method Full-Discretization Method.

Stépán et al. [6-7], investigated chatter stability of up milling and down milling operations with two different analytical methods namely, Finite element analysis in time

(FEAT) and Semi-Discretization. Milling system is modeled with a single degree of freedom. It's shown that FEAT method is more efficient than Semi-Discretization for low radial immersion milling. The reason is that while FEAT discretizes only the time in cut while Semi-Discretization discretizes all the principle period. However Semi-Discretization method can be applied to more general cases of milling processes such as variable spindle speeds or multiple delay situations. Proposed chatter stability methods are validated experimentally in the second part of the paper.

Stépán et al. [8] presented analytical models for determination of the multiple chatter frequencies arise during milling operations. They found that during both stable and unstable milling operations, tooth passing excitation frequency with its harmonics and the damped natural frequency of the tool arise. Furthermore in unstable cases, other frequencies such as Hopf type or period doubling (flip) arise, too. They verified their results with experimental data.

Gradišek et al. [9] investigated the chatter stability of milling operation both with Zero Order Approximation and the Semi-Discretization methods. The system is modeled with two degrees of freedom. They showed that in high radial immersion milling cases these two methods give similar results. However as the radial immersion decreases their differences grow considerably. They showed that Semi-Discretization method can predict additional stability lobes representing the period doubling or flip bifurcations which cannot be caught by Zero Order Approximation. They verified their models with experimental work.

Insperger et al. [10] presented Semi-Discretization techniques using zeroth, first and higher-order approximations of the delayed terms. They showed that if time-periodic coefficients are approximated by piecewise constant functions, there's no need to use higher than the first order approximations for the delayed term. They demonstrated the effects of the order on the delayed Mathieu's equation.

Insperger et al. [11] investigated the effect of tool run-out on chatter frequencies. They considered the systems principle period as spindle period instead of tooth period due to tool run-out. They pointed out that period doubling chatter is in fact period one chatter in case of tool run-out

Insperger [12] compared Full-Discretization with zeroth and first order Semi-Discretization methods regarding their convergence, computational complexity. Their similarities and differences are discussed. He showed that first order semi-discretization method provides faster convergence on the other hand computational time for the full discretization method for a fixed approximation parameter is less than these two semi-discretization methods. However the difference in computational times vanishes as the approximation parameter is increased.

Henninger and Eberhard [13] investigated the computational cost of semi-discretization method. They stated that computation of the approximate monodromy matrix takes most of the time consumed for the calculation of stability lobes. They proposed some methods for increasing the computational efficiency of this method. Proposed methods can be used for reducing the dimension of the monodromy matrix and efficient multiplication of p consecutive matrices computed for every time interval. Significant improvement in computation time was reported.

The literature on variable pitch and variable helix end mills had been very limited up until last few years. Their positive effect on chatter stability was first shown decades ago on significant papers. Slavicek [14] applied orthogonal stability theory to irregular pitch end mills having linear pitch variation using a rectilinear tool motion approximation. A stability limit expression as a function of the variation in the pitch was represented. Vanhreck [15] presented an analytical method for variable pitch end mills having linear or nonlinear variation of the tooth pitch. The milling structure is modeled as a single degree of freedom system. Also tools with alternating helix were investigated. The authors in [14, 15] assumed rectilinear tool motion and infinite tool diameter. Opitz et al. [16] used averaged directional factors and investigated the chatter stability of tools having alternating pitch variation. According to the predictions and the experimental results, significant increase in stability was demonstrated.

Doolan et al. [17] developed a method to design a face-mill having variable pitch blades in order to minimize vibration considering forced excitation only, i.e. regenerative chatter is neglected. They stated that when the dynamic frequency response of a machine-tool-workpiece system is known, a special milling tool can be designed to minimize the relative cutter-workpiece vibration for a particular spindle speed. Nonlinear least-squares and random search are used in order to choose the pitch angles.

9

They showed a reduction in noise and vibration with a special-designed tool comparing with a regular one.

Tlusty et al. [18] investigated the effects of special milling tools on stability of milling. They showed that these special tools, which have cutting teeth having variable pitch, alternating helix, serrated cutting edges and harmonically varied helix angle, can be effective in suppressing chatter type vibrations. For end mills which have variable pitch angles between their teeth, based on the dynamics of the system and the pitch variation angles, it's shown that these tools can be effective in particular spindle speed ranges. This is attributed to the fact that according to spindle speeds, lengths of the waves left on the cut surface change. That's why some pitch variations are effective in lower spindle speeds while some others become effective in higher spindle speeds. Variable helix angles also show similar effect since at different heights of the cutter the pitch angle between subsequent teeth changes. They also investigated serrated end mills and observed that serrated end mills lower total tool-workpiece contact length at any immersion angle which decreases the effective axial depth of cut. It's found out that this situation increases the absolute stability considerably while adding extra stability pockets in to the diagram. The simulations are done using both time domain solutions and a simplified approach.

Budak [19, 20] proposed an analytical design method for end mills having variable pitch angles. It's shown that for a given milling system and a chatter frequency, it's possible to suppress chatter type vibrations for a chosen spindle speed by designing an end mill with the proposed model. The main idea behind this study is to place cutting teeth according to the vibration waves left on the cut surface so that subsequent cutting teeth catch the waves with a controlled phase difference. This way the regeneration is suppressed and the stability limits are increased. Proposed method also applied to example milling operations and its effectiveness was verified by force, surface and sound measurements with custom designed variable pitch cutters.

Turner et al. [21] investigated the stability performance of variable pitch and variable helix end mills using analytical models and time domain simulations. It's shown experimentally that the tools having variable helix angles have better performance than variable pitch end mills.

Zatarain et al. [22] investigated the effect of helix angle on milling stability. They included the effect of helix angle into the multifrequency chatter stability model proposed by Budak and Altıntas [23, 24]. In this study, it's observed that the influence of the helix angle on main lobes of the stability diagram is negligible however its effect on flip lobes needs to be considered. Some islands of instability in the stability diagram are formed if the helix angle is taken into account.

Sims et al. [25] proposed three different methods for stability prediction of variable helix and variable pitch end mills. First two methods are based on semi-discretization method. The first one is the application of semi-discretization method with a state-space approach. This method can predict the stability lobes of milling operations with variable helix and variable pitch end mills both for low and high radial immersions. The second one is called time-averaged semi-discretization method. This method uses the average terms of the directional coefficients during one tool revolution similar to the approach in Zero Order Solution [1]. In time-averaged semi-discretization method, the approximate monodromy matrix is constructed at one step instead of p repeated multiplications in discretized time steps of the system's principle period which is one spindle period for variable helix, variable pitch or serrated end mills. Because of this reason the method is superior to the first one in regard of computational complexity. With the eigenvalues of the Monodromy matrix stability of the system is analyzed. First two methods are compared to each other and other published work and a good agreement is observed.

Wan et al. [26] investigated the effects of feed per tooth, helix angle, cutter run-out and non-constant tooth pitch on milling stability. Their stability prediction method is based on Updated Semi-Discretization Method [27]. They included the multiple delays occurring from cutter run-out and non-constant tooth pitch.

Campomanes [28] presented a mechanics and dynamics model for serrated end mills which have sinusoidal type serration on their cutting teeth. Milling forces are modeled by using Linear Edge Force model proposed by Budak et al. [29] which calculates the cutting force coefficients by transforming orthogonal cutting data into oblique conditions using the necessary geometrical properties of the oblique cutting conditions. He proposed a kinematics of milling model for the calculation of the local chip thickness. In this study an analytical prediction method based on [1] for milling operations using serrated end mills.

Wang and Yang [30] presented a force model in frequency and angle domains for cylindrical end mills which have sinusoidal serrated cutting teeth. They investigated the effect of serration wave profile, wavelength and amplitude on milling forces. They observed that with the appropriate feed per tooth values, at one axial point only one cutting tooth removes material while other teeth do not remove any material at all. Because of this behavior chip thickness for that axial level and for that tooth becomes equal to the feed per revolution value.

Merdol and Altıntas [31] proposed a force model for cylindrical and tapered end mills with serrated cutting teeth. Serrations on cutting teeth are modeled using cubic splines which allow inclusion of different serration forms into the force and stability models. In addition a time domain stability model was presented.

Dombovari et al. [32] proposed a stability model for serrated end mills. Unlike previous works, they solved the stability of milling with serrated end mills by using Semi-Discretization Method.

The literature on mechanics and dynamics of harmonically varying helix angles is rather limited. There are only three papers in the literature investigating the effects of these tools on milling stability. First known publication on these tools is Tlusty et al.'s "Use of special cutters against chatter" [18]. They demonstrated the effect of harmonically varying helix angle on milling stability. They investigated a cutter whose cutting teeth have one full sine wave and adjacent teeth have a phase shift. Following works were published recently. Although these studies include mechanics and stability models, they all lack experimental data.

Dombovari and Stepan [33] investigated the effects of end mills with harmonically varying helix angles. This study is one of the few works investigating the effects of harmonically varied helix angles on milling stability. They introduced a mechanical model to predict the linear stability of these tools. They state that these tools distribute the regeneration. The stability of corresponding time periodic distributed delay differential equations are analyzed by Semi-Discretization Method. They showed that these tools are effective for chatter suppression in both low and high spindle speeds.

Otto and Radons [34] presented an analytical approach for the stability analysis of milling operations with variable pitch and variable helix tools in frequency domain.

They analyzed the stability of the system by examining the eigenvalues of a multifrequency matrix. Since the method is in frequency domain, dynamical parameters of the system can be directly incorporated with the model as frequency response functions and including many vibration modes can be used without any extra computational effort. The results of the proposed method are compared with the results of Semi-Discretization and a good agreement is observed.

The publications on optimization of special milling tools are limited too. The first study after Budak's work [19, 20] on optimization of variable helix and variable pitch tools is the work of Yusoff and Sims [35]. They optimized variable pitch and variable helix angles for a given milling system by using Differential Evolution and Semi Discretization Method proposed in [25]. They obtained a fivefold increase in stability comparing to regular end mills.

The optimization algorithm used in [35] was presented by Storn and Price. It's a population based global optimization method over continuous spaces. Differential Evolution Algorithm uses the following procedures in order to find the optimal parameter sets for a given objective function within a given search space: initialization, mutation, crossover and selection. These set of actions are similar to Genetic Algorithm.

As a summary, the literature on special milling tools is limited to predictive methods for cutting forces and chatter stability. Although there are very few studies on optimal design of variable pitch and helix tools, no work has been reported on selection or optimization of serrated end mills.

CHAPTER 2

MECHANICS AND DYNAMICS OF MILLING WITH VARIABLE PITCH AND VARIABLE HELIX END MILLS

In this chapter mechanics and dynamics of milling operations with variable pitch and variable helix end mills are investigated. Geometry of the end mills and the process are defined and milling forces are modeled for these tools. Chatter stability of these special tools is also investigated and a stability model based on First Order Semi-Discretization Method including the multiple delay effect is presented. The predictions of the stability model are compared with previously published results from the literature.

Before the force formulations, the coordinate system and the tool geometry, which constitute an important part of both force and stability models, will be given.

2.1. Tool Geometry
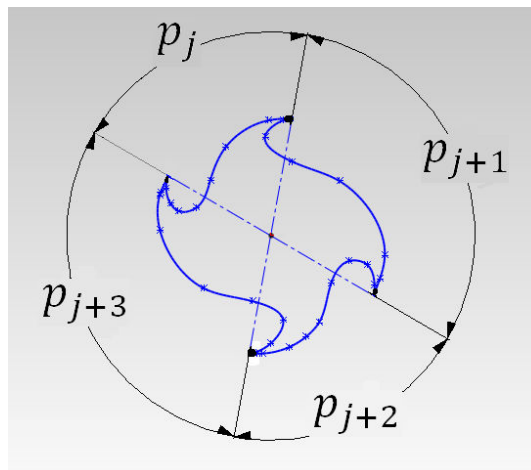
Figure 2.1. Cross section of variable pitch end mill geometry showing different pitch angles

As stated before variable pitch end mills have non-constant spacing between the cutting teeth. Variable helix end mills with constant pitch have similar cross sections along the tool axis. Pitch angle of the jth tooth is defined at the tip of the cutter where $z=0$, as the angular difference between the jth and the previous teeth.
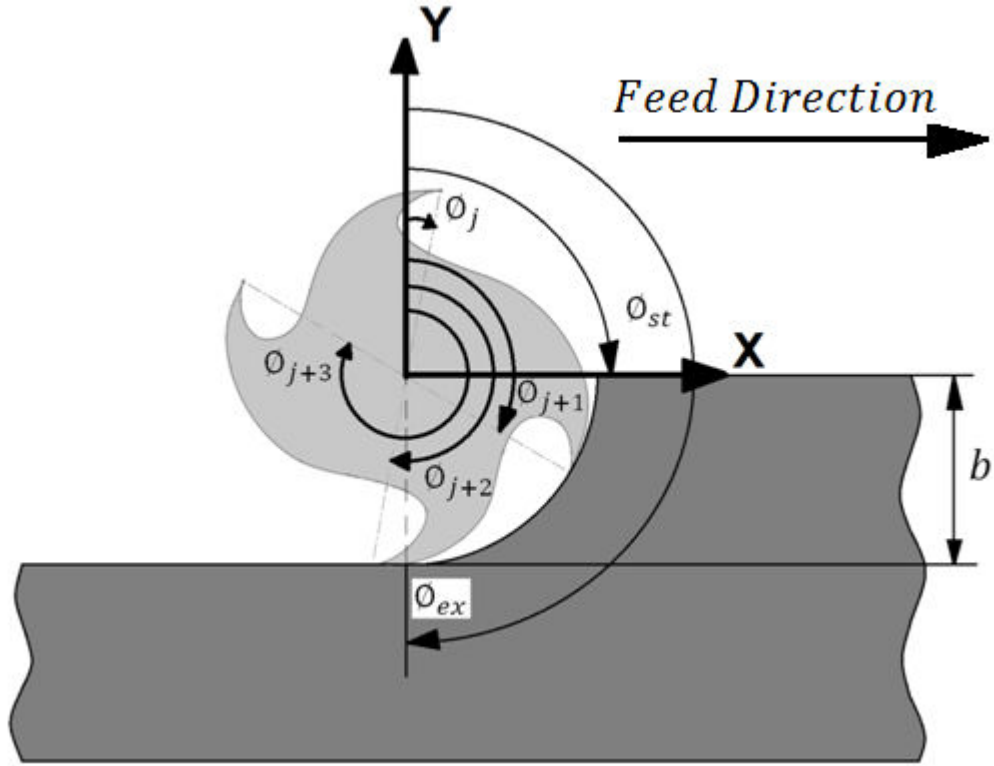
Figure 2.2. Process coordinates and angular positions of the cutting teeth for a given z level (Down milling)

Angular position of the jth tooth at height z is given below.

$$\emptyset_j(z) = \emptyset + p_t(j) - \frac{\tan{(\beta_j)}}{R} z \qquad (2.1)$$

where $\emptyset_j(z)$ is the angular position of the jth tooth at axial height z, $\emptyset$ is the rotation angle of the end mill which starts from 0 and ends at 2π, $p_t(j)$ is the total pitch angle for j^{th} tooth, β_j is the helix angle of the jth tooth and R is the radius of the cutter. $p_t(j)$ is defined as follows where N_t represents the number of cutting teeth.

$$p_t(j) = \sum_{s=1}^{s=j} p(s) \quad j = 1,2, \dots, N_t \qquad (2.2)$$

In order to include the effect of variable pitch and variable helix angles properly, the end mill is divided into disk elements with uniform thickness along the tool axis.
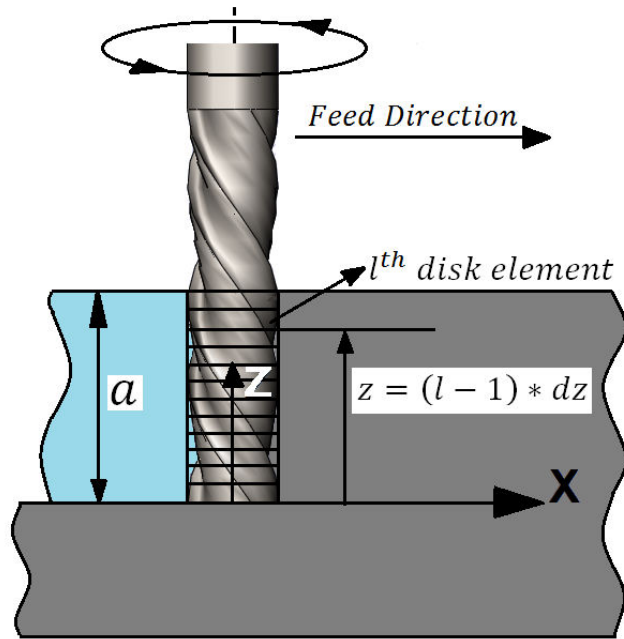
Figure 2.3. Disk elements along the tool axis

Total axial depth of cut, a, is divided into L number of disk elements. The number of disk elements is kept high (e.g 1mm is divided into 100 disk elements) in order to have reliable results. The height of disk elements is very small, thus taking the height of an element as its lowest or highest point does not affect the results. Angular engagement limits, $\emptyset_{st}$ and $\emptyset_{ex}$ shown in Figure 2.2. $\emptyset_{st}$ is the angular position where the teeth start to remove material until angular position $\emptyset_{ex}$. It should be noted that the cutting teeth remove chip only between these angular positions. $\emptyset_{st}$ and $\emptyset_{ex}$ formulated for both up milling and down milling operations as follows:

For up milling:

$$\emptyset_{st} = 0$$

$$\emptyset_{ex} = acos\left(\frac{1-b}{R}\right)$$

(2.3)

For down milling:

$$\emptyset_{st} = \pi - acos\left(1 - \frac{b}{R}\right)$$

$$\emptyset_{ex} = \pi$$

(2.4)

where b represents the radial depth of cut. (Figure 2.2)

For up-milling and down-milling conditions, a unit step function which determines whether the tooth is in cut or not is used

$$g(\emptyset_j) = \begin{cases} 1, & \emptyset_{st} < \emptyset_j < \emptyset_{ex} \\ 0, & \emptyset_j < \emptyset_{st} \ or \ \emptyset_j > \emptyset_{ex} \end{cases} \qquad (2.5)$$

In order to express the angular positions of the cutting teeth along tool axis, tool circumference is unfolded and illustrated in Figure 2.4 for two different tools. The properties of the tools are given in Table 2.1. Tool 1 has both variable pitch and variable helix while Tool 2 is a regular, equal pitch, equal helix end mill.

Table 2.1. Tool Properties

Tool No	R	# of Teeth	Pitch Angles	Helix Angles	Flute Length
1	12 mm	4	[80°,100°,80°,100°]	[42°,28°,42°,28°]	10 mm
2	12 mm	4	[90°, 90°, 90°, 90°]	[30°, 30°, 30°, 30°]	10 mm
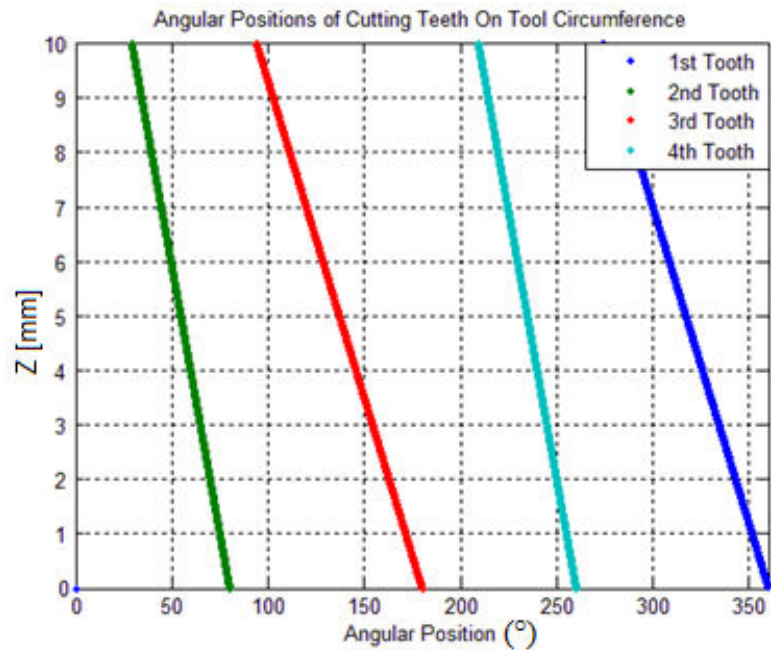
a)
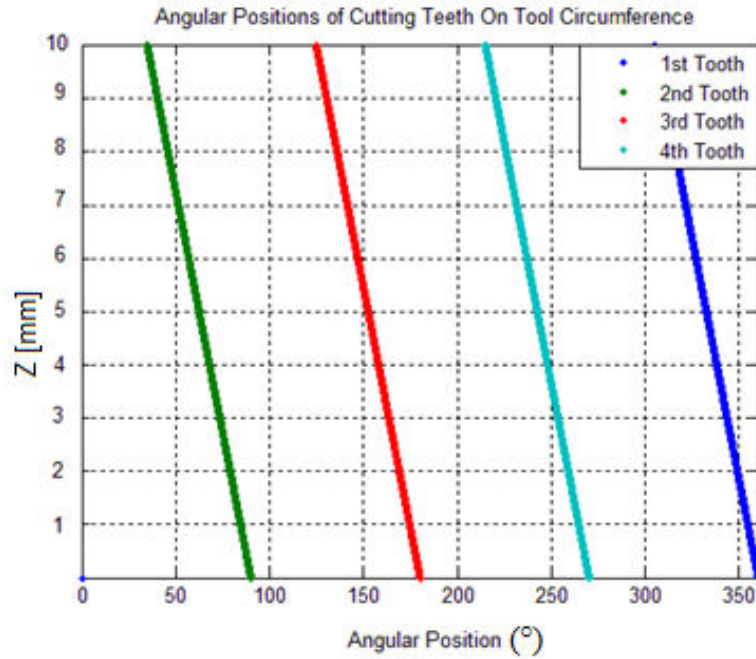
b)

Figure 2.4. Angular positions of cutting teeth for a) Tool 1 b) Tool 2

As can be seen in Figure 2.4 a), because of both variable pitch and variable helix angles the angular difference between cutting teeth at every z level is different. This difference will be represented with $\delta\emptyset(j,z)$, and be called Separation Angle. It is defined in equation (2.6) as follows:

$$\delta\emptyset(j,z) = \emptyset_{j+1}(z) - \emptyset_j(z) \qquad (2.6)$$

where $\emptyset_j(z)$ is the angular position of the jth tooth at axial height z, $\delta\emptyset(j,z)$ is the Separation Angle of the jth tooth at axial height z. Separation Angle is the angular difference between the jth and $(j+1)^{th}$ teeth at axial height z.

The difference between angular positions of the cutting teeth has a great importance on local feed per tooth. Thus local feed per tooth for j^{th} tooth at axial height z is defined as follows:

$$f_t(j,z) = \frac{\delta\emptyset(j,z)}{2\pi}(f * Nt) \qquad (2.7)$$

18

where Nt is number of teeth, f is the feed per tooth, z is the axial height and $\delta\emptyset(j, z)$ is the separation angle of the jth tooth at axial height z.

2.2. Force Model
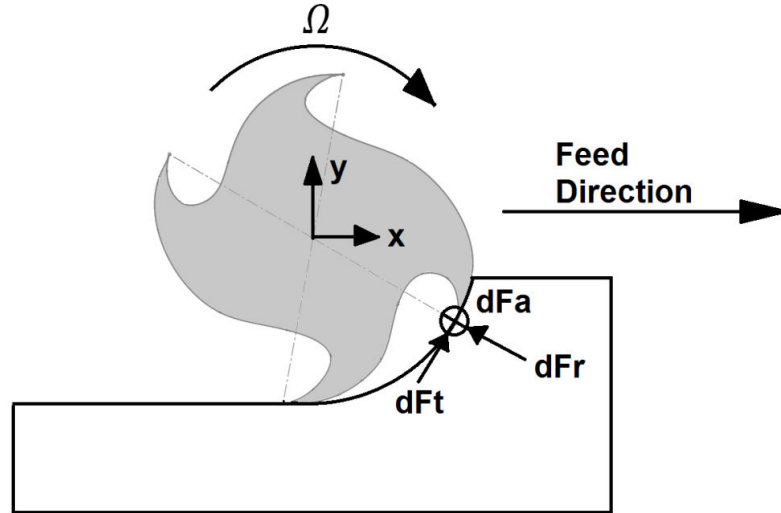
Figure 2.5. Differential forces and their directions acting on the tool during milling

For milling forces Linear Edge Force model [29], where edge forces are assumed not to change with the chip thickness is adopted. For each axial disk element; differential axial, radial and tangential forces are calculated for every rotation for one full spindle revolution:

$$
\begin{aligned}
dFa_j(\emptyset_j, z) &= g(\emptyset_j)\big[K_{ae} + K_{ac}\, h_j(\emptyset_j, z)\big]dz \\
dFr_j(\emptyset_j, z) &= g(\emptyset_j)\big[K_{re} + K_{rc}\, h_j(\emptyset_j, z)\big]dz \\
dFt_j(\emptyset_j, z) &= g(\emptyset_j)\big[K_{te} + K_{tc}\, h_j(\emptyset_j, z)\big]dz
\end{aligned}
\tag{2.8}
$$

where K_{ae}, K_{re}, K_{te} are the edge force coefficients; K_{ac}, K_{rc}, K_{tc} are the cutting force coefficients for axial, radial and tangential directions, respectively and dz is the height of one axial disk element. The chip thickness $h_j(\emptyset_j, z)$ for angular position of $\emptyset$ and j^{th} tooth at the axial height of z can be expressed as follows:

$$
h_j(\emptyset_j, z) = f_t(j, z) * \sin(\emptyset_j)
\tag{2.9}
$$

19

Cutting force coefficients K_{ac}, K_{rc}, K_{tc} are transformed from orthogonal data into oblique cutting conditions using the method in [29].

$$K_{tc} = \frac{\tau_s}{\sin(\theta_n)} \frac{\cos(\beta_n - \alpha_n) + \tan(\beta)\tan(\eta)\sin(\beta_n)}{\sqrt{(\cos(\emptyset_n + \beta_n - \alpha_n))^2 + (\tan(\eta))^2(\sin\beta_n)^2}}$$

$$K_{rc} = \frac{\tau_s}{\sin(\theta_n)\cos(\beta)} \frac{\sin(\beta_n - \alpha_n)}{\sqrt{(\cos(\emptyset_n + \beta_n - \alpha_n))^2 + (\tan(\eta))^2(\sin\beta_n)^2}} \qquad (2.10)$$

$$K_{ac} = \frac{\tau_s}{\sin(\theta_n)} \frac{\cos(\beta_n - \alpha_n)\tan(\beta) - \tan(\eta)\sin(\beta_n)}{\sqrt{(\cos(\emptyset_n + \beta_n - \alpha_n))^2 + (\tan(\eta))^2(\sin\beta_n)^2}}$$

Here τ_s is the shear stress, β_n is the normal friction angle, α_n is the normal rake angle, η is the chip flow angle, θ_n is the normal shear angle, β is the oblique angle (helix angle for milling tools).

Using differential forces in axial, radial and tangential directions, milling forces in the process coordinates (X, Y, and Z) can be expressed as follows:

$$dF_{xj}(\emptyset_j, z) = -dF_{ri}(\emptyset_j, z).\sin(\emptyset_j) - dF_{tj}(\emptyset_j, z).\cos(\emptyset_j)$$
$$dF_{yj}(\emptyset_j, z) = -dF_{rj}(\emptyset_j, z).\cos(\emptyset_j) + dF_{tj}(\emptyset_j, z).\sin(\emptyset_j) \qquad (2.11)$$
$$dF_{zi}(\emptyset_i, z) = -dF_{ai}(\emptyset_i, z)$$

Differential milling force contributions coming from all cutting teeth and disk elements are summed for every rotation angle, and milling forces in X, Y and Z directions for immersion angle $\emptyset$ are obtained as follows:

$$F_x(\emptyset) = \sum_{z=0}^{z=a} \sum_{j=1}^{j=Nt} dF_{xj}(\emptyset_j, z)$$

$$F_y(\emptyset) = \sum_{z=0}^{z=a} \sum_{j=1}^{j=Nt} dF_{yj}(\emptyset_j, z) \qquad (2.12)$$

$$F_z(\emptyset) = \sum_{z=0}^{z=a} \sum_{j=1}^{j=Nt} dF_{zj}(\emptyset_j, z)$$

2.3. Stability Model for Variable Pitch and Variable Helix End Mills

2.3.1. Formulation of the Governing Equation
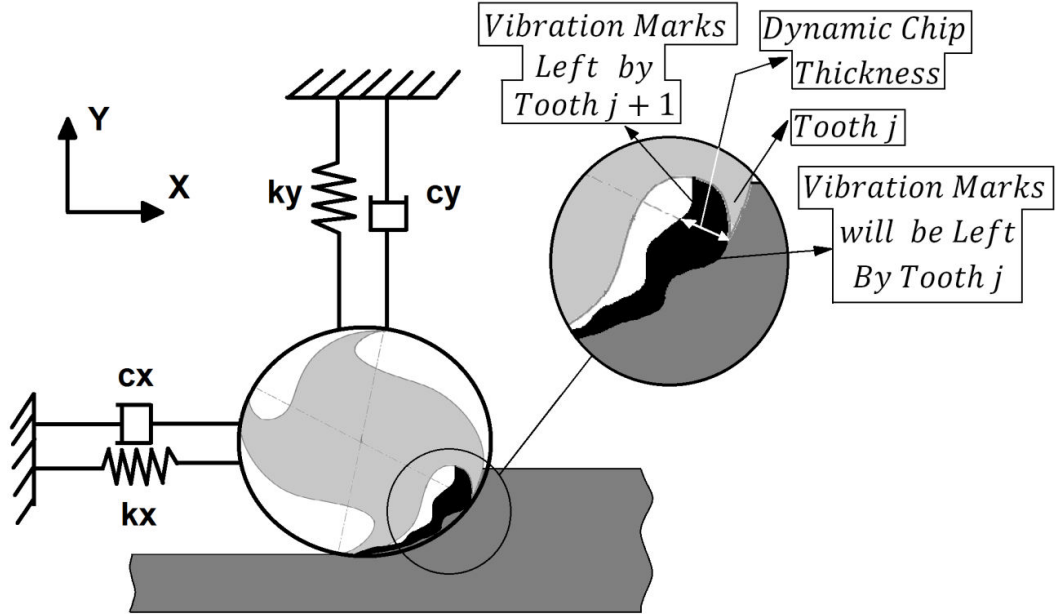
Figure 2.6. Dynamic chip thickness and two orthogonal degrees of freedom

Milling processes need to be considered as dynamic systems. In this part, milling system will be modeled considering the effect of dynamic chip thickness, dynamically changing milling forces and structural parameters of the milling system. In this thesis, the milling system is modeled with two orthogonal degrees of freedom with the dynamic parameters in the tool-workpiece contact area. In figure 2.5, vibration marks left by the tooth $j + 1$ and vibration marks will be left by the tooth j is illustrated and resulting dynamic chip thickness is shown. In equation (2.13) equations of motion in X and Y directions are given as follows:

$$m_x\ddot{x}(t) + c_x\dot{x}(t) + k_x x(t) = F_x(t) \qquad (2.13)$$
$$m_y\ddot{y}(t) + c_y\dot{y}(t) + k_y y(t) = F_y(t)$$

where m_x, m_y are the modal masses, c_x, c_y are the modal dampings, k_x, k_y are the modal stiffnesses in X and Y directions respectively. $\ddot{x}(t)$, $\ddot{y}(t)$ are the time dependent vibration accelerations, $\dot{x}(t)$, $\dot{y}(t)$ are vibration velocities, $x(t)$, $y(t)$ are the vibration amplitudes, $F_x(t)$ and $F_y(t)$ are the milling forces in X and Y directions respectively.

The chip thickness changes dynamically because of the vibration marks of the previous cutting teeth and the cutting teeth currently in the cut. Thus, milling system needs to be considered as a delayed dynamic system. The effect of the vibrations on the chip thickness is taken into account by the equations in (2.14) as follows:

$$h_j(z, \emptyset) = \left[\Delta x \sin(\emptyset_j) + \Delta y \cos(\emptyset_j)\right]$$
$$\Delta x = x(t) - x(t - \tau_j(z)) \tag{2.14}$$
$$\Delta y = y(t) - y(t - \tau_j(z))$$

where Δx and Δy are the time dependent vibration amplitude differences in X and Y directions respectively. $\tau_j(z)$ is the time delay between the jth tooth and $(j+1)^{th}$ at axial height z. Thus $x(t - \tau_j(z))$ and $y(t - \tau_j(z))$ represent the dynamic displacements of tooth $j + 1$, $x(t)$ and $y(t)$ represent the dynamic displacements of tooth j in X and Y directions respectively. The effect of vibrations is taken into account in chip thickness $h_j(z, \emptyset)$ by translating the vibrations into X and Y directions. Since variable pitch and helix angles introduce variable time delays into the systems, they need to be considered in the model as can be seen from the dynamic displacement representations.

$$dFr_j(\emptyset, z) = g(\emptyset_j)\left[K_{re} + K_{rc} \, h_j\right]dz$$
$$dFt_j(\emptyset, z) = g(\emptyset_j)\left[K_{te} + K_{tc} \, h_j\right]dz$$
$$dFx_j(\emptyset, z) = -dFr_j \sin(\emptyset_j) - dFt_j \cos(\emptyset_j) \tag{2.15}$$
$$dFy_j(\emptyset, z) = dFt_j \sin(\emptyset_j) - dFr_j \cos(\emptyset_j)$$

Edge force coefficients are neglected since they do not contribute to the regeneration mechanism. Similarly the static part of the chip thickness is also neglected in stability analysis.

Delay values for j^{th} teeth at the axial level z, i.e. $\tau_j(z)$, are calculated with the help of separation angle $\delta\emptyset(j, z)$ and the spindle speed as follows:

$$\tau_j(z) = \frac{\delta\emptyset_j(z) \, T}{2\pi}$$
$$T = \frac{60}{\Omega} \tag{2.16}$$

22

An end mill having only variable pitch angles has the same delay along the tool axis. For instance a variable pitch end mill having 70°, 110°, 70°, 110° pitch angles with the constant helix have two different delay values. However if variable pitch and variable helix angles are combined, more delay values will be introduced into the system.

Dynamic milling forces are revised to include the effect of vibrations on the chip thickness:

$$dFx_j = -K_{rc}(\Delta x\, sin\emptyset_j + \Delta y cos\emptyset_j)sin\emptyset_j - K_{tc}(\Delta x\, sin\emptyset_j + \Delta y\, cos\emptyset_j)cos\emptyset_j$$

$$dFy_j = K_{tc}(\Delta x\, sin\emptyset_j + \Delta y cos\emptyset_j)sin\emptyset_j - K_{rc}(\Delta x\, sin\emptyset_j + \Delta y\, cos\emptyset_j)cos\emptyset_j$$

$$dFx_j = (\Delta x\,(-K_{rc}\, sin\emptyset_j sin\emptyset_j - K_{tc}\, sin\emptyset_j cos\emptyset_j) + \Delta y(-K_{rc}cos\emptyset_j sin\emptyset_j \qquad (2.17)$$
$$- K_{tc}cos\emptyset_j cos\emptyset_j))dz$$

$$dFy_j = (\Delta x\,(K_{tc}\, sin\emptyset_j sin\emptyset_j - K_{rc}\, sin\emptyset_j cos\emptyset_j) + \Delta y(K_{tc}cos\emptyset_j sin\emptyset_j$$
$$- K_{rc}cos\emptyset_j cos\emptyset_j))dz$$

In equation (2.17), the effect of dynamic displacements is taken into account in dynamic differential milling forces. Dynamic milling forces are rearranged in order to construct the coefficients of dynamic displacement differences in X and Y directions as follows:

$$dFx_j = \Delta x(a_{xx}) + \Delta y(a_{xy}) \qquad (2.18)$$

$$dFy_j = \Delta x(a_{yx}) + \Delta y(a_{yy})$$

where directional coefficients are given as in reference [1]

$$a_{xx} = g(\emptyset_j)(sin\emptyset_j(-K_{rc}\, sin\emptyset_j - K_{tc}cos\emptyset_j))dz$$

$$a_{xy} = g(\emptyset_j)(cos\emptyset_j(-K_{rc}\, sin\emptyset_j - K_{tc}cos\emptyset_j))dz$$

$$a_{yx} = g(\emptyset_j)(sin\emptyset_j(K_{tc}\, sin\emptyset_j - K_{rc}cos\emptyset_j))dz \qquad (2.19)$$

$$a_{yy} = g(\emptyset_j)(cos\emptyset_j(K_{tc}\, sin\emptyset_j - K_{rc}cos\emptyset_j))dz$$

Here, directional coefficients are calculated for every cutting tooth at every z level, i.e. disk elements, in the range of given axial depth of cut. They are going to be labeled with their corresponding values:

$$a_{xx}(l, j, r, t) \qquad\qquad (2.20)$$

Above expression represents the a_{xx} directional coefficient of lth axial element, j^{th} cutting teeth at time t. r represents delay label of that directional coefficient. The different delay values in the system are kept in a vector and lined up from the smallest one to the biggest. Every element in the delay matrix is labeled with its column number.

Equations of motion are rearranged as follows:

$$\ddot{x}(t) + 2\zeta_x \omega_{nx}\, \dot{x}(t) + \omega_{nx}^2\, x(t) = \frac{F_x(t)}{m_x}$$

$$\ddot{y}(t) + 2\zeta_y \omega_{ny}\, \dot{y}(t) + \omega_{ny}^2\, y(t) = \frac{F_y(t)}{m_y} \qquad\qquad (2.21)$$

where ω_{nx}, ω_{ny} represent the natural angular frequencies, ζ_x, ζ_y represent the damping ratios of the most dominant vibration modes of the system in X and Y directions.

System equations are written as follows before they are transformed into first order.

$$\begin{Bmatrix} \ddot{x}(t) + 2\zeta_x \omega_{nx}\, \dot{x}(t) + \omega_{nx}^2\, x(t) \\ \ddot{y}(t) + 2\zeta_y \omega_{ny}\, \dot{y}(t) + \omega_{ny}^2\, y(t) \end{Bmatrix} = \sum_{r=1}^{r=N_D} \left[[DC_r(t)] \begin{bmatrix} x(t) - x(t - \tau_r) \\ y(t) - y(t - \tau_r) \end{bmatrix} \right] \qquad (2.22)$$

DC_r (t) matrix consists of directional coefficients which are grouped according to their delay values. This is because the variable tool geometry introduces multiple delays into the system. The number of different delays in the system is represented with N_D. For a variable pitch cutter, number of different delays can be at most equal to the number of teeth. However, for variable pitch and helix combination this number increases. According to the number of disk elements that tool is divided into and the number of time intervals which the principle period is divided into, number of delays varies in the case of variable helix tools. This will be revisited in the following parts of this Chapter. Elements of DC_r (t) are given below.

$$DC_{r,t}(1,1) = \frac{1}{m_x} \sum_{l=1}^{l=L} \sum_{j=1}^{Nt} a_{xx}(l,j,r,t)$$

$$DC_{r,t}(1,2) = \frac{1}{m_x} \sum_{l=1}^{l=L} \sum_{j=1}^{Nt} a_{xy}(l,j,r,t)$$

$$DC_{r,t}(2,1) = \frac{1}{m_y} \sum_{l=1}^{l=L} \sum_{j=1}^{Nt} a_{yx}(l,j,r,t) \qquad (2.23)$$

$$DC_{r,t}(2,2) = \frac{1}{m_y} \sum_{l=1}^{l=L} \sum_{j=1}^{Nt} a_{yy}(l,j,r,t)$$

$DC_r(t)$ represents the directional coefficient matrix at time t, which have the sum of all contributions coming from all cutting teeth and disks having the same delay label, r.

The governing equation of the multiple delays milling dynamics equations are transformed into first order.

$$\dot{\mathbf{X}}(t) = A(t)\mathbf{X}(t) + \sum_{r=1}^{r=N_D} B_r(t)U(t - \tau_r)$$

$$U(t) = D\mathbf{X}(t), \qquad D = \begin{bmatrix} 1 & 0 & 0 & 0 \\ 0 & 1 & 0 & 0 \end{bmatrix} \qquad (2.24)$$

Above we see a delay differential equation with time periodic coefficients and multiple delays. In equations (2.24) when the system is transformed into first order a new variable $\mathbf{X}(t)$ is introduced.

$$\mathbf{X}(t) = \begin{Bmatrix} x(t) \\ y(t) \\ \dot{x}(t) \\ \dot{y}(t) \end{Bmatrix} \qquad (2.25)$$

The coefficients of the first order governing equation are time-periodic in principle period of the system which is spindle period in the case of special milling tools and tooth passing period in the case of regular end mills.

$$A(t) = A(t + T) \tag{2.26}$$
$$B_r(t) = B_r(t + T)$$

$A(t)$, $B_r(t)$ are time periodic coefficient matrices.

$$A(t) = \begin{bmatrix} [\mathbf{0}] & [\mathbf{I}] \\ [E(t)] & [W] \end{bmatrix} \tag{2.27}$$

$A(t)$ is a 4x4 matrix, $\mathbf{0}$ and $\mathbf{I}$ are 2x2 zeros and identity matrices respectively. Elements of $E(t)$ and W are stated as follows:

$$E_t(1,1) = -\omega_{nx}^2 + \sum_{r=1}^{r=N_D} DC_{r,t}(1,1)$$

$$E_t(1,2) = \sum_{r=1}^{r=N_D} DC_{r,t}(1,2)$$

$$E_t(2,1) = \sum_{r=1}^{r=N_D} DC_{r,t}(2,1) \tag{2.28}$$

$$E_t(2,2) = -\omega_{ny}^2 + \sum_{r=1}^{r=N_D} DC_{r,t}(2,1)$$

$$W = \begin{bmatrix} -2\zeta_x \omega_{nx} & 0 \\ 0 & -2\zeta_y \omega_{ny} \end{bmatrix}$$

The matrix $E(t)$ has the contributions of all the directional coefficients at time t, regardless of their delay label. On the other hand the matrix $B_r(t)$ has the contributions coming from directional coefficients with the delay label r only.

$$B_r(t) = DC_r(t) \tag{2.29}$$

In this part of Chapter 2, the governing equation of milling dynamics is formulated. A delay differential equation with multiple time delays is obtained. The stability of this

equation (2.24), i.e. stability of milling with multiple delays, will be analyzed with Semi-Disretization method.

2.3.2. Semi – Discretization Method

Semi-discretization method is used for the stability analysis of linear – time periodic delay differential equations [39]. Main steps of the semi-discretization method for multiple delays proposed by Insperger and Stépán [39] will be applied to the dynamic milling problem with multiple delays.

For the first order semi-discretization analysis of the governing dynamic milling equation formulated in the previous part of this chapter, higher order method will be adopted directly from [10,39] and applied to our problem with necessary changes. Main steps of semi-discretization method will be presented next.

2.3.2.1. General Formulation for Higher Order Semi-Discretization Method

The difference between the higher order and the other methods of semi-discretization is the way of approximating the delayed terms. Other semi discretization methods approximate the delayed terms by piece-wise constant ones over each discretization step. However, in higher order methods the delayed terms are approximated by higher order polynomials of time t.

One of the main ideas which semi-discretization methods are based on is to divide the principle period T of the system into p discrete time intervals.

$$\Delta t = \frac{T}{p} \tag{2.30}$$

where p is the principle period resolution, Δt is the length of discrete time intervals. Discrete time scheme will be introduced to the governing equation (2.24). For convenience below changes will be made for the representation of time dependent terms in the formulation.

$$\mathbf{X}_i \coloneqq \mathbf{X}(t_i) \tag{2.31}$$

$$U_i \coloneqq U(t_i)$$

where $t_i = i\Delta t$, $i \in Z$

Time dependent coefficient matrices will be approximated by constant ones. Their values are averaged for each discrete time interval $[t_i, t_{i+1})$, $i = 1,2, \dots, p$

$$A_i = \frac{1}{\Delta t} \int_{t_i}^{t_{i+1}} A(t)dt$$

$$B_{r,i} = \frac{1}{\Delta t} \int_{t_i}^{t_{i+1}} B_r(t)dt \tag{2.32}$$

where $r = 1,2, \dots, N_D$

The approximate semi-discrete system can be given as

$$\dot{Y}(t) = A_i Y(t) + \sum_{r=1}^{ND} B_{r,i} \Gamma_{\mathbf{r}}^{(\mathbf{q})}(t - \tau_r), \quad t \in [t_i, t_{i+1}) \tag{2.33}$$

$$\Gamma_{\mathbf{r}}^{(\mathbf{q})}(t - \tau_r) = \sum_{k=0}^{q} \left(\prod_{l=0,\; l \neq k}^{q} \frac{t - \tau_r - (i - l - DR_r)\Delta t}{(k - l)\Delta t} \right) v(t_{i+k-DR_r})$$

The delayed term $\Gamma_{\mathbf{r}}^{(\mathbf{q})}(t - \tau_r)$ is a q$^{\text{th}}$ order Lagrange polynomial interpolation.
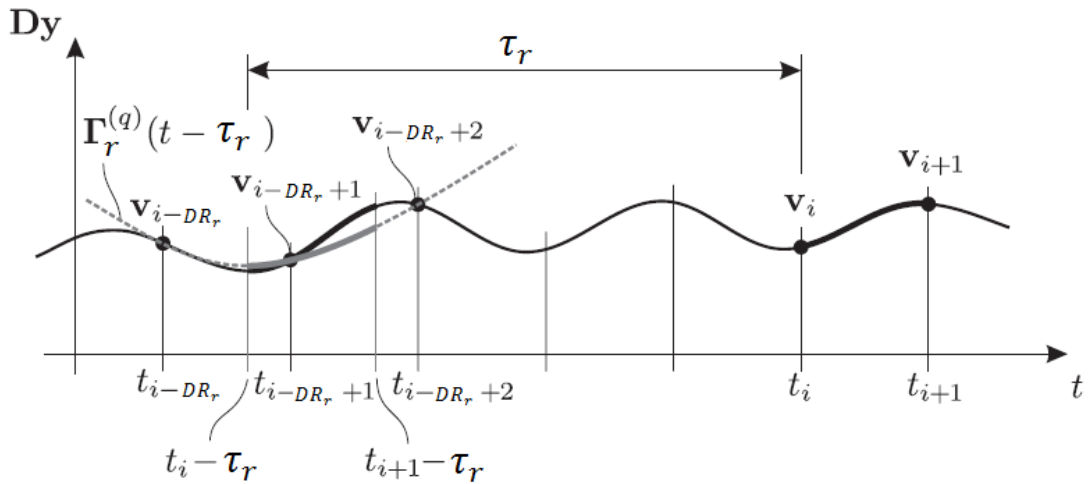
Figure 2.7. Approximation of the delayed term with a Lagrange polynomial [39]

28

The delay resolution for the rth delay value is calculated as follows:

$$DR_r = int\left(\frac{\tau_r}{\Delta t} + \frac{q}{2}\right), \quad r = 1, 2, \dots, N_D \tag{2.34}$$

where q is the order of the Lagrange polynomial for the approximation of the delayed term. int function indicates the integer part, e.g. $int(4.8) = 4$.

The approximate system given in (2.33) has an analytical solution over the time interval $t \in [t_i, t_{i+1})$ with the initial values of $\mathbf{Y_i}$ and v_{i-k-DR_r}, $k = 1, 2, \dots, q$, $r = 1, 2, \dots, N_D$ in the form

$$\mathbf{Y_{i+1}} = P_i \mathbf{Y_i} + \sum_{r=1}^{N_D} \sum_{k=0}^{q} \left(R_{r,i,k} v_{i+k-DR_r}\right) \tag{2.35}$$

where

$$P_i = e^{A_i \Delta t}$$

$$R_{r,i,k} = \int_{t_i}^{t_{i+1}} e^{A_i(t_{i+1}-s)} \left(\prod_{l=0, l\neq k}^{q} \frac{s - \tau_r - (i - l - DR_r)\Delta t}{(k - l)\Delta t} \right) B_{r,i} ds \tag{2.36}$$

$$= \int_{0}^{\Delta t} e^{A_i(\Delta t - s)} \left(\prod_{l=0, l\neq k}^{q} \frac{s - \tau_r - (l - DR_r)\Delta t}{(k - l)\Delta t} \right) B_{r,i} ds$$

And the discrete map is given as

$$z_{i+1} = G_i z_i \tag{2.37}$$

Where G_i is the transition matrix which links the states at time interval i to the next interval $i + 1$.

$$z_i = (\mathbf{Y_i} \ v_{i-1} \ v_{i-2} \ \dots \ v_{i-DR})^{\mathrm{T}} \tag{2.38}$$

Since we have p discrete time intervals, p repeated applications of (2.37) gives the monodromy matrix which links the states at time interval i to the states one principle period later.

$$z_p = \Phi z_0 \tag{2.39}$$

$$\Phi = G_{p-1} G_{p-2} \ldots G_0$$

Stability of the system is analyzed with the eigenvalues of the monodromy matrix Φ according to the Floquet theory. If the largest complex eigenvalue of the monodromy matrix has an absolute value bigger than 1 the system is unstable, if it is equal to 1 the system is on the stability boundary or if it is less than 1 than the system is stable. Resulting monodromy matrix is a finite dimensional approximation of the infinite dimensional monodromy operator.

2.3.2.2. First Order Semi-Discretization Method

In this part, the first order application of the higher order semi-discretization formulation and the structure of the transition matrix G_i will be given. Some useful comments on the application of the method to the milling operations with multiple delays will be added at the end of this part.

Approximate semi-discrete form of the problem stated in (2.24) with the first order semi-discretization method is as follows:

$$\dot{\mathbf{Y}}(t) = A_i \mathbf{Y}(t) + \sum_{r=1}^{N_D} B_r \left(\beta_{r,0}(t) \mathbf{v}\left(t_{i-DR_r}\right) + \beta_{r,1}(t) \mathbf{v}\left(t_{i-DR_r+1}\right) \right), \quad t \in [t_i, t_{i+1})$$

$$\mathbf{v}(t_i) = D\mathbf{Y}(t_i) \tag{2.40}$$

where

$$\beta_{r,0}(t) = \frac{\tau_r + (i - DR_r + 1)\Delta t - t}{\Delta t}$$

$$\beta_{r,1}(t) = \frac{t - (i - DR_r)\Delta t - \tau_r}{\Delta t}$$

(2.41)

The solution over one discrete time step is

$$\mathbf{Y}_{i+1} = P_i \mathbf{Y}_i + \sum_{r=1}^{ND} \left(R_{r,i,0} \mathbf{v}_{i-DR_r} + R_{r,i,1} \mathbf{v}_{i-DR_r+1} \right)$$

(2.42)

where

$$P_i = e^{A_i \Delta t}$$

$$R_{r,i,0} = \int_0^{\Delta t} \frac{\tau_r - (DR_r - 1)\Delta t - s}{\Delta t} e^{A_i(\Delta t - s)} ds B_{r,i}$$

(2.43)

$$R_{r,i,1} = \int_0^{\Delta t} \frac{s - \tau_r + DR_r \Delta t}{\Delta t} e^{A_i(\Delta t - s)} ds B_{r,i}$$
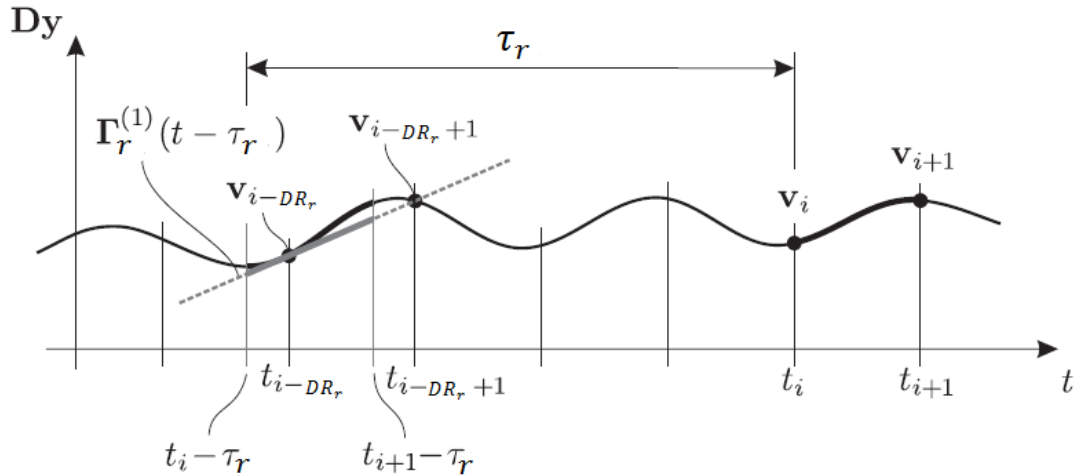
Figure 2.8. Approximation of the delayed term with 1$^{\text{st}}$ order Lagrange polynomial interpolation [39]

If A_i^{-1} exists then $R_{r,i,0}$, $R_{r,i,1}$ are given as follows:

$$R_{r,i,0} = \left(A_i^{-1} + \frac{1}{\Delta t} \left(A_i^{-2} - (\tau_r - (DR_r - 1)\Delta t) A_i^{-1} \right) \left(I - e^{A_i \Delta t} \right) \right) B_{r,i} \tag{2.44}$$

$$R_{r,i,1} = \left(-A_i^{-1} + \frac{1}{\Delta t} \left(-A_i^{-2} + (\tau_r - DR_r \Delta t) A_i^{-1} \right) \left(I - e^{A_i \Delta t} \right) \right) B_{r,i}$$

The discrete map for one discrete time interval is given as:

$$z_{i+1} = G_i z_i \tag{2.45}$$

The transition matrix G_i has the final form as follows:

$$\tag{2.46}$$

$$G_i = \begin{bmatrix} P_i & 0 & \cdots & 0 & 0 \\ D & 0 & \cdots & 0 & 0 \\ 0 & I & \cdots & 0 & 0 \\ \vdots & \vdots & \ddots & \vdots & \vdots \\ 0 & 0 & \cdots & I & 0 \end{bmatrix} + \sum_{r=1}^{ND} \begin{bmatrix} 0 & 0 & \cdots & 0 & R_{r,i,1} & R_{r,i,0} & 0 & \cdots & 0 \\ 0 & 0 & \cdots & 0 & 0 & 0 & 0 & \cdots & 0 \\ 0 & 0 & \cdots & 0 & 0 & 0 & 0 & \cdots & 0 \\ \vdots & \vdots & \ddots & \vdots & \vdots & \vdots & \vdots & \ddots & \vdots \\ 0 & 0 & \cdots & 0 & 0 & 0 & 0 & \cdots & 0 \end{bmatrix}$$

(columns labeled: 1, $DR_r - 1$, DR_r, DR_{max})

p repeated applications of (2.45) gives the monodromy matrix of the system, i.e. the matrix which links the states at time i to the states one principle period later.

$$z_p = \Phi z_0 \tag{2.47}$$

$$\Phi = G_{p-1} G_{p-2} \cdots G_0$$

The dimension of the monodromy matrix is $(2DR_{max} + 4) \times (2DR_{max} + 4)$ where DR_{max} is the delay resolution of the system's largest delay value.

In another expression

$$DR_{max} = int \left(\frac{\tau_{max}}{\Delta t} + \frac{1}{2} \right)$$

The convergence of the method is strongly dependent on the period resolution p. As p is increased, the dimension of the monodromy matrix increases, too. Computation time needs to be considered carefully because as the matrix dimension increases two disadvantages arise. First one is that the transition matrix is multiplied p times in order to approximate the infinite dimensional monodromy matrix with a finite one. Second one is that as the dimension of the monodromy matrix grows it becomes difficult to compute the characteristic multipliers, i.e. eigenvalues, of the system. These constraints need to be taken into account for the construction of the stability charts.

In order to decrease computational complexity of the method, Henninger and Eberhard [13] proposed some methods like reducing the dimension of the monodromy matrix and efficient multiplication of p transition matrices. There's another method proposed by Sims et al. [25] called time-averaged semi-discretization method. The difference between formulation made here and the proposed method by Sims et al. is that instead of constructing the monodromy matrix with p repeated multiplications, it's constructed at one step.

Semi-discretization method originally divides the principle period in to p time intervals and approximates the time-periodic coefficient matrices A_i and $B_{r,i}$ with their average values within each of these intervals. In Sims et al.'s method, instead of averaging the time-periodic coefficient matrices for each of these intervals, they are averaged within the principle period of the system, which is one full revolution of the tool for special milling tools. They stated that this approach is similar to the idea behind Zero Order Approximation given in [1].

The benefit of this method is that instead of p repeated multiplications of the transition matrices for each time interval, the monodromy matrix is constructed at one step without multiplying p matrices.

$$A = \frac{1}{T} \int_{t_i}^{t_{i+p}} A(t)dt$$

$$B_r = \frac{1}{T} \int_{t_i}^{t_{i+p}} B_r(t)dt \qquad (2.48)$$

$$z_p = \Phi z_0$$

$$\Phi = G$$

In the next part, an application of the method formulated here and Zero Order Approximation version of it will be given. These methods will be applied to milling cases with both variable pitch and regular tools. Also the method formulated here will be compared with previously published results from the literature.

2.4. Application of the Stability Prediction Method on Variable Pitch Cutters

Proposed method is applied to the following milling cases with the given parameters.

Table 2.2. Case 1 Regular Tool

Tool Diameter	# of Teeth	Pitch Angles	Helix Angle	Radial DOC	Milling Mode
19.05 mm	4	90°, 90°,90°, 90°	30°	9.525 mm	Down Milling

Modal parameters of the system and the cutting force coefficients are given in the following table.

Table 2.3. Modal Parameters and Cutting Force Coefficients

ω_{nx}	ζ_x	m_x	ω_{ny}	ζ_y	m_y	Ktc	Krc
563.6*2π (rad/sec)	0.02872	11.125 (Kg)	516*2π (rad/sec)	0.0250	1.199 (Kg)	697 (MPa)	255.8 (MPa)

In the following figure, stability predictions with two different methods from the literature [25, 40] for Case 1 are presented.
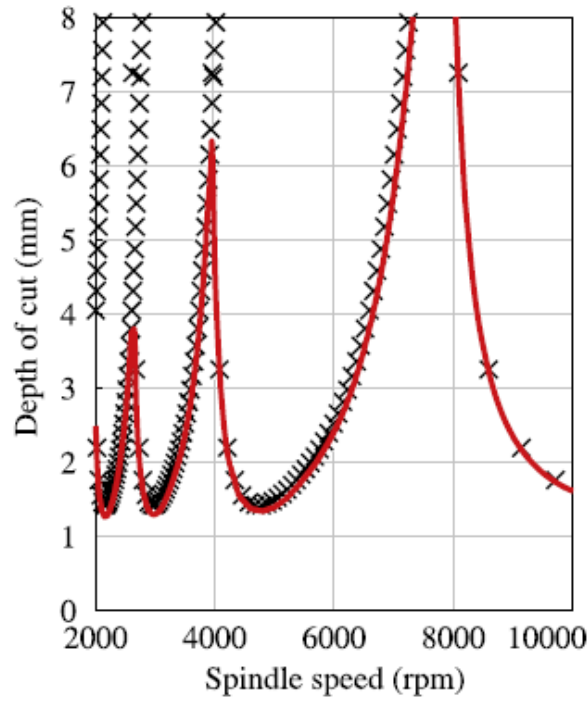
Figure 2.9. Results from literature: Red Curve Time-Averaged Semi-Discretization Method [25], X method of Altintas et al. [40]
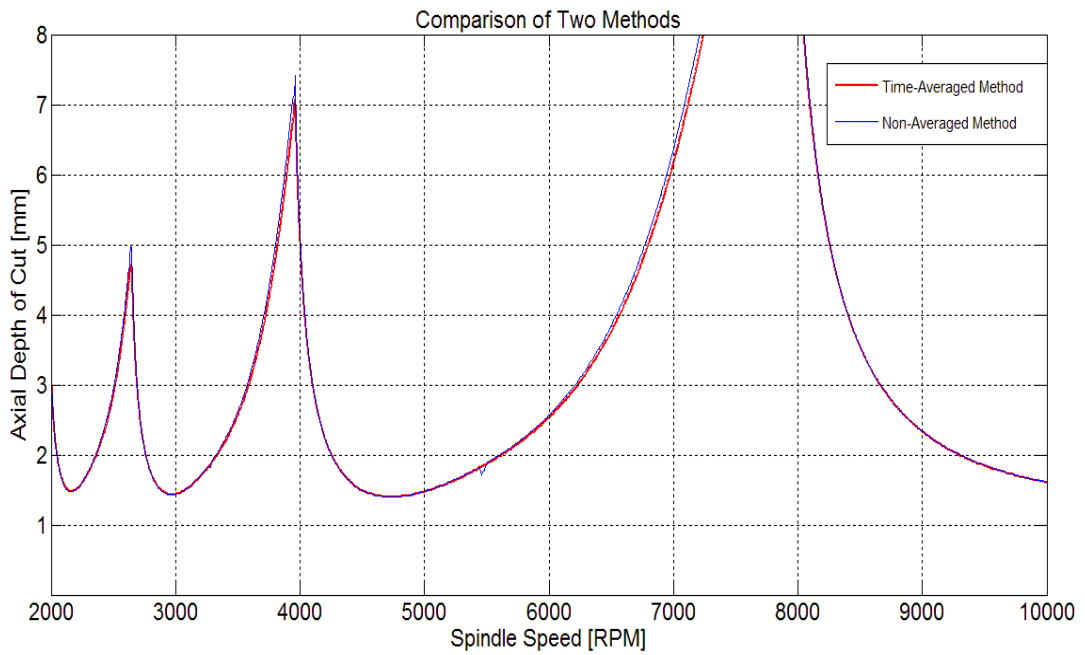
Figure 2.10. Stability Prediction for Case 1 using the methods presented in part (2.3.2.2)

35

As can be seen from the figures, presented methods are in a very good agreement with the previously published results from the literature. Also it can be seen that time-averaged and non-averaged methods presented here are in a good agreement too.

Table 2.4. Case 2 Variable Pitch Tool

Tool Diameter	# of Teeth	Pitch Angles	Helix Angle	Radial DOC	Milling Mode
19.05mm	4	70°, 110°,70°, 110°	30°	9.525mm	Down Milling

Table 2.5. Modal Parameters and Cutting Force Coefficients

ω_{nx}	ζ_x	m_x	ω_{ny}	ζ_y	m_y	Ktc	Krc
563.6*2π (rad/sec)	0.028722	11.125 (kg)	516*2π (rad/sec)	0.025004	1.199 (kg)	697 (MPa)	255.8 (MPa)

For Case 2, there are three published results which are used for comparisons here.

a)   b)
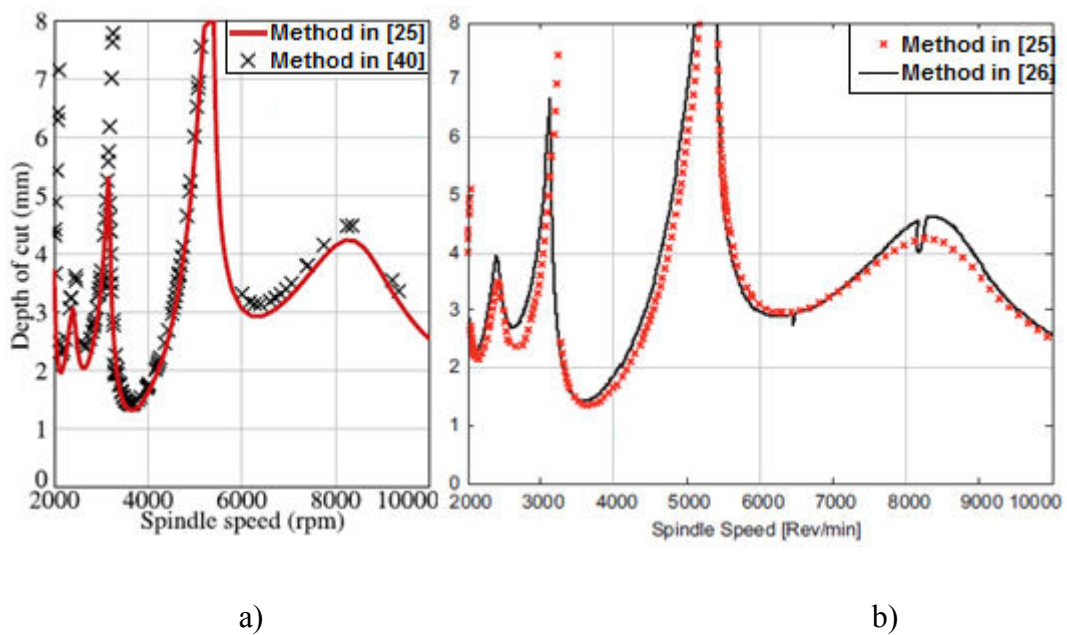
Figure 2.11. Comparisons of methods from the literature, a) [25, 40], b) [25, 26] for Case 2

36

In [25] time averaged semi-discretization method with state-space approach is used while in [26] an alternative semi-discretization method called Updated Semi-Discretization is used.
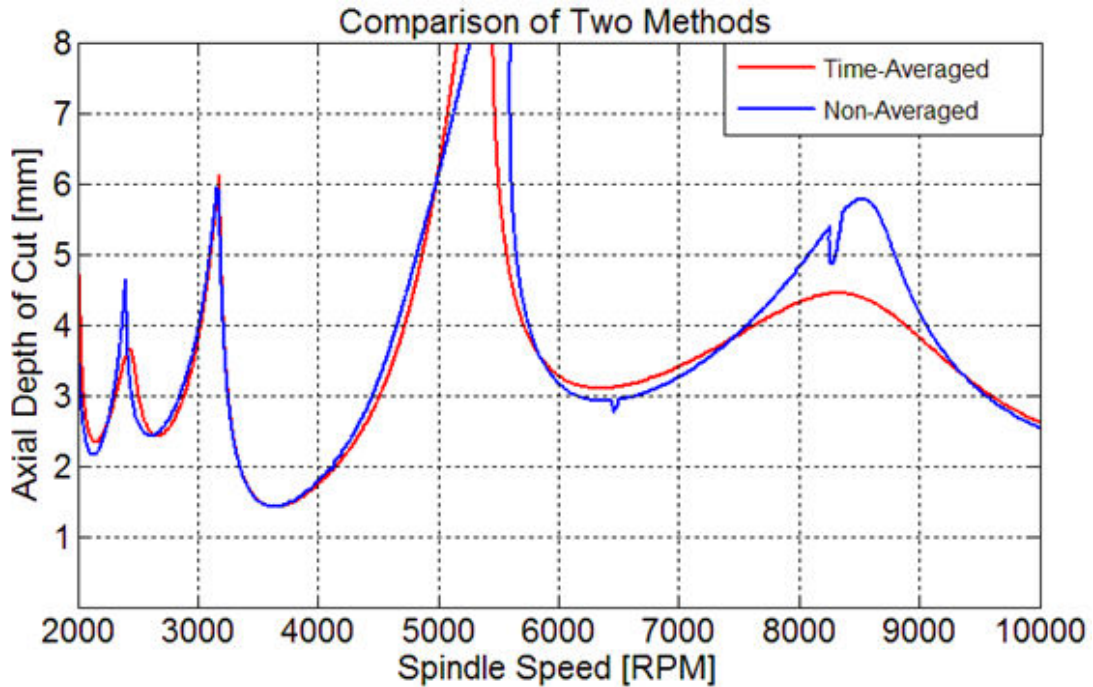
Figure 2.12. Comparison of methods presented in the previous part for Case 2

From the results of the stability prediction methods, both variable pitch and regular end mills' stability behaviors are predicted successfully with the presented first order semi-discretization methods including multiple delays.

In case 1, both time-averaged method and the non-averaged one predict the stability behavior of a regular end mill. There is not too much difference between two methods for regular end mills. However for case 2, in some regions of the stability chart there are some small differences between two methods but in the rest of the chart both methods behaves with the same trend. In Figure 2.12 the biggest difference between two methods occurs around 8500 RPM. In Figure 2.11 same trend is observed on the results from the literature too. This difference might be attributed to the number of intervals which the principle period is divided into.

It was stated earlier that the time-averaged version requires less time to compute the stability diagram. The stability diagrams in Figure 2.12 are constructed for (400x320) spindle speed and axial depth of cut pairs with the principle period resolution, p=144.

On a laptop having 2GB RAM and 2.3 GHz Dual-Core CPU it took 15773 seconds for the non-averaged version and 5560 seconds for the time-averaged version to construct the stability diagrams. The software used for the calculations is MATLAB R2009a.

In this section, the stability prediction methods presented in this chapter are used for known milling cases from the literature. The results of the presented methods are compared with both other stability prediction methods from the literature and with each other. It's observed that the results are in a very good agreement.

Also it's important to note that time averaged version of the method gives reasonably close results with the non-averaged method. Because time-averaged version computes the monodromy matrix at one step, not with p repeated multiplications, the amount of time required to obtain the stability chart is reduced significantly. Considering these in the following sections, the stability of serrated end mills will be analyzed with the time-averaged first order semi-discretization method with multiple delays.

2.5. Optimization of Variable Pitch Angles for Chatter Suppression

In this section variable pitch angles are optimized using the analytical design method proposed by Budak [19, 20]. Method will be explained briefly. Three variable pitch cutters are designed for given modal parameters and a spindle speed. Resulting cutters' stability is analyzed with first order semi-discretization method including multiple delays using time-averaged coefficient matrices. The chatter stability performances of these designed tools are compared with each other.

Variable pitch tools have variations between their cutting teeth. The phase delay between the surface being cut currently and the surface which was cut by previous tooth can be given as:

$$\varepsilon_j = \omega_c T_j \quad , \quad j = 1,2,\dots, N_t \tag{2.49}$$

where ω_c is the chatter frequency and T_j is the tooth pass period of jth cutting tooth.

This phase delay can also be expressed as

38

$$\varepsilon_j = \varepsilon_1 + \Delta\varepsilon_j \quad , \quad j = 2, \dots, N_t \tag{2.50}$$

where $\Delta\varepsilon_j$ is the phase difference between tooth j and the 1st tooth.

Regardless of the tool type, variable pitch, variable helix or regular end mill, the number of waves left on the cut surface because of the vibrations is expressed as follows:

$$m = \frac{\omega_c}{\Omega} \tag{2.51}$$

where Ω is the spindle speed (rad/sec).

The corresponding angular wavelength of one full wave is given as

$$\theta = \frac{2\pi}{m} \tag{2.52}$$

The pitch angle variation ΔP is determined as:

$$\Delta P = \frac{\Delta\varepsilon}{2\pi}\theta \tag{2.53}$$

With the help of the pitch angle variation ΔP, optimal variable pitch tools can be designed in order to increase chatter stability. According to the number of cutting teeth, optimal $\Delta\varepsilon$ values vary.
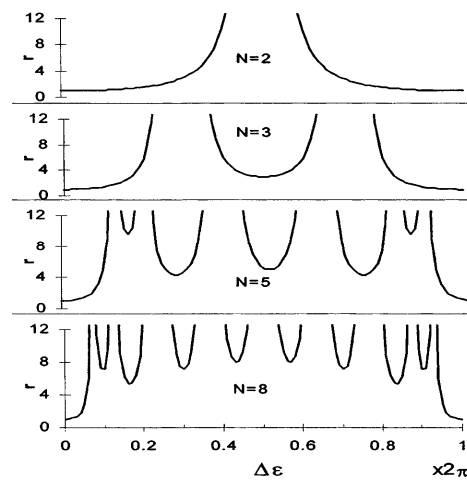
Figure 2.13. The effect of number of cutting teeth on optimal $\Delta\varepsilon$ [19]

39

There are different pitch variations such as linear, alternating and sinusoidal.

Linear pitch variation: $P_0, P_0 + \Delta P, P_0 + 2\Delta P, P_0 + 3\Delta P, ...$

Alternating pitch variation: $P_0, P_0 + \Delta P, P_0, P_0 + \Delta P, ...$

Sinusoidal pitch variation: $P_0, P_0 + \Delta P, P_0, P_0 - \Delta P, P_0, ...$

In the next part of this section, variable pitch variation will be determined with the method proposed in [19, 20] for given modal parameters and a desired spindle speed. Linear, alternating and sinusoidal pitch variations will be formed and their chatter stability behaviors will be analyzed.

2.5.1. Application of Variable Pitch Optimization

The method will be applied to design a variable pitch end mill having 4 cutting teeth in order to increase chatter stability at a given spindle speed.

The modal parameters of the system and cutting force coefficients are given in the below table

Table 2.6. Modal parameters and cutting force coefficients

ω_{nx} (rad/sec)	ζ_x	m_x (Kg)	ω_{ny} (rad/sec)	ζ_y	m_y (Kg)	K_{tc} (MPa)	K_{rc} (Mpa)
$1440*2\pi$	0.02503	0.1246424	$1440*2\pi$	0.02503	0.12464	697	255.8

Desired spindle speed is chosen as 4800 rpm

Total number of waves left on the surface after one tool rotation is calculated as follows:

$$m = \frac{\omega_c}{\Omega} = \frac{1440}{\left(4800/60\right)} = 18 \tag{2.54}$$

The angular wavelength of a one full wave is given as:

$$\theta = \frac{2\pi}{m} = \frac{2\pi}{18} = 20° \qquad (2.55)$$

According to the figure given in part 2.5 for even number of teeth, $\Delta\varepsilon$ is chosen as 0.5 ΔP for given modal parameters and 4800rpm spindle speed is $10°$.

Resulting variable pitch variations are given below:

Linear pitch variation: $P_0, P_0 + \Delta P, P_0 + 2\Delta P, P_0 + 3\Delta P = 360°$

Pitch values of the cutting teeth are 75°, 85°, 95° and 105°

Alternating pitch variation: $P_0, P_0 + \Delta P, P_0, P_0 + \Delta P = 360°$

Pitch values of the cutting teeth are 85°, 95°, 85° and 95°

Sinusoidal pitch variation: $P_0, P_0 + \Delta P, P_0, P_0 - \Delta P = 360°$

Pitch values of the cutting teeth are 90°, 100°, 90° and 80°

Stability charts for designed variable pitch cutters and a regular end mill will be constructed for a half immersion milling case.

As can be seen from the Figure 2.13, for 4800RPM stability limit is around 1mm. We expect to increase this stability limit for 4800RPM with the optimal pitch variations calculated in this section. In the following a comparison of those pitch variations will be given.
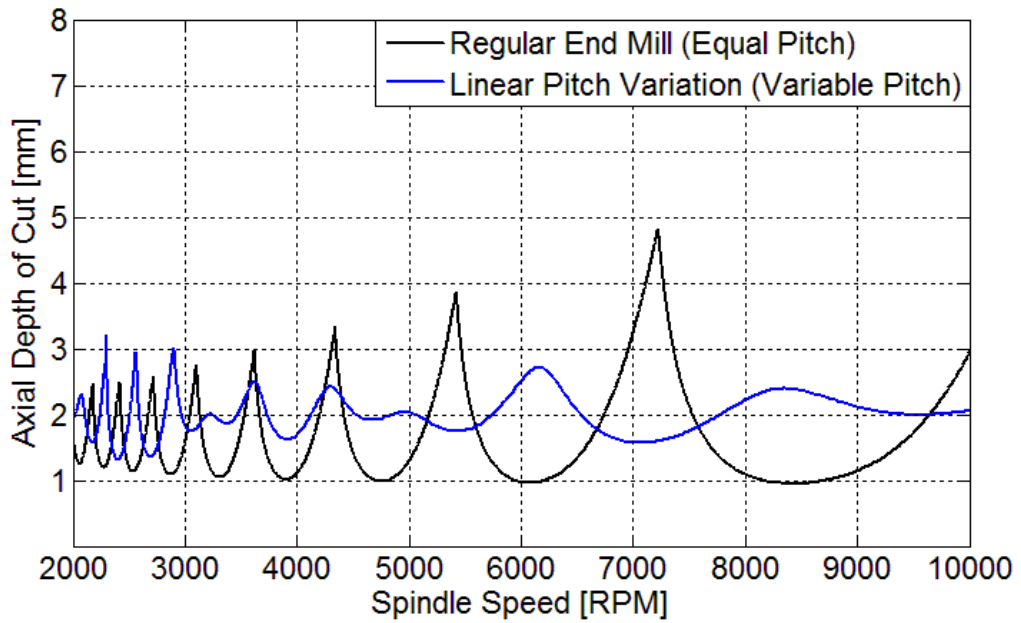
Figure 2.14. Stability diagrams: Comparison of regular and variable pitch milling tool with linear pitch variation (Half immersion, down milling case)
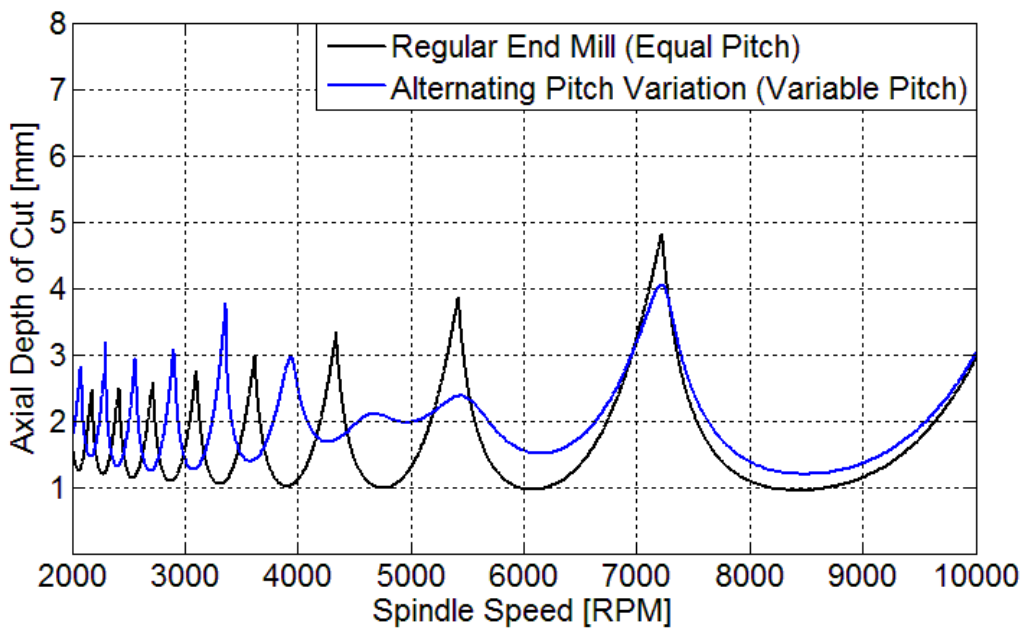
Figure 2.15. Stability diagrams: Comparison of regular end mill and variable pitch tool with alternating pitch variation (Half immersion, down milling case)
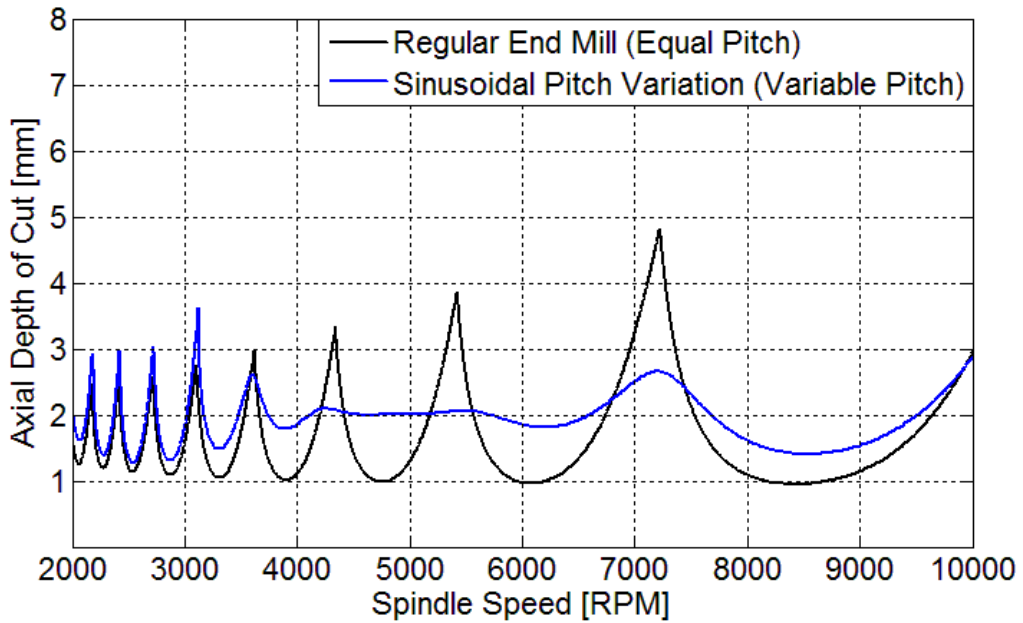
Figure 2.16. Stability diagrams: Comparison of regular end mill and variable pitch tool with sinusoidal pitch variation (half immersion, down milling case)

As can be seen from the comparison figures, all three variable pitch tools doubled the stability limit for the given spindle speed 4800RPM. The method proposed by Budak [19, 20] was verified experimentally in [20]. Here, the effectiveness of the method is shown on stability diagrams. Stability analysis of the designed variable pitch tools are made with time-averaged first order semi-discretization method including multiple delays presented in this chapter.
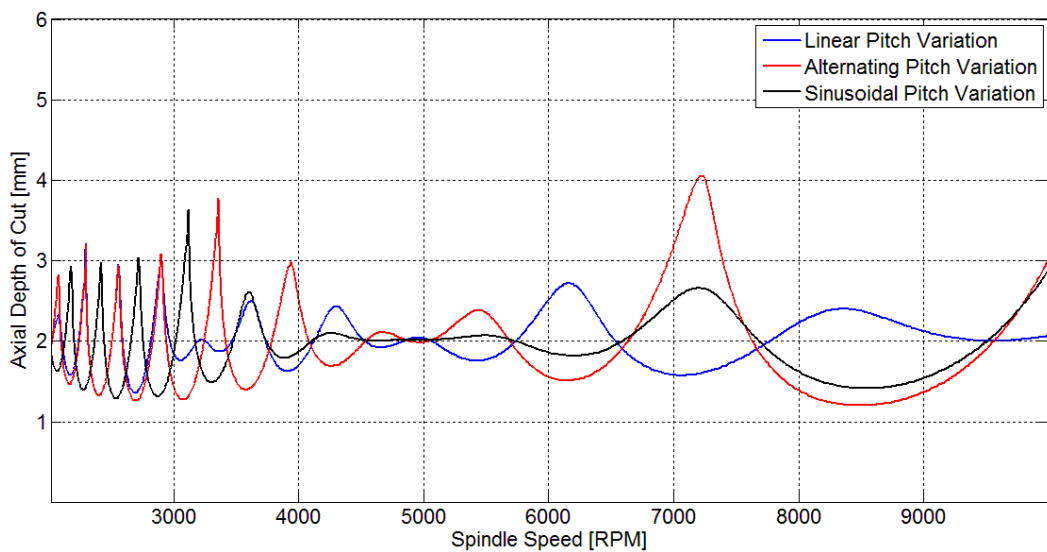
Figure 2.17. Comparison of optimal variable pitch patterns

As can be seen from the diagram above, each and every one of the variable pitch patterns reach the same stability limit at the desired spindle speed.

In this chapter, mechanics and dynamics of variable pitch, variable helix end mills are modeled. Milling forces are modeled based on Linear Edge Force model. Governing equation of milling stability with multiple time delays is constructed. Stability of the resulting delay differential equation with time-periodic coefficients is analyzed with semi-discretization method. First order semi-discretization method including multiple delays is formulated for milling stability problem with multiple time delays. Also presented semi-discretization method is slightly altered with Zero Order Approximation where coefficient matrices are averaged for one tool period instead of every time interval within the tool period. This approximation leads to the construction of the monodromy matrix in one step without p repeated multiplications of the transition matrices. According to the comparisons made, Zero Order Approximation gives reasonably close results to the main solution method while accelerating the stability analysis. The formulation is tested for previously published milling cases from the literature and very good agreement is observed.

In the last section of this chapter, the design method for variable pitch end mills proposed by Budak [19, 20] is applied to a milling case. Three different milling tools are designed to increase chatter stability for a given spindle speed considering the modal parameters of the system, and their stability behaviors are compared. As a result, every one of the designed variable pitch cutters doubled the stability limit for the given spindle speed compared to regular end mills.

Although validity of this variable pitch design method was experimentally verified, the overall performance of the optimized variable pitch tools in different spindle speeds hasn't been investigated so far. In this study, the performance of the optimized variable pitch tools are investigated with the stability charts. An important result is observed that optimized variable pitch tools are not only effective for the particular spindle speed they are optimized for but a wider range of spindle speeds. This observation has a great value in practice because of the practical advantages it introduces. During machining operations, machine tool spindles might not be able to perform at a given RPM. However with the observed results, even though spindle speed changes, the systems will remain stable.

Analytical optimization method adopted here considers one single chatter frequency, which is generally around the natural frequency of the most dominant mode. However, since machine tools are complex assemblies with a lot of different structural parts, the Frequency Response Functions at tool-workpiece contact area might have more than one dominant vibration mode. If the natural frequencies and the amplitudes of these multiple modes are close to each other, it is difficult to choose the most dominant one. However with the observed results, chatter suppression can be achieved for different chatter frequencies. This extends the effect of optimized variable pitch tools significantly.

Tool life is dependent on tool and workpiece materials and also cutting speed. Even if a particular milling operation is planned and the tooling is done, if a problem occurs regarding to tool life, spindle speed can be reduced than the planned spindle speed. According to the performance results, this change would not affect the stability of the operation. This is another important result which makes the optimized variable pitch tools more versatile and flexible in terms of cutting speed.

CHAPTER 3

MECHANICS OF MILLING WITH SERRATED END MILLS

Serrated end mills have been used commonly in the machining industry because of their ability to decrease total milling forces and allow higher stable depths of cut. Serrated cutting teeth have undulations on their flank faces. This undulation can have different forms such as sinusoidal, circular and trapezoidal. With the help of these forms, serrated cutting teeth get in contact with the material to be removed at only certain axial levels. There are two important characteristics which help the total milling forces to decrease:

- Total contact length between cutting tool and the workpiece decreases
- Chip load increases in certain axial levels, resulting in a decrease in cutting force coefficients. Also if serrated tools are properly designed another advantage is introduced with the help of increased rake angles in some portions of the cutting edge which also results in a decrease in cutting force coefficients.

In this chapter mechanics of milling with serrated end mills will be investigated in detail. Serrated end mill geometry representations will be given. Cutting tooth geometries, differences between regular and serrated cutting teeth will be discussed. Angle definitions for cutting force model along with the differential force calculations and directions will be presented. Commonly used serration forms, i.e. sinusoidal, circular and trapezoidal, will be formulated parametrically.

At the end of the chapter, the results obtained from force model will be compared with the force measurements during milling tests with serrated end mills.

3.1 Serrated End Mill Geometry

It is essential to understand the details of serrated tooth geometry in order to model both mechanics and dynamics of the milling operations in which these tools are employed. Because of the waveforms ground on the flank face of the cutting teeth, differential

force directions, uncut chip thickness values change significantly, and these features alter the whole process mechanics and dynamics.

Because of the waves on its cutting teeth, the tool radius is not constant but variable in the axial direction.

In figures 3.1 a) and b) the effect of serrations on local radius of the cutting teeth is illustrated.

a)

b)
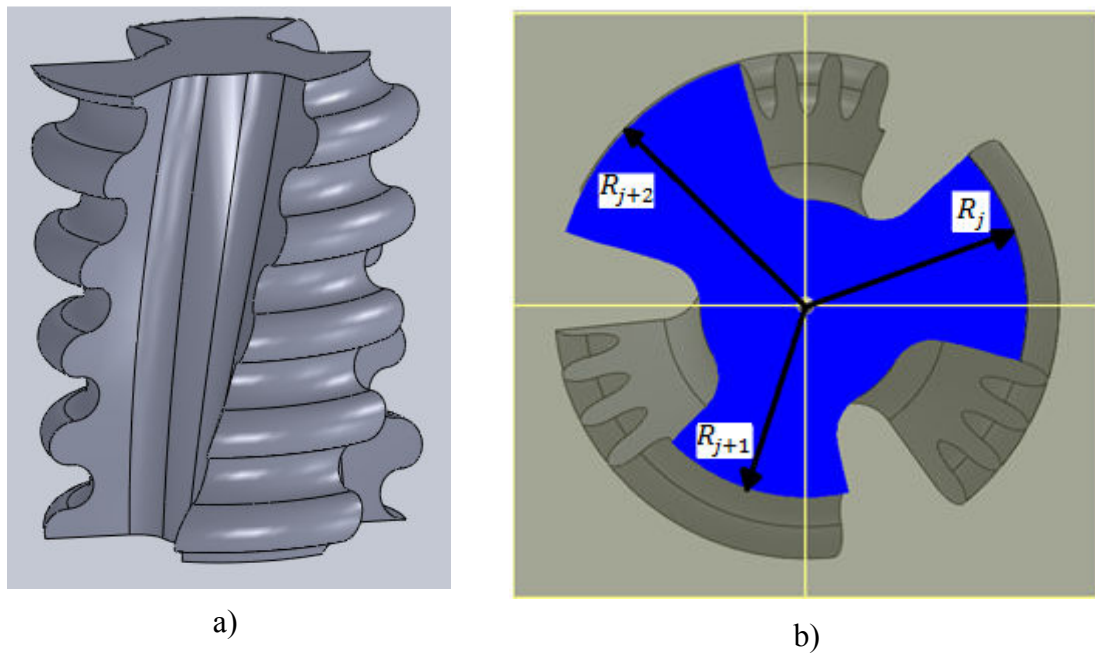
Figure 3.1. a) The effect of serrations on local tool radius, b) cross-section of a serrated tool

In the above figures serrated cutting edges are shown. Figure 3.1 b) illustrates the tool radius for a cross-section of the tool. It is seen that consecutive cutting teeth have different radii at a certain z level. This is because the waves on cutting teeth are placed with a phase shift in z direction in order to distribute the chip thickness. Thus, at a certain z level, only one cutting tooth removes material. This is the main mechanism behind serrated cutting teeth, which reduces cutter-workpiece contact length, and thus milling forces.
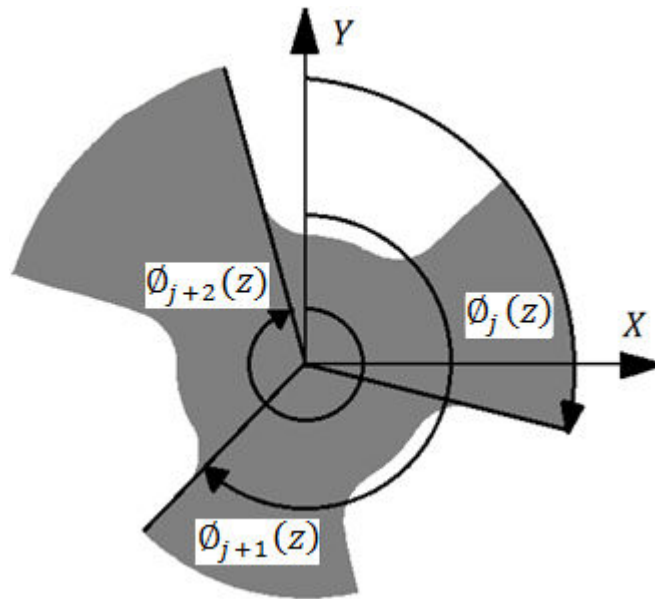
Figure 3.2. The angular positions of cutting teeth

The local radius definitions will be given in the following for different serration waveforms.

Another result of the serrations on cutting teeth is that surface tangent vectors change, which directly affects the directions of the differential milling forces.
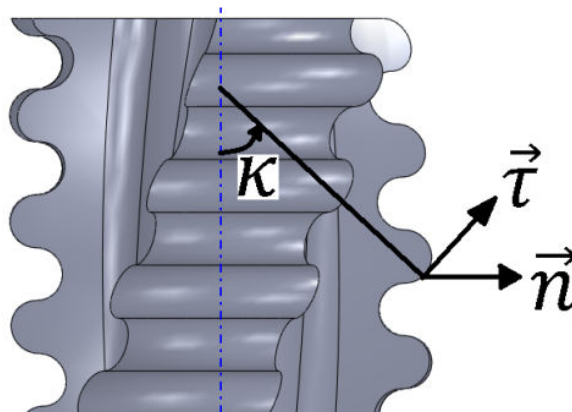
Figure 3.3. Surface tangent vector $\vec{\tau}$, surface normal vector $\vec{n}$ and axial immersion angle κ

Surface tangent vector, $\vec{\tau}$ is given as follows [31]:

$$\vec{\tau_j}(z) = \begin{Bmatrix} \left(\cos\left(\emptyset_j(z)\right)\right)\left(-\dfrac{tan(\beta_j)}{R_t}\right)R_j(z) \\ \left(-\sin\left(\emptyset_j(z)\right)\right)\left(-\dfrac{tan(\beta_j)}{R_t}\right)R_j(z) \\ 1 \end{Bmatrix} + \begin{Bmatrix} \left(\sin\left(\emptyset_j(z)\right)\right)\dfrac{\partial}{\partial z}R_j(z) \\ \left(\cos\left(\emptyset_j(z)\right)\right)\dfrac{\partial}{\partial z}R_j(z) \\ 0 \end{Bmatrix} \quad (3.1)$$

where, j indicates the tooth number, R_t indicates the radius of the tool, $R_j(z)$ indicates local radius for j^{th}, at axial level z, β_j is the helix angle of jth tooth, $\emptyset_j(z)$ is the angular position of the jth cutting teeth at axial level z.

Surface normal vector, $\vec{n}$ is given as follows [31]:

$$\vec{n_j}(z) = \begin{Bmatrix} \sin\left(\emptyset_j(z)\right) \\ \cos\left(\emptyset_j(z)\right) \\ 0 \end{Bmatrix} \quad (3.2)$$

$\kappa_j(z)$, axial immersion angle, which has a great importance for material removing mechanics is defined as the angle between surface tangent and surface normal vectors as follows [31]:

$$\vec{\tau_j}(z) \cdot \vec{n_j}(z) = \left|\vec{\tau_j}(z)\right|\left|\vec{n_j}(z)\right| \cos\left(K_j(z)\right)$$

$$\kappa_j(z) = \text{acos}\left[\frac{\vec{\tau_j}(z) \cdot \vec{n_j}(z)}{\left|\vec{\tau_j}(z)\right|}\right] \quad (3.3)$$

Another important issue is to represent the local radius change for a given serration waveform, and wave phase shift direction. Following are the parametric waveform and radius formulations for sinusoidal, circular and trapezoidal serration forms.

3.2. Serration waveform and local radius representations

3.2.1. Sinusoidal serration form

Sinusoidal serration form is defined with a sinewave.
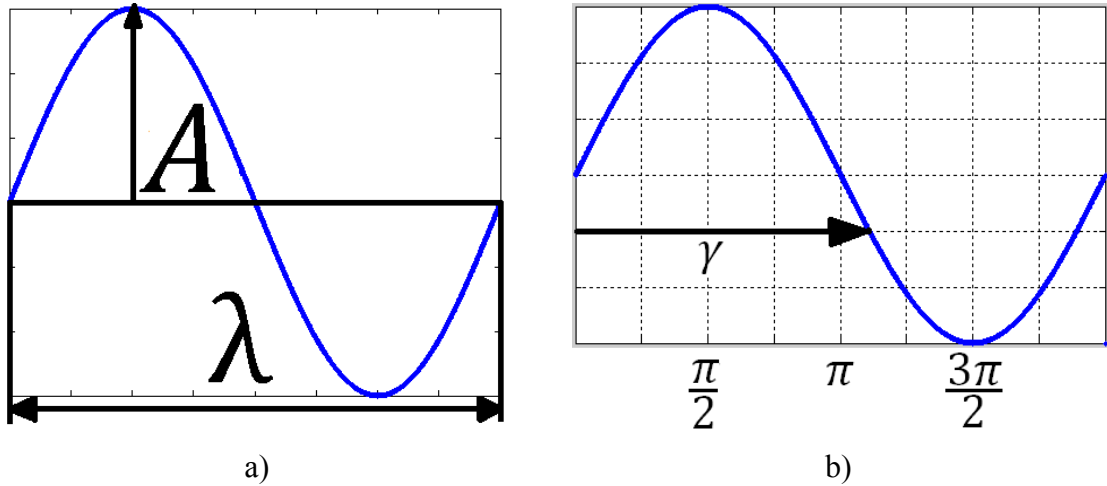
Figure 3.4. a)Sine wave and its parameters, b) serration angle λ

In figure 3.4, sine wave form and its defining parameters A, amplitude of the sine wave, and λ, wavelength of the sine wave, are shown.

Local radius $R_j(z)$ is defined as follows for sinusoidal serrated end mills:

$$R_j(z) = (R_t - A) + A(\sin(\gamma(z,j))) \qquad (3.4)$$
$$\gamma(z,j) = z/(\lambda + 2\pi + pd(j))$$

where $\gamma(z,j)$ is the serration angle as shown in figure 3.4 b), $pd(j)$ is the phase difference of the serration wave between the 1st and the jth tooth.

As an example, local radius and κ variations for a 4 teeth end mill with sinusoidal serration is given below. Serration parameters are: A=0.3mm, λ=4mm. R_t= 6mm.
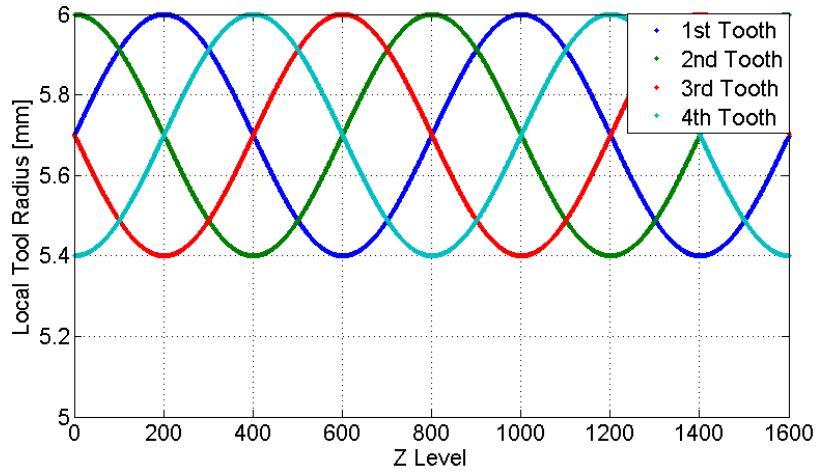
Figure 3.5. Local radius variation for an end mill with sinusoidal serrations.

In figure 3.5. the phase shift between consequtive teeth can be seen. Phase shift between every cutting teeth is defined as (λ/Nt) .

κ angle variation for resulting form is given in the next figure.
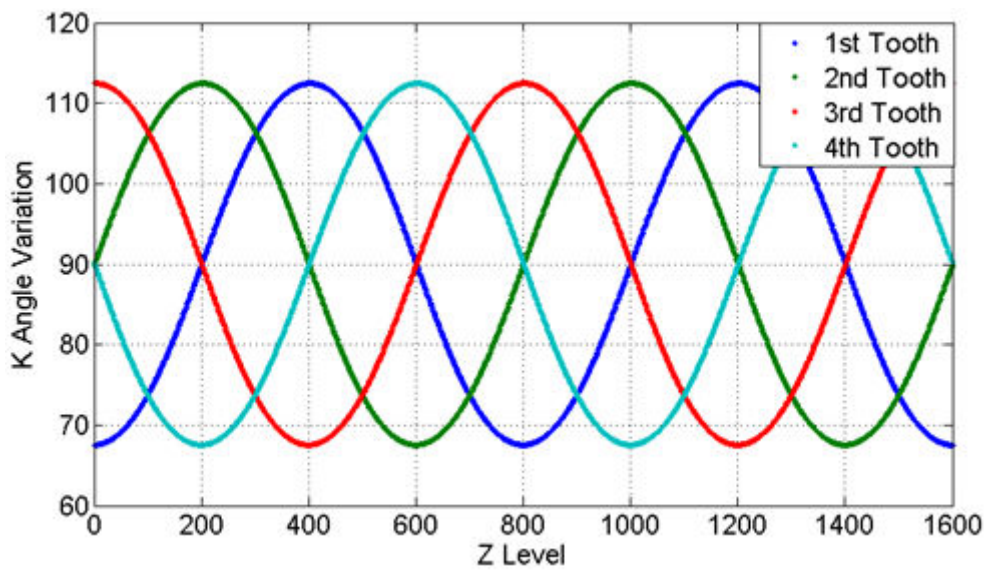
Figure 3.6. κ angle variation

As κ angle variates, the directions of the differential milling forces change too. This effect will be discussed in force modeling.

51

3.2.2. Circular serration form

Circular serration wave is defined with two tangent arcs.
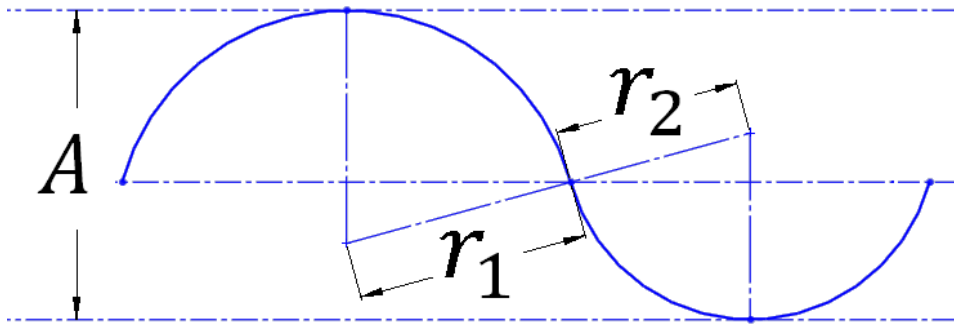
Figure 3.7. Circular serration wave

The parameters in order to define the circular serration form are radius of the outer arc r_1, radius of the inner arc r_2 and amplitude of the wave A. In this study the serration waves are defined with least possible number of parameters in order to decrease the complexity of optimization process, which will be presented in the next chapter.

In order to calculate the local radius for every tooth at every axial level, i.e disk element, one full circular serration wave is divided into four zones:
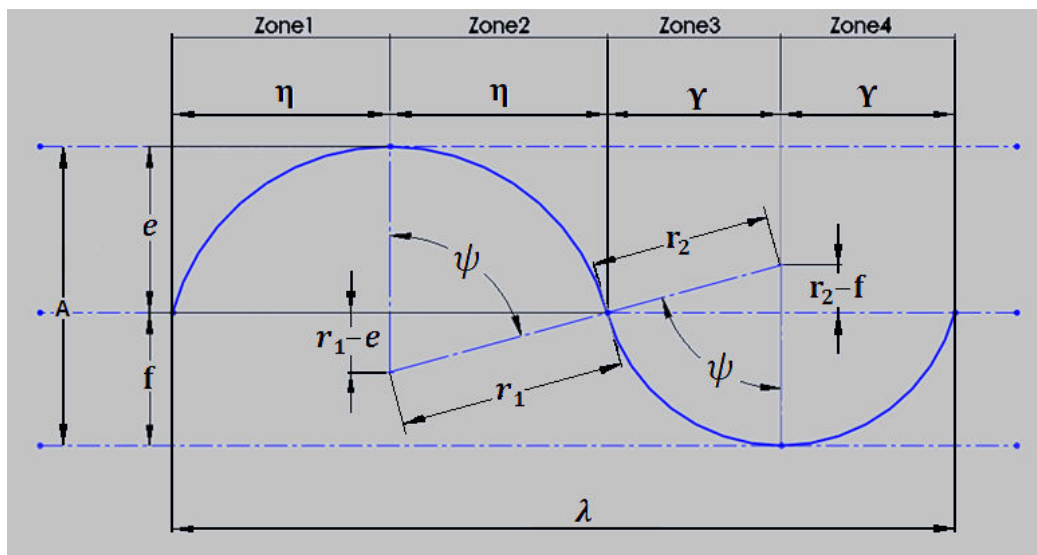
Figure 3.8. Circular serration wave divided into zones with necessary dimensions shown

where shown dimensions are calculated as follows:

$$e = \frac{A * r_1}{r_1 + r_2}$$

$$\psi = acos\left(\frac{r_1 - e}{r_1}\right)$$

$$f = A - e$$

$$\eta = (sin(\psi)) * r_1$$

$$\Upsilon = (sin(\psi)) * r_2$$

$$\lambda = 2 * (\eta + \Upsilon)$$

(3.5)

3.2.2.1. Zone 1
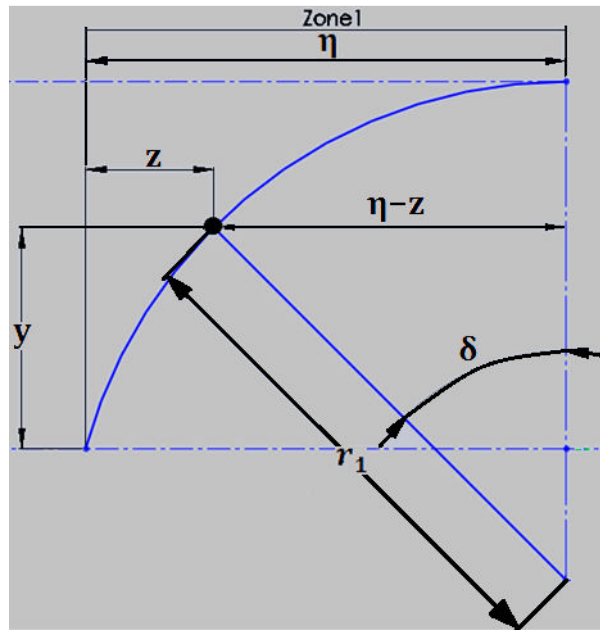
Figure 3.9. Dimensions of zone 1

As explained in chapter 2, the cutting tool is divided into disk elements along the axial direction. In order to calculate the local radius for every tooth at every z level, every disk element is traced starting from the tool tip up to the axial depth of cut. For every z level, the zone number is determined according to wavelength, phase shift and z level. Then, the local radius, $R_j(z)$ is calculated.

$$z_1 = \big(dz(l-1)\big) + pd(j)$$

$$z = mod(z_1, \lambda)$$

$$\delta = asin\left(\frac{(\eta - z)}{r_1}\right)$$

(3.6)

$$y = r_1\big(cos(\delta)\big)$$

$$R_j(z) = R_t - r_1 + y$$

The formulation for the local radius calculation in Zone 1 is given in (3.6)

3.2.2.2. Zone 2
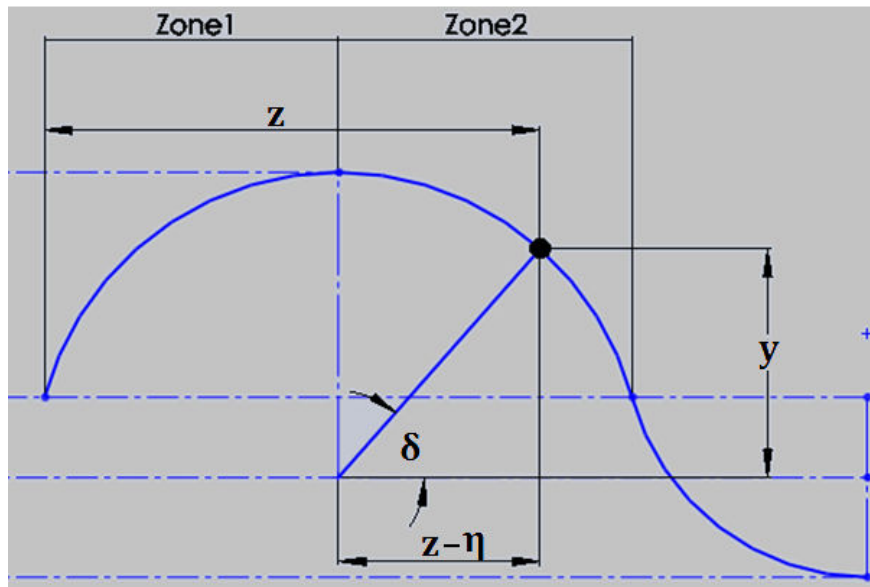
Figure 3.10. Dimensions of zone 2.

$$\delta = acos\left(\frac{z - \eta}{r_1}\right)$$

(3.7)

$$y = r_1\big(sin(\delta)\big)$$

$$R_j(z) = R_t - r_1 + y$$

The formulation for the local radius calculation for zone 2 is given in (3.7)

3.2.2.3. Zone 3
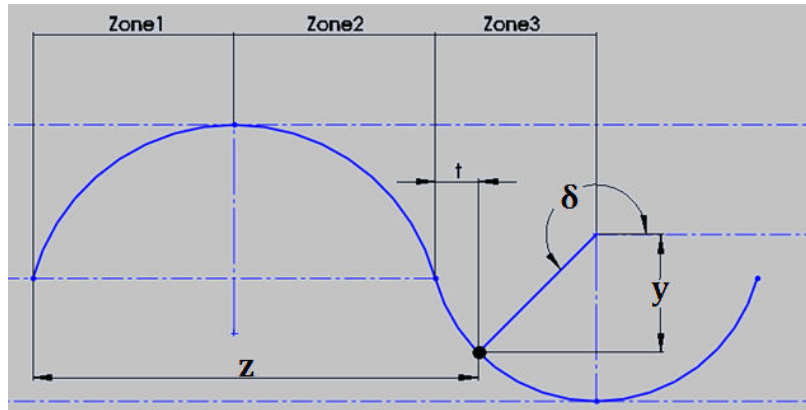
Figure 3.11.: Dimensions of zone 3.

$$t = Y - \left(z - (2\eta)\right)$$

$$\delta = acos\left(\frac{-t}{r_2}\right)$$

$$y = r_2\left(sin(\delta)\right)$$

$$R_j(z) = (R_t - A) + (r_2 - abs(y))$$

(3.8)

The formulation for the local radius calculation in zone 3 is given in (3.8)

3.2.2.4. Zone 4
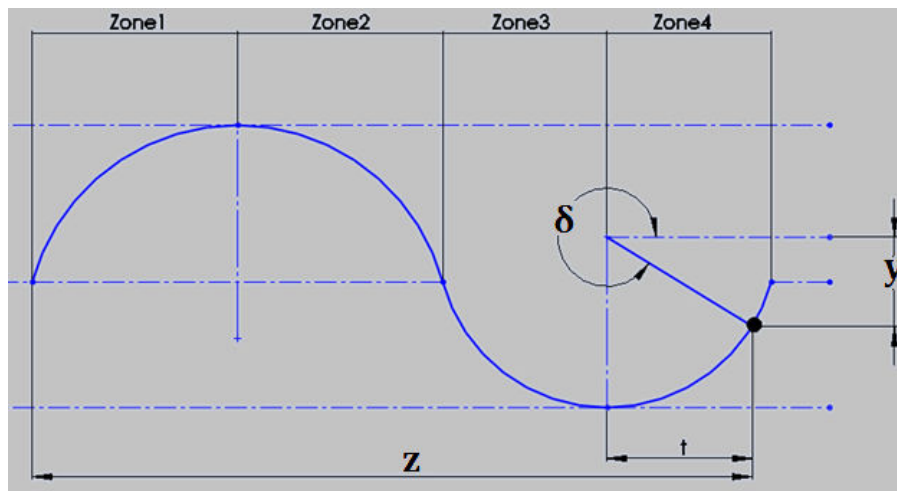
Figure 3.12. Dimensions of zone 4.

$$t = (z - (2\eta)) - Y$$

$$\delta = acos\left(\frac{t}{r_2}\right)$$

(3.9)

$$y = (sin(\delta))r_2$$
$$R_j(z) = (R_t - A) + (r_2 - abs(y))$$

The formulation for the local radius calculation for Zone 4 is given in (3.9)

As an example, local radius of a circular serrated tool will be given. Serration wave parameters are $r_1 = 5mm, r_2 = 2mm, A = 1mm$.
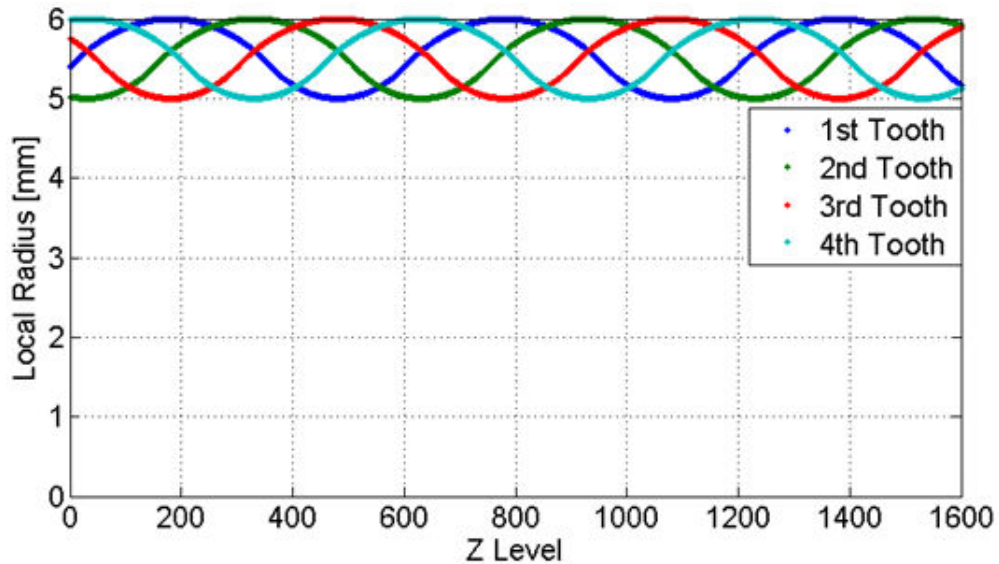
Figure 3.13. Local radius of the circular serrated end mills' teeth
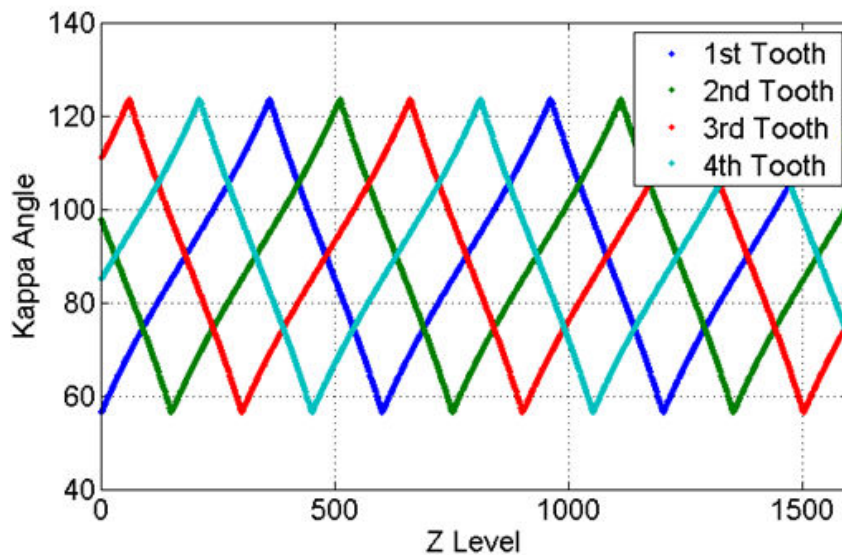
Figure 3.14. Local κ angle variation of the circular serrated end mill's teeth

In figure 3.13. local radius variations of cutting teeth along the tool axis are illustrated. As can be seen from the figure 3.13. the local radii of cutting teeth vary between R_t and

56

$R_t - A$. In figure 3.14 local κ angle variation of the circular serrated end mill's teeth is illustrated. If figure 3.14. and figure 3.6 are compared, it can be seen that the effect of serration wave type and parameters directly affect the κ angle variation. This will directly affect the differential milling force directions.

3.2.3. Trapezoidal Serration Form

Another serration wave used in industry is trapezoidal wave. Trapezoidal wave form is defined as follows:
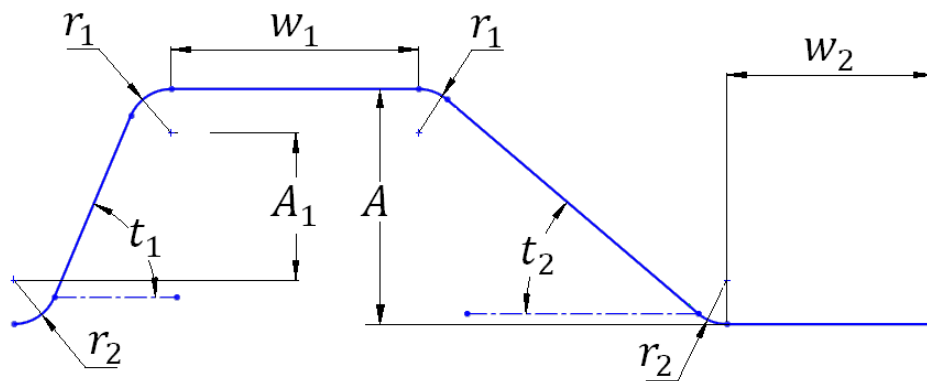
Figure 3.15. Trapezoidal serration wave and its parameters

Local radius definitions for trapezoidal serration wave are also done in the same fashion as circular serration. One full wave of the serration form is divided into 8 zones.
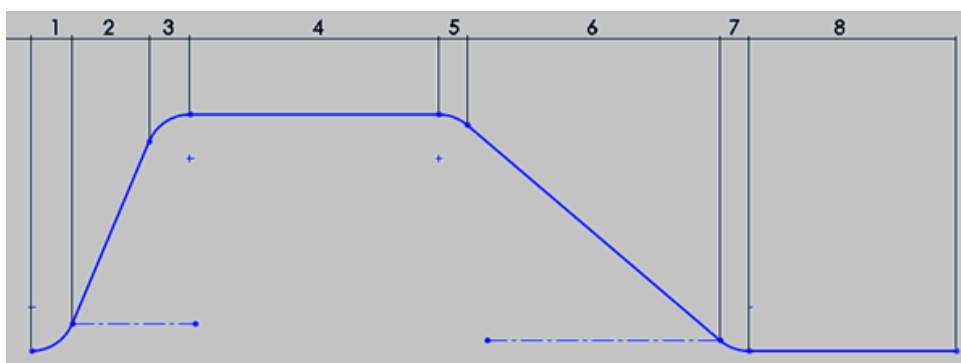
Figure 3.16. Trapezoidal serration wave divided into zones

An example trapezoidal serrated end mill's local radius will be represented here. Serration parameters for the example trapezoidal form are given below.

Table 3.1. Parameters for a trapezoidal serration wave

w_1	w_2	t_1	t_2	A	$r_1 \& r_2$
0.4 mm	0.5 mm	60°	30°	0.6 mm	0.2 mm

Resulting tool radius variation for a 12mm diameter tool is illustrated in figure 3.17.
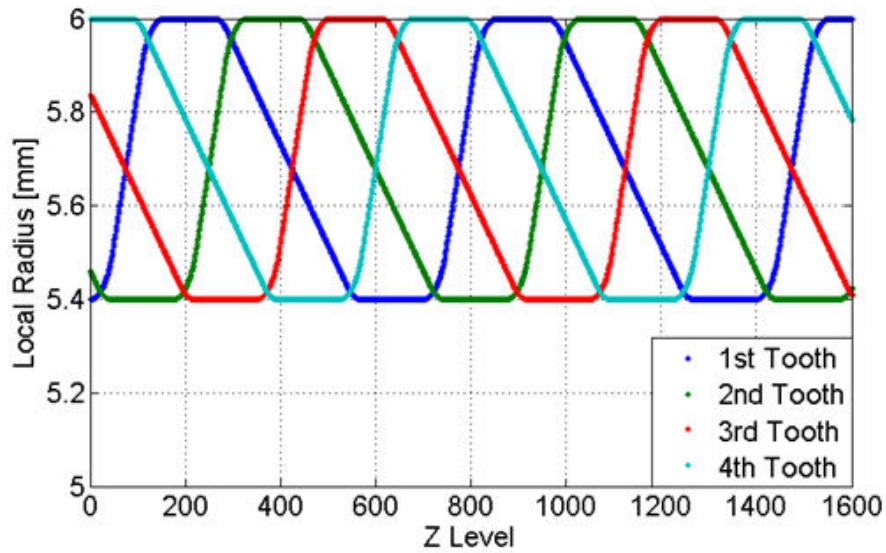
Figure 3.17. Illustration of local radius variation for the example trapezoidal serrated end mill.
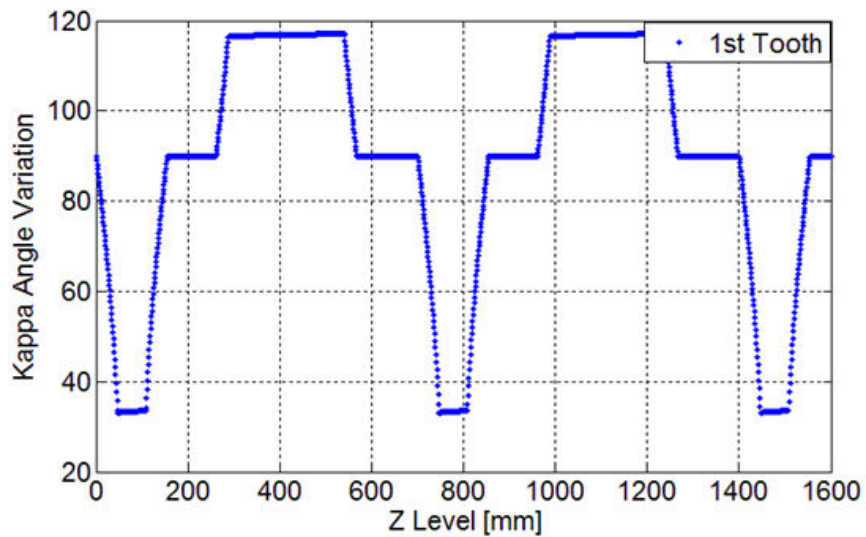
Figure 3.18. κ angle variation of the first tooth of the example trapezoidal serrated end mill

As can be seen from the figure 3.17, in some portions of the trapezoidal serrated cutting teeth local radii do not change. Because of this, if properly designed these serrated end mills can be employed in finishing operations where a flat surface is required. Other serration wave forms can not be used for finishing, because of their geometry, sinusoidal and circular ways always leave some material on the cut surface. In figure 3.18, the portions of the cutting edge where local radius is constant, κ angle does not variate. This is also the same with the regular end mills.

3.3. On Rake and Oblique Angle Variations Caused by Serrations

The cutting edges of serrated teeth have variable geometry. Because of this, rake and oblique angles vary along theses cutting edges. This variable character of the edges needs to be considered and included into the chip removal mechanics. In order to explain the variable angles, orthogonal and oblique cutting models are used.
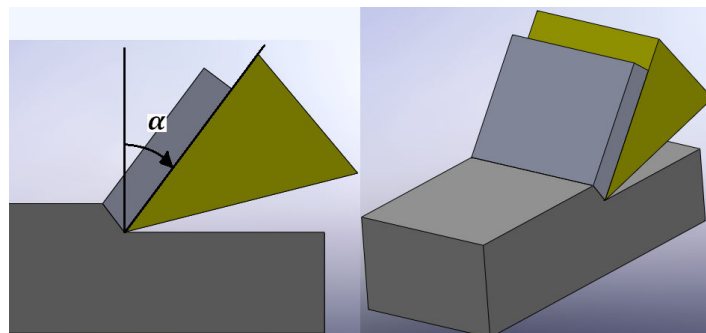
a)
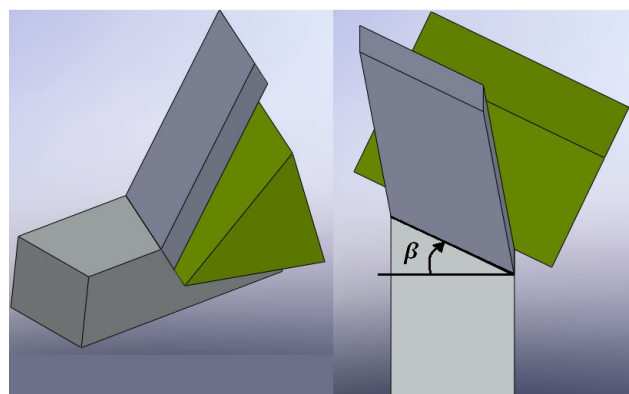
b)

Figure 3.19. a) Orthogonal Cutting, b) Oblique Cutting

In figure 3.19, α and β represent the global rake and oblique angles, respectively. With the introduction of the obliquity into the cutting system, the local or effective cutting angles change which also alters the shearing mechanism.

In the following figure, a fraction of a serrated cutting tooth is presented. The axis represents the rotation axis of the end mill.
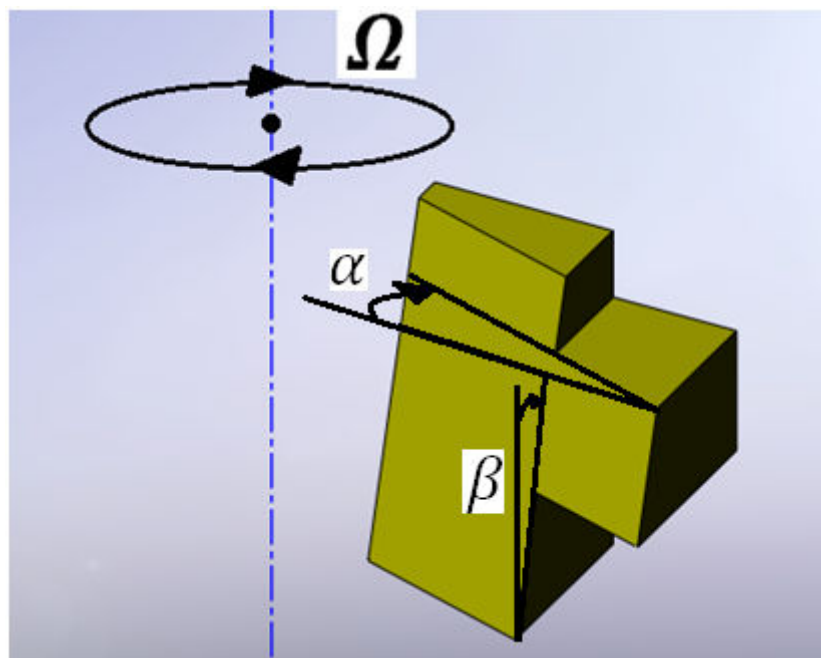
Figure 3.20. A fraction of a cutting edge having rectangular serration, global rake and oblique angles α and β respectively

In order to explain the variable rake and oblique angles better, a fraction of the cutting edge of an end mill having rectangular serration is presented.
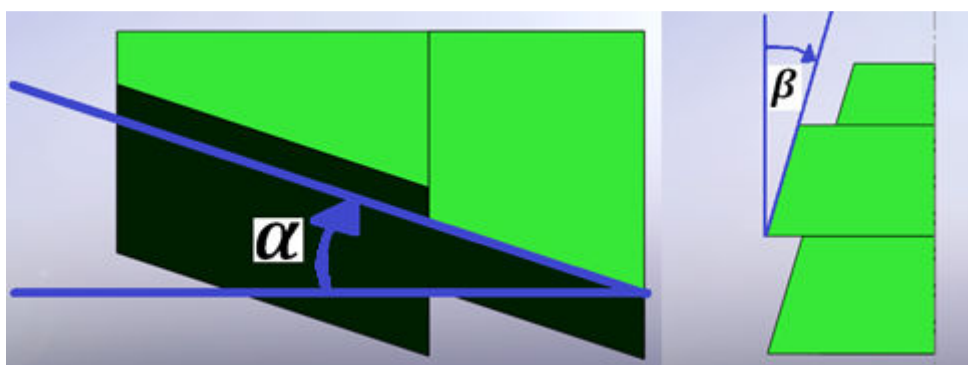
Figure 3.21. Global rake and oblique angles of the end mill respectively

In figure 3.21 global rake and oblique angles of the end mill are shown. These angles would be valid along the whole cutting edge if there were no serrations. However in serrated case, the angular orientation of the tooth defined by these angles affect the local rake and inclination angles on different parts of the cutting edge. This situation will be explained by showing the rake and oblique angles for three different parts of the serrated cutting edge.
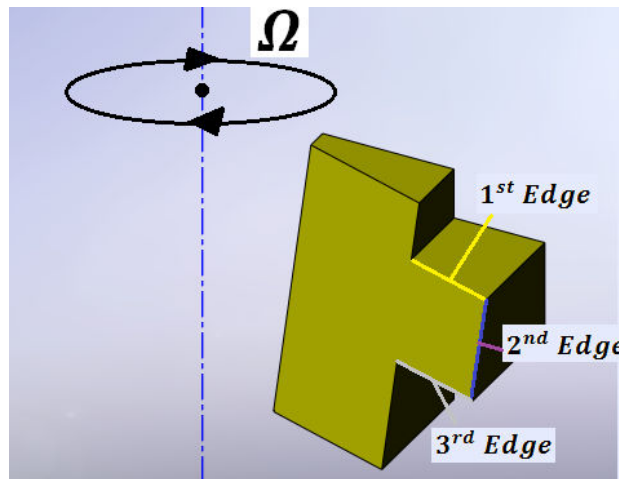
Figure 3.22. Three different parts of the serrated cutting edge

3.3.1. 1st Edge

In the 1st edge, because of the chip removal directions, the global oblique angle of the tooth due to helix becomes the local rake angle (negative) and the global rake angle on the flute becomes the oblique angle on this edge illustrated in figure 3.23.
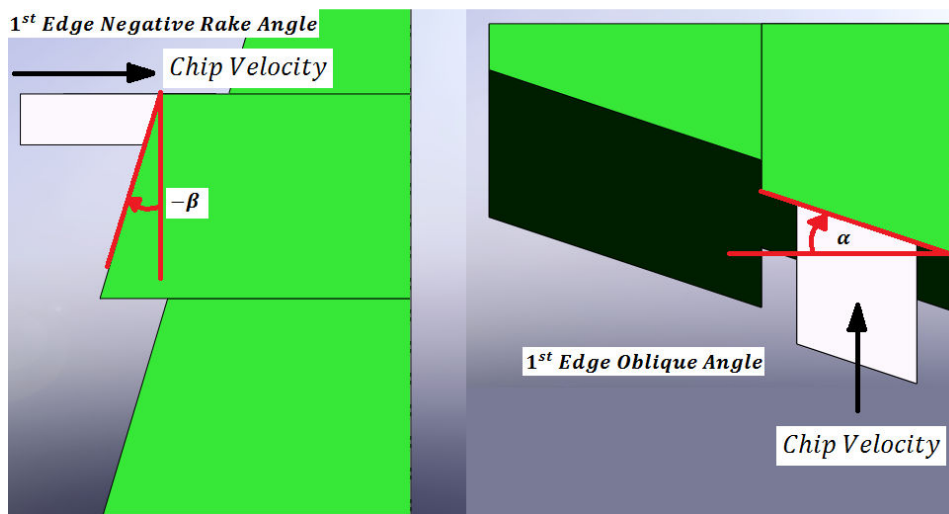
Figure 3.23. Resulting rake and oblique angles for 1st edge

3.3.2. 2nd Edge

2nd edge has the same global cutting angles with the end mill. Thus the local rake angle on this edge is equal to α and the local oblique angle is equal to the helix angle, β.
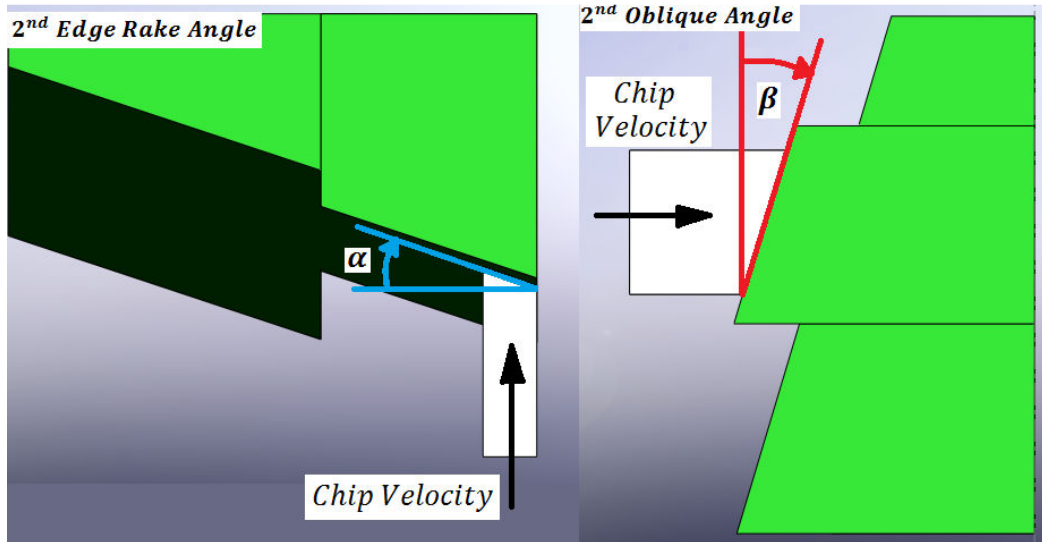
Figure 3.24. Resulting rake and oblique angles on 2nd edge

3.3.3. 3rd Edge

3rd edge has a bigger local rake angle than the other 2 edges as illustrated in figure 3.27. It's shown that for this rectangular serration type, the resulting local rake angle for this edge is equal to the helix angle of the end mill, β, and the resulting local oblique angle is the global rake angle of the end mill, α .
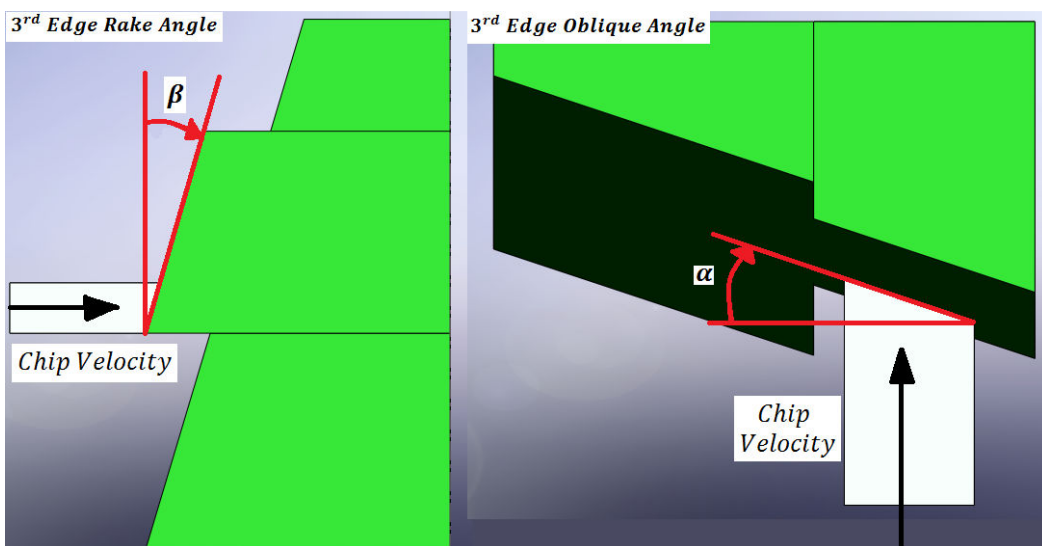
Figure 3.25. Resulting rake and oblique angles on 3rd edge

A rectangular serration type is analyzed in order to show the variable cutting angles on different portions of the serrated tools. In this case it is relatively easy to see the resulting angles, however for complicated serration geometries the local angles must be calculated for every cutting edge for each axial disk element. It has been a known fact and proved with both analytical and experimental studies that as the increasing rake angle affects the shearing mechanism positively. It results in decreased cutting force coefficients as it becomes easier to shear the material with higher rake angles. When selecting or designing serrated end mills, one can prefers to exploit this phenomenon in order to decrease cutting forces. However, in order to use this as an advantage, cutting edge strength needs to be taken into account, too. When using rectangular serration type, the stress distribution on corners of the edges needs to observed carefully. Also as rake angle increases cutting edge becomes weaker, this should be another concern in serrated tool design.

It is also to be noted that for most oftenly used serration types such as sinusoidal, circular and trapezoidal, resulting change in the rake and oblique angles is not as drastic as in the case of rectangular or square wave types. Another required comment is that serrated end mills are employed with lower feed per tooth values, which decreases the immersed part of the cutting edges, and thus local angle variations. However, for a complete mechanics of milling model for serrated end mills this, local angle variations should be taken into account. To the author's knowledge, local angle variations and their effects on milling mechanics has not been made until this study.

In order to take advantage of this situation, serration waves need to be ground on flank faces of the teeth in such a way that the portions of the cutting edge where rake angles are higher should remove material instead of the lower rake angle sections. One can actually achieve this by reversing the phase shift of the serration waves of consecutive teeth. It's been observed that the serrated end mills available on the market has forward phase shift as explained in the following:

$$pd(j) = \left(\lambda/_{Nt}\right) * (j - 1) \tag{3.10}$$

Phase shift is given according to the equation above. First cutting tooth starts with the full wave. The second tooth starts with a (Full Wave – pd(2)), and so on. It's explained in the figures:
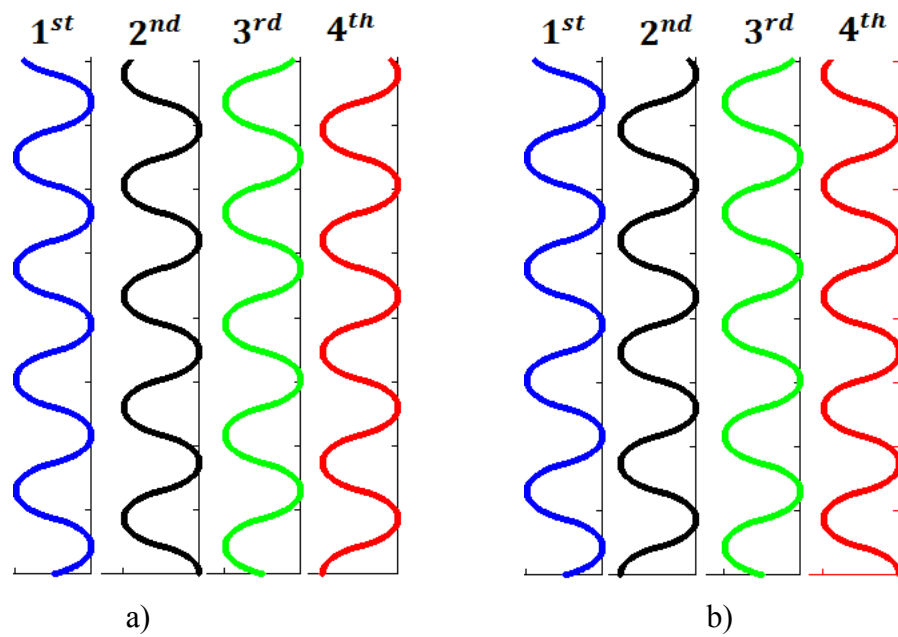
Figure 3.26. a) Forward phase shift, b) reverse phase shift

In figure 3.26, difference between forward and reverse phase shifts is shown by plotting the serration waves on consecutive cutting teeth.

If we plot the chip thickness for these phase shift types, one can understand its effect better.
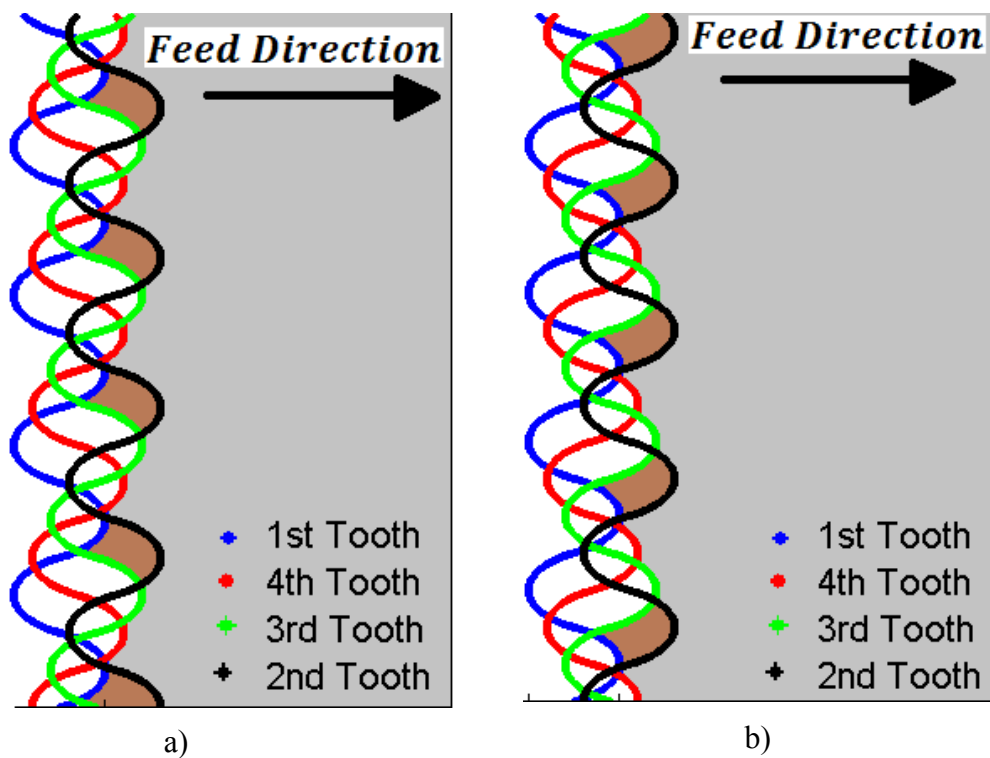
Figure 3.27. a) Forward phase shift, b) reverse phase shift

64

In figure 3.27, the difference between forward phase shift and revese shift is clearly seen. In these figures, profiles of the cutting edges are plotted with a given feed per tooth value for right-hand milling tools. From the figure 3.1 b), the way cutting teeth are numbered can be seen. After the 1st cutting tooth, 4th cutting tooth enters the workpiece then 3rd and 2nd respectively. The parts colored brown are the chip removed by the 2nd cutting tooth.

It's shown that with the reverse phase shift, the portions of the cutting edge where rake angles are higher remove the material. However, the effect of this advantage only can be significant when higher feed rates are used, i.e there is chip-tool contact all around the serrated edge. Having said that, another important aspect, which will be revisited in detail in the following sections, is that serrated end mills do not perform well when higher feeds are used. Considering these, a small amount of improvement would be introduced with reverse phase shift.

3.4. Chip Thickness Formulation

Chip thickness calculations for serrated end mills are different than regular end mills. This originates from the fact that some portions of the cutting edges do not remove material at certain axial levels. However, as a result of the process the same amount of material as the regular end mills is removed. This is possible due to the fact that some portions of the cutting teeth, remove more material.

Chip thickness for a cutting teeth on an axial disk element is calculated for each immersion angle $\emptyset_j(z)$ as follows:

$$h_j(\emptyset, z) = \max\left(0, h_j val\right)$$
$$h_j val(\emptyset, z) = \min\left[R_j(z) - R_m(z) + k * ft * \sin\left(\emptyset_j(z)\right)\right]$$
$$k = 1,2, \dots, Nt \tag{3.11}$$
$$m = \begin{cases} Nt & \leftarrow \ if \ j-k = 0 \\ & else \\ \mod\left((j-k), Nt\right) \end{cases}$$

The chip thickness is found by checking the chip removed by the previous cutting teeth.

As an example, a given serrated end mill and a regular end mill are compared in terms chip thickness they remove in one tool revolution in figure 3.28. Both tools have 4 cutting teeth and 12mm diameter. Radial immersion is 6mm, ft=0.05mm, axial depth of cut is 8mm. The serrated end mill has the circular serration wave with parameters $r_1 = 0.5mm, r_2 = 0.5mm, A = 0.6mm$. Milling operation is in down milling mode.
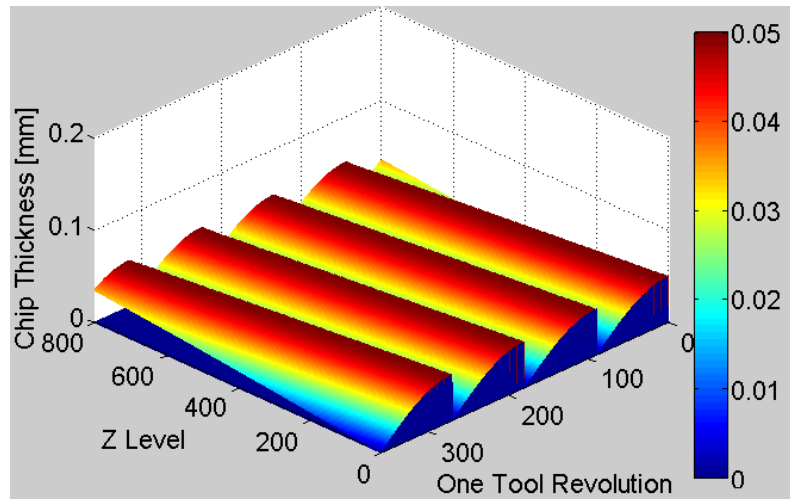
a)
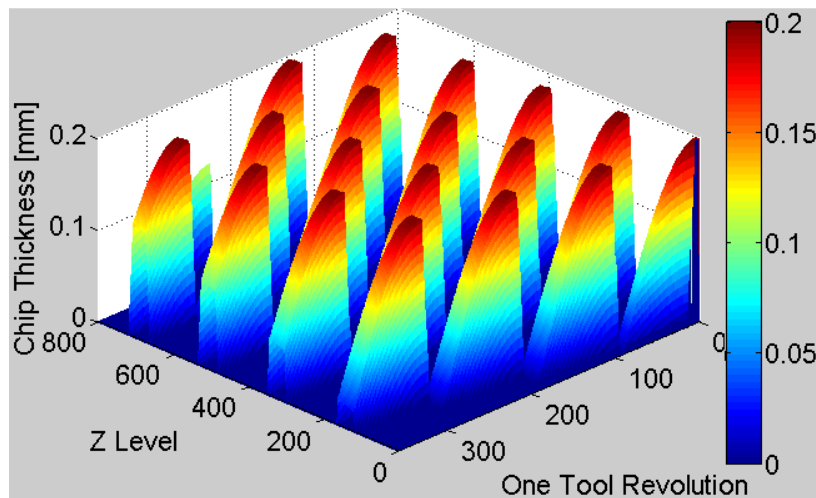
b)

Figure 3.28. a) Chip load for a regular end mill, b) Chip load for a serrated end mill

Figure 3.28 illustrates the difference between chip loads of regular end mills and serrated end mills. As stated earlier some portions of the cutting teeth do not remove any material at all. For the chip removing portions of the cutting teeth, chip thickness increases up to number of teeth times feed per tooth (Nt.ft). Because of this the contact length between cutting tool and the workpiece decreases drastically. Consequently a great amount of reduction in edge forces is obtained. Another improvement comes from

66

the cutting force coefficients which are decreased by the increased uncut chip thickness values.

3.5. Force Model

In order to present a force model for serrated end mills, required geometrical formulations were given in the previous sections of this chapter. In this section, differential milling forces will be calculated for every cutting tooth and immersion angle at every axial disk element in one full revolution of the cutter. Force contributions coming from every tooth and every disc element are summed to determine total milling forces at certain for every immersion angle. The differences between serrated end mills and regular end mills will be discussed in terms of force models. For a given milling operation, both regular and serrated end mills will be employed and differences will be discussed. At the end of this chapter, the results obtained from force model and experiments will be compared.
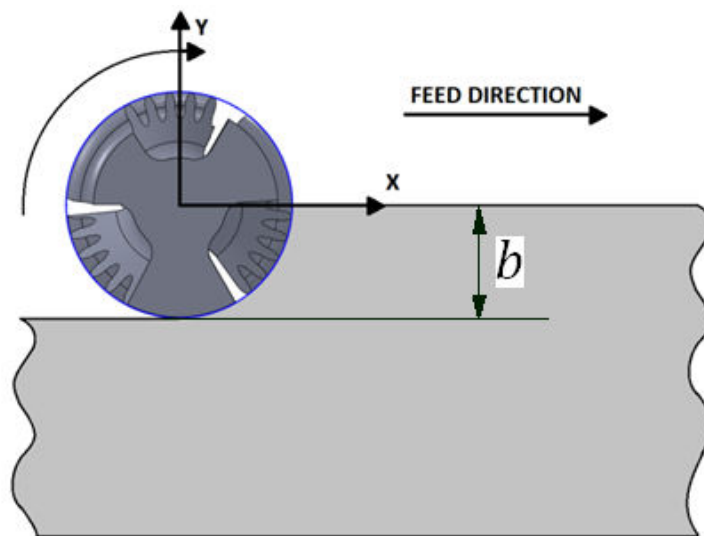
Figure 3.29. Milling process geometry

Because of the serration form, the directions of the differential forces vary along the cutting edges.
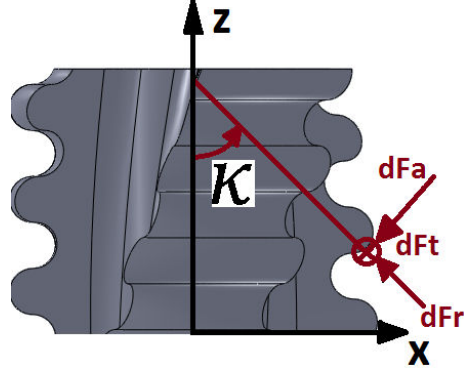
Figure 3.30. Differential forces acting on the cutting edge and their directions

Milling forces are calculated with the Linear Edge force model [14].

$$dFa_j(\emptyset_j, z) = g(\emptyset_j)[K_{ae} + K_{ac}\, h_j(\emptyset_j, z)]db$$
$$dFr_j(\emptyset_j, z) = g(\emptyset_j)[K_{re} + K_{rc}\, h_j(\emptyset_j, z)]db \qquad (3.12)$$
$$dFt_j(\emptyset_j, z) = g(\emptyset_j)[K_{te} + K_{tc}\, h_j(\emptyset_j, z)]db$$
$$db = {dz}\big/{\sin(\kappa(z,j))}$$

$dFa_j(\emptyset_j, z)$, $dFr_j(\emptyset_j, z)$, $dFt_j(\emptyset_j, z)$ represent the axial, radial and tangential differential forces acting on the jth tooth at axial level z for the immersion angle $\emptyset$. db represents the chip width.

According to the up-milling and down-milling conditions, a unit step function which determines whether the tooth is in cut or not is used.

$$g(\emptyset_j) = \begin{cases} 1, & \emptyset_{st} < \emptyset_j < \emptyset_{ex} \\ 0, & \emptyset_j < \emptyset_{st}\ or\ \emptyset_j > \emptyset_{ex} \end{cases} \qquad (3.13)$$

Cutting force coefficients are calculated with orthogonal-to-oblique transformation as explained in chapter 2.

Differential forces acting on the cutting edges are calculated as follows [31]:

$$dF_{xj}(\emptyset_j, z) = -dF_{rj}sin(\kappa)\sin(\emptyset_j) - dF_{aj}\cos(\kappa)\sin(\emptyset_j) - dF_{tj}\cos(\emptyset_j)$$

$$dF_{yj}(\emptyset_j, z) = -dF_{rj}\sin(\kappa)\cos(\emptyset_j) - dF_{aj}\cos(\kappa)\cos(\emptyset_j) + dF_{tj}\sin(\emptyset_j) \quad (3.14)$$

$$dF_{zj}(\emptyset_j, z) = dF_{rj}\cos(\kappa) - dF_{aj}\sin(\kappa)$$

Differential milling force contributions coming from all cutting teeth and disk elements are summed to obtain milling forces in X, Y and Z directions as follows:

$$F_x(\emptyset) = \sum_{z=0}^{z=a}\sum_{j=1}^{j=Nt} dF_{xj}(\emptyset_j, z)$$

$$F_y(\emptyset) = \sum_{z=0}^{z=a}\sum_{j=1}^{j=Nt} dF_{yj}(\emptyset_j, z) \quad (3.15)$$

$$F_z(\emptyset) = \sum_{z=0}^{z=a}\sum_{j=1}^{j=Nt} dF_{zj}(\emptyset_j, z)$$

In the following an example milling case will be simulated with the proposed force model. First, a comparison will be given with using regular and serrated end mills. Process and tool parameters are given in the table below:

Table 3.2. Process and tool parameters for the force model example

R_t	N_t	β	Serration Type	$r_1 = r_2$	W_1	W_2	$t_1 = t_2$	A
6mm	4	30°	Trapezoidal	0.2 mm	0.3 mm	0.2m m	45°	0.5 mm
Axial DOC *(a)*			**Radial Immersion** *(b)*		***ft***			
10mm			6mm		0.05mm/tooth			
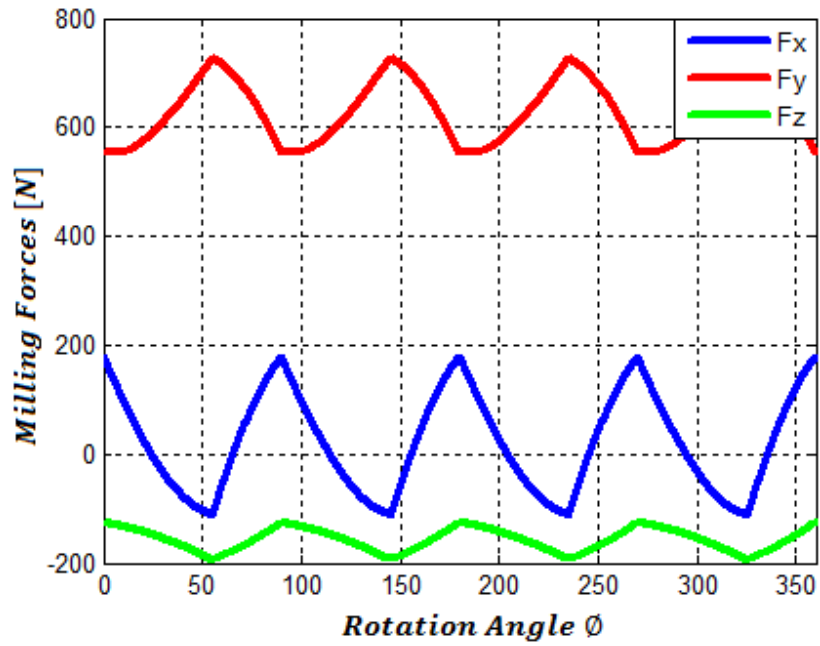
a)
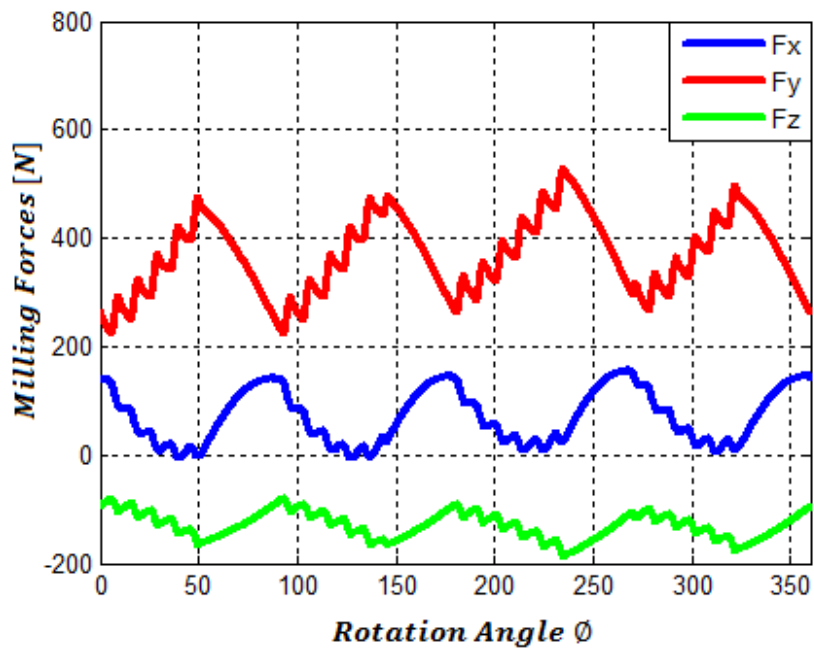
b)

Figure 3.31. Comparison of a) regular and b) serrated end mills in terms of cutting forces

In figure 3.31 it is shown that serrated end mills reduce total milling forces significantly. There are two reasons behind this.

The first and the most significant one is the reduction in contact length between the cutter and the workpiece. It was already shown that the cutter engage with the workpiece only at certain axial levels because of the serrations on the cutting edges. As explained both in chapter 2 and earlier in this one, there are two main force contributions coming from two main mechanisms namely, shearing and ploughing.

The forces needed to shear the material are calculated with the help of cutting force coefficients and shearing area. Ploughing forces acting on the cutting edge dependent on the workpiece-cutter contact length, cutting edge geometry, workpiece and cutter materials. Contributions of these forces are represented with the edge force coefficients in milling force formulations.

The second one is the reduction in the cutting force coefficients. This originates from the fact that the chip load accumulates on certain portions of the cutting edge and is increased by the number of teeth. In general, as the uncut chip thickness increases, the rake face friction decreases and the shear angle increases reducing the cutting forces [42]. Another reason for the reduction of the cutting force coefficients is the increase of the local rake angles in some portions of the serrated cutting edges. This situation was explained in 3.3 in detail. The reduction in cutting force coefficients due to this effect is much less compared to the reduction due to the edge forces.

The milling scenario given in table 3.2 is revisited in order to show these effects. All parameters except axial depth of cut, which is now taken as 8 mm, and radial depth of cut, which is now taken as 3mm, are the same.
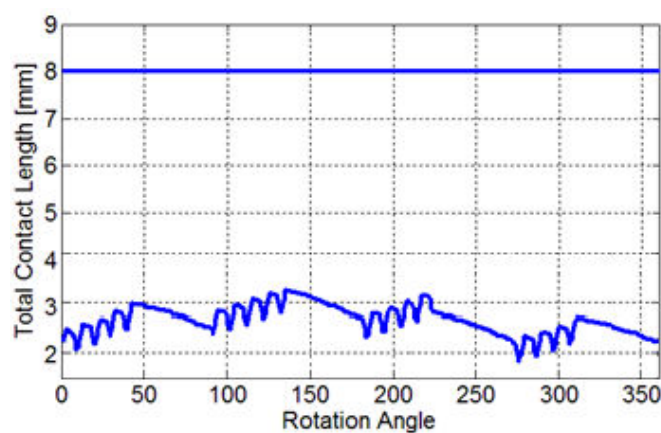
Figure 3.32. Contact length for regular end mill (8mm), contact length for serrated end mill (the curve at the bottom)

In figure 3.32, a comparison of regular and serrated end mills is given considering the cutter-workpiece contact length. As can be seen serrated end mills show a drastic decrease in cutter-workpiece contact length, resulting in a significant amount of decrease in edge forces.
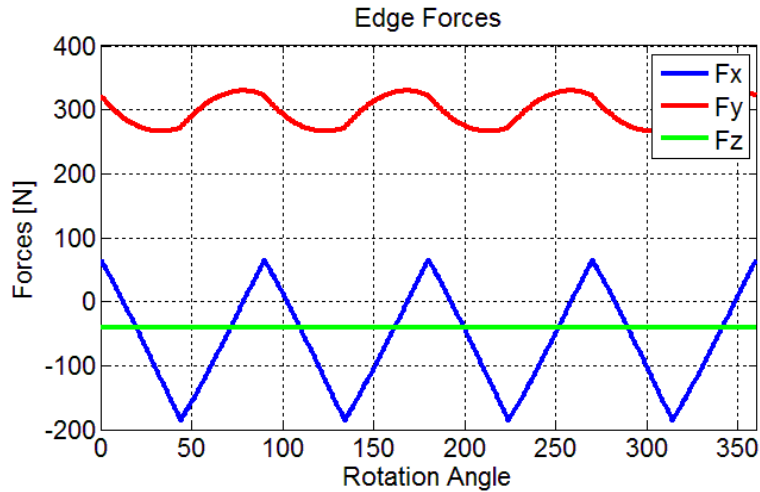
a)
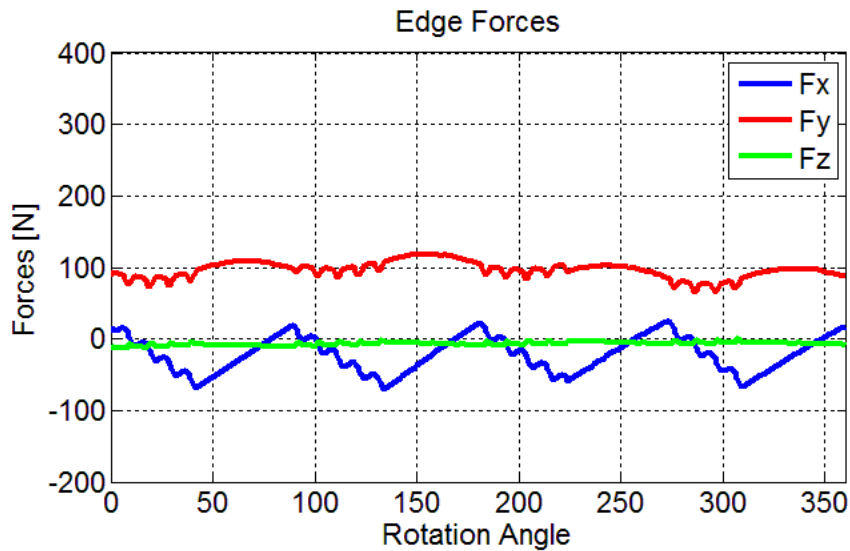
b)

Figure 3.33. Edge force components for the a) regular end mill b) serrated end mill.

In figure 3.33 a comparison of regular and serrated end mills is given considering the edge forces. As can be seen, the decrease in the cutter-workpiece contact length directly affects the edge force contributions of the milling system.

3.6. Experimental Verification

In this section numerous milling tests are done with serrated end mills. Resulting forces in X, Y and Z directions are measured with Kistler table type dynamometer. Force data is collected with using LabVIEW software. Milling experiments are done on a DMG 5 axis machining center.

Figure 3.34. Test set-up: dynamometer mounted on machine tool table, workpiece mounted on dynanometer

Workpiece material is chosen as Al7075-T6 alloy. End mills used in the tests are all uncoated carbide tools which were applied in down milling mode. Material database for Al7075-T6 alloy is as follows:

Table 3.3. Material data base for Al7075-T6 alloy [42]

$$\tau_s = 297.1 + 1.1\alpha_r \ \text{[MPa]}$$
$$\beta_f = 18.8 + 6.7h + 0.0076V_c + 0.26\alpha_r$$
$$\emptyset_c = 24.2 + 36.7h + 0.005V_c + 0.3\alpha_r$$
$$K_{te} = 23.4N/mm$$
$$K_{re} = 35.2N/mm$$
$$K_{ae} = 5 \ N/mm$$

The workpiece is mounted on the table dynamometer on the machine tool's table rigidly in order to ensure a stable milling operation. Also milling cutter is mounted in the tool holder with a small overhang as possible in order to increase its rigidity.

Table 3.4. Parameters of the serrated end mill used in cutting tests

Tool No	R_t	N_t	β	Serration Type	$r_1=r_2$	W_1	W_2	$t_1=t_2$	A
1	6 mm	4	30°	Trapezoidal	0.2 mm	0.3 mm	0.2 mm	45°	0.5 mm
2	6 mm	4	30°	Circular	r_1	r_2		A	
					0.5 mm	0.5 mm		0.6 mm	

Table 3.5. Process parameters of the cutting tests

Test No	Axial DOC	Tool No	Radial DOC (b)	f_t	Ω (RPM)
1	8mm	1	3mm	0.05mm/tooth	1500
2	8mm	1	6mm	0.05mm/tooth	1500
3	8mm	1	3mm	0.1mm/tooth	1500
4	8mm	2	3mm	0.05mm/tooth	1500
5	8mm	2	3mm	0.1mm/tooth	1500

The comparisons of experimental data and force model results are given in the following figures. Also following the experimental verification, the same milling cases are simulated with regular end mills, and the results are given for comparison.

3.6.1. Test1
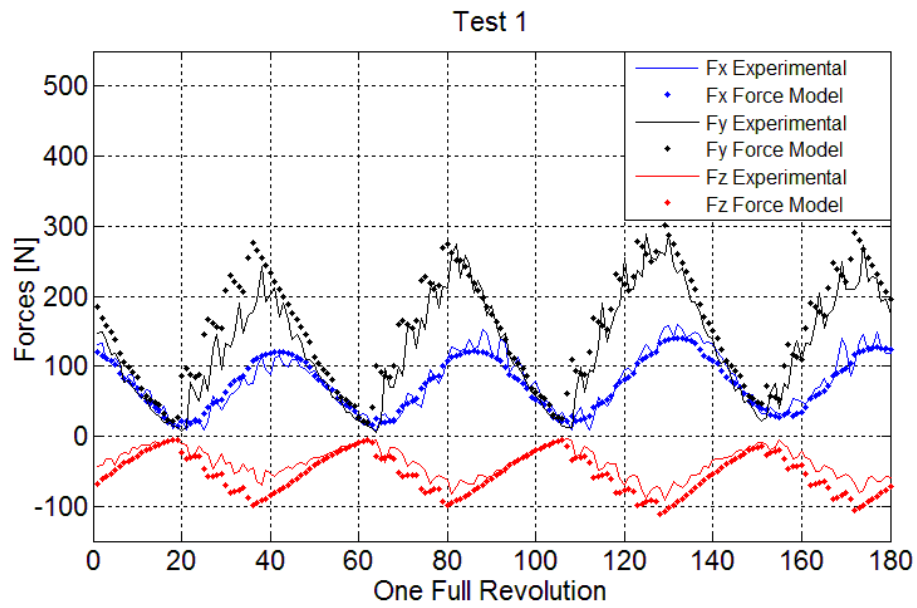
Figure 3.35. Comparison of experimental and predicted results for Test1

It should be noted that one full revolution of the tool is represented with 180 data points in order to prevent the data overflow with the data acquisition system. Thus in every 2° force data point is collected.
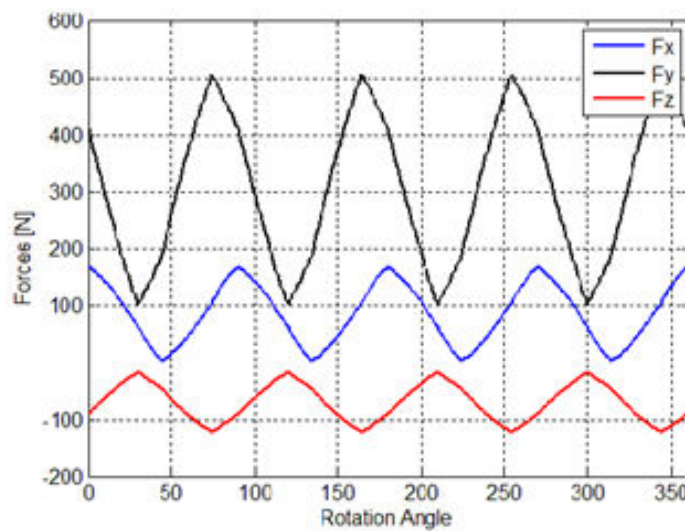
Figure 3.36. Test 1: Force model simulation for the milling parameters for test 1 with regular end mill

In figure 3.35, the same milling case is simulated for the force model with a regular end mill. As can be seen from figure 3.34 and figure 3.35 serrated tools lower milling forces drastically. Both simulations and test data represent one tool revolution.

3.6.2. Test 2
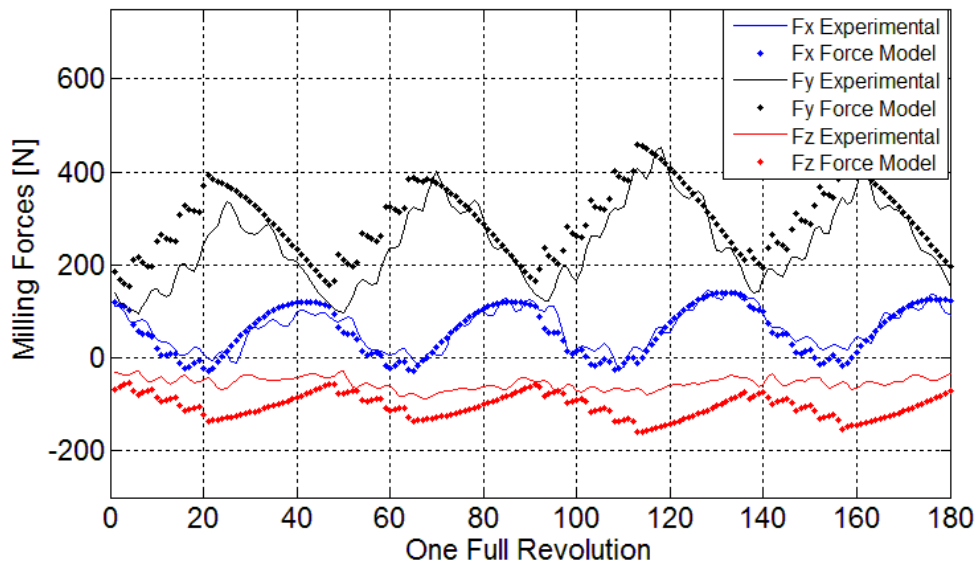
Figure 3.37. Comparison of experimental and predicted results for Test 2
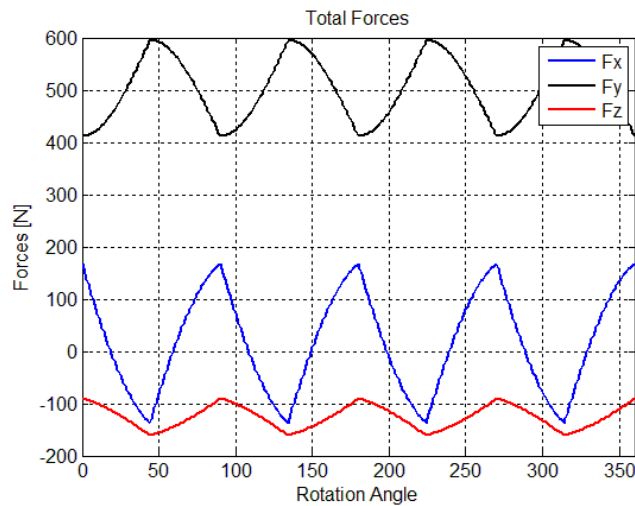
Figure 3.38. Test 2: Force model simulation for the milling parameters for test 2 with regular end mill

3.6.3. Test 3
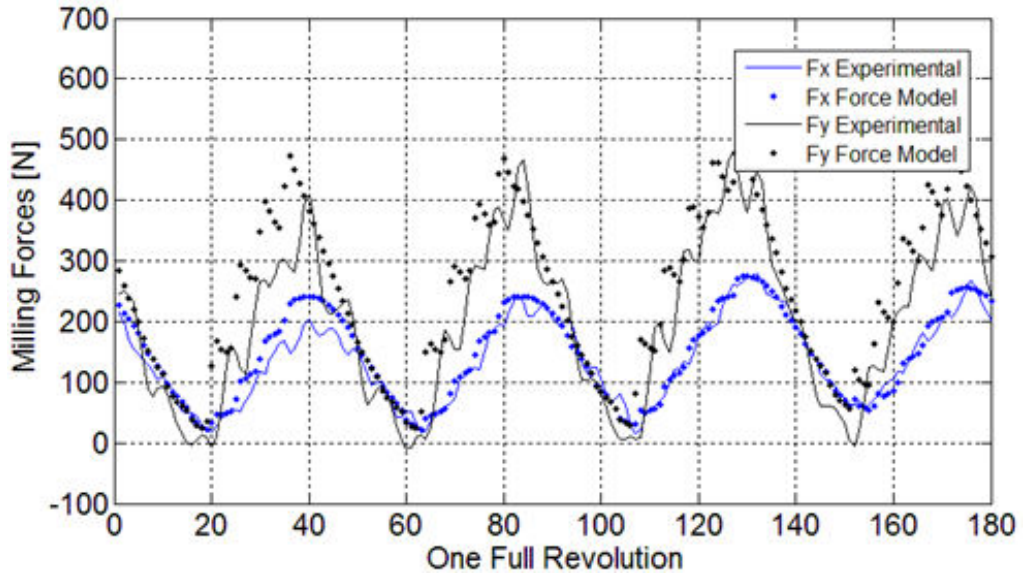
Figure 3.39. Comparison of experimental and predicted results for Test 3
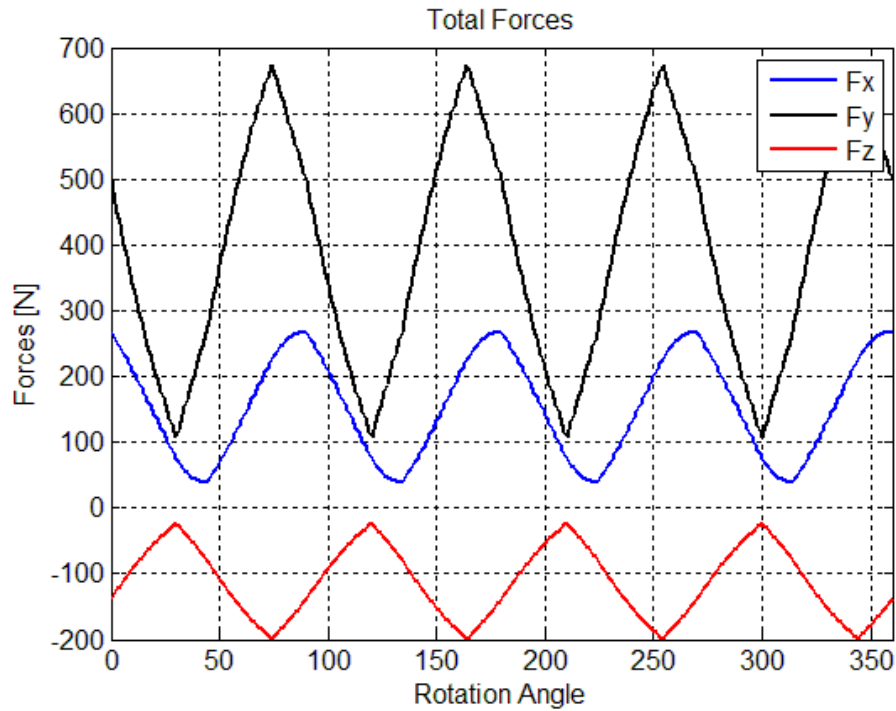
Figure 3.40. Test 3: Force model simulation for the milling parameters for test 3 with regular end mill

In the following tests, a circular serrated end mill is used whose parameters are given in table 3.4.

3.6.4. Test 4
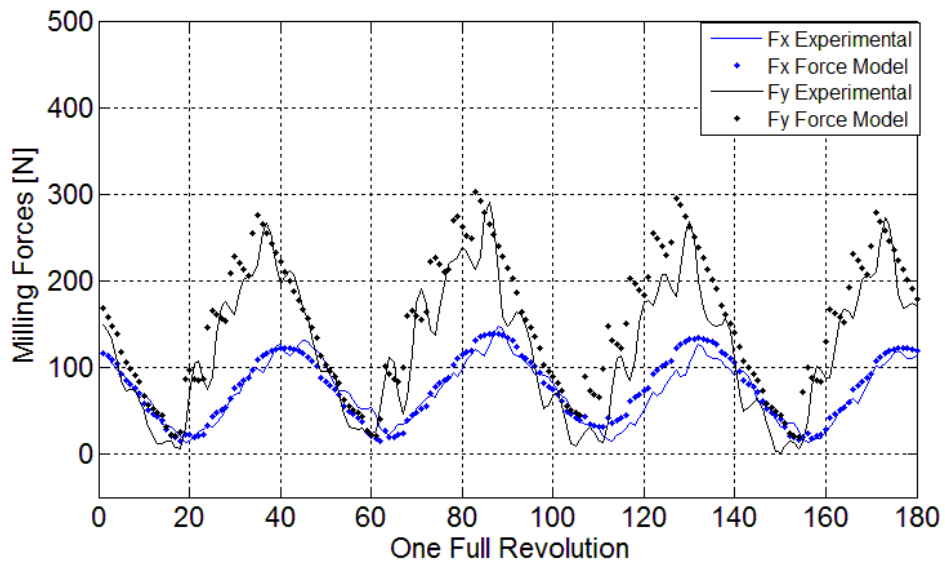
Figure 3.41. Comparison of experimental and predicted results for Test 4
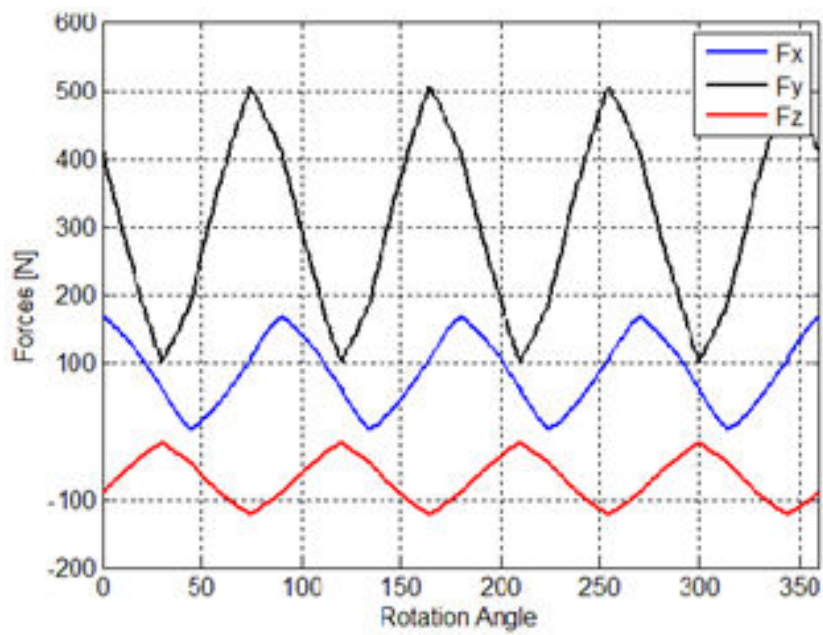
Figure 3.42. Test 4: Force model simulation for the milling parameters for test 4 with regular end mill

3.6.5. Test 5
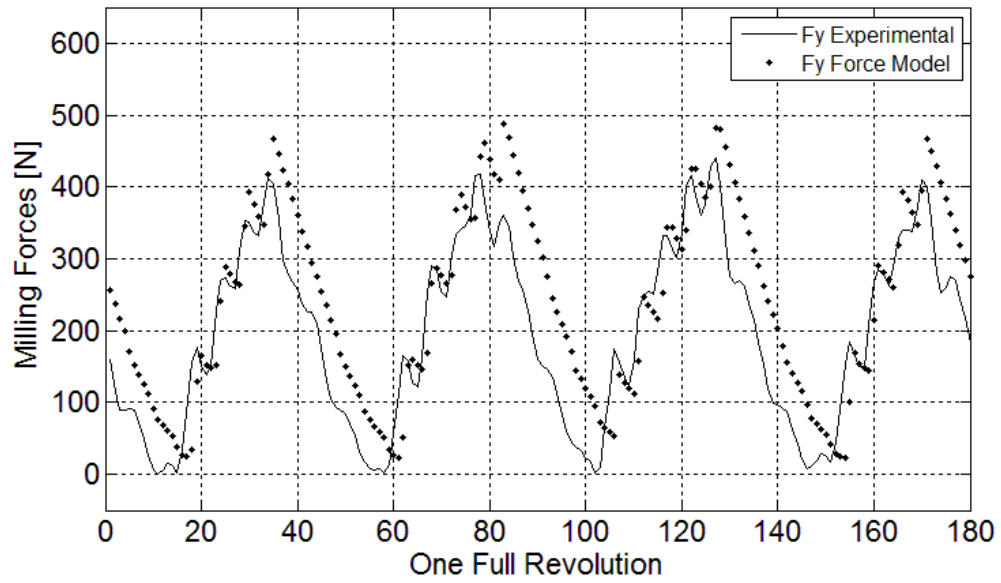
a)
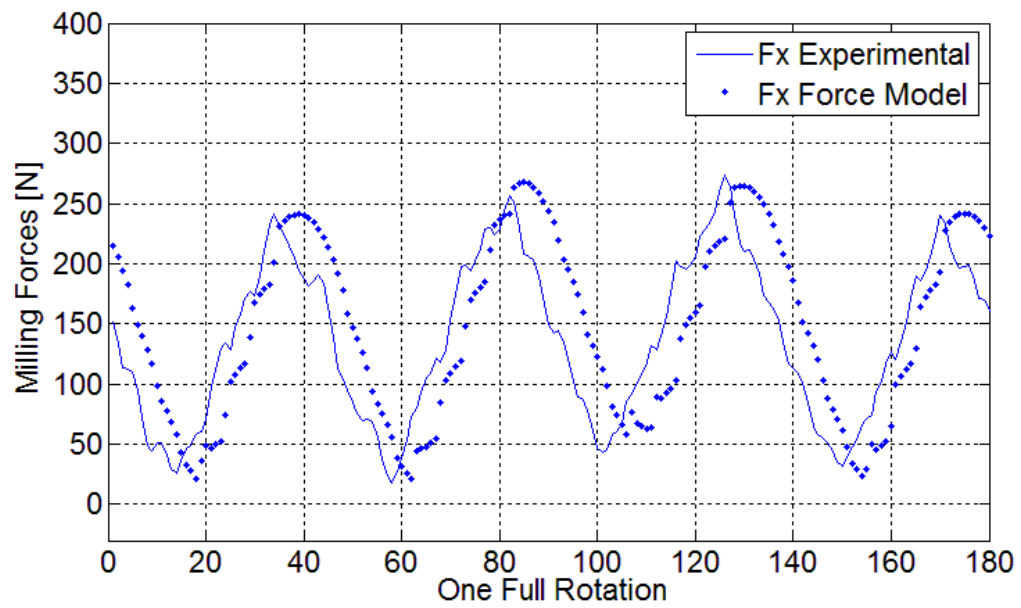
b)

Figure 3.43. Comparison of experimental and predicted results for Test 5
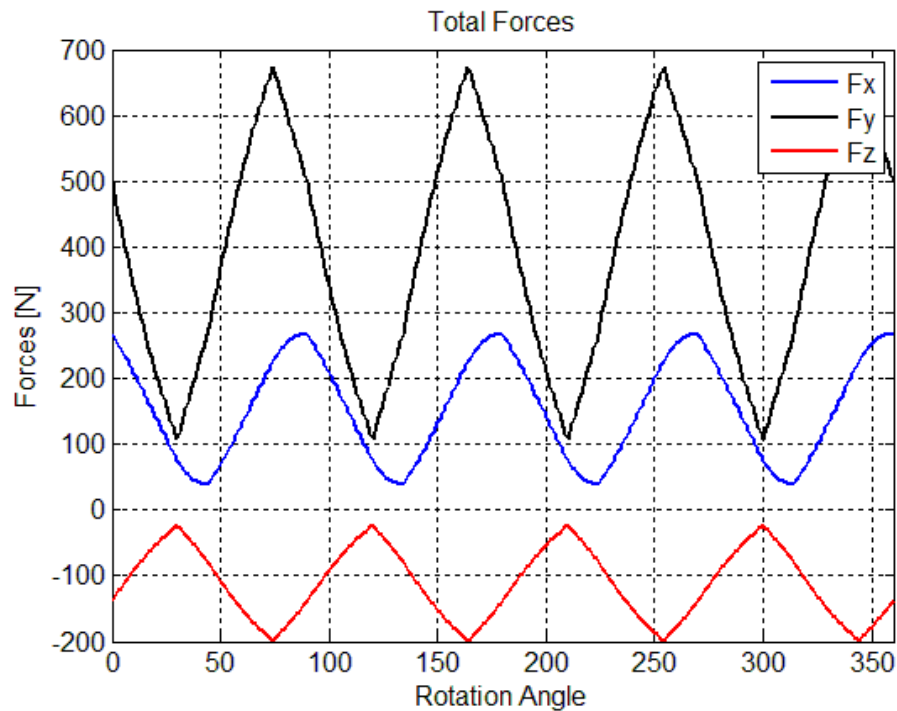
Figure 3.44. Test 5: Force model simulation for the milling parameters for test 5 with regular end mill

Experimental data and results generated with the force model are in a good agreement. However for Fz forces, the force model results do not agree well with the measured ones. This can be attributed to a few reasons. First of all, the maginitude of forces in the z direction are very small compared to the ones in x and y directions. Thus, S/N ration and thus the measurement accuracy are low for Fz. On the modeling side, tool bottom contact is not taken into account in the force model. Similarly, small chamfers on tool tip are not included in the force model, either. Another reason might be some flaws regarding to the cutting force coefficient in the axial direction, K_{ac}. The maximum difference between measured and predicted Fxmax, Fymax values are around %6.6 while it is smaller for mean forces. Predicted forces are slightly higher than the measured ones.

In this chapter of the thesis, mechanics of milling with serrated end mills is investigated in detail. The geometrical differences between regular end mills and serrated end mills are stated. Required geometrical formulations are given in order to represent the serrated cutting edges. Chip thickness formulation is presented, the effects of forward and reverse phase shift are discussed. Milling forces are modeled, and the effects of serrated cutting edges on milling forces are shown both with the presented force model

and cutting tests. Force model predictions and experimental data showed good agreement.

The effects of phase shift of waveforms on cutting teeth for serrated tool design and milling mechanics is investigated in detail. Resulting variable rake and helix angles on cutting teeth because of the serrations, which hasn't been studied before in the literature, are stated and explained. It's found out that by simply reversing the phase shift between cutting teeth an amount of performance increase can be achieved. This is very practical since reversing the phase shift does not introduce any complication into end mill manufacturing. Also it doesn't complicate the local chip loads. Because of these reasons it should be used in tool design however the available serrated end mills in the market lack this design quality.

CHAPTER 4

OPTIMIZATION OF SERRATION WAVE PARAMETERS FOR LOWER MILLING FORCES

Serrated end mills have been used in milling operations for decades. There are several different serration geometries available in the market from different cutting tool manufacturers. Most commonly used serration waveforms are sinusoidal, circular and trapezoidal waves. However the defining parameters of these wave forms vary considerably. The selection or design of these tools is usually done by experience based or try-error methods. The literature about these tools especially on their cutting force and chatter stability characteristics is limited. There is no published work on design, optimization or selection of these waveforms for higher performance.

In this chapter of the thesis, selection, design and optimization of serrated end mills will be studied. For the first time in the literature, the geometrical parameters of serrated end mills are optimized for higher performance by minimizing milling forces generated by them. Wave forms defined parametrically in the previous chapter will be used in the analysis. In order to simplify the optimization process, the least possible number of parameters is used in constructing the wave geometries.

The optimization process will be handled by using two methods, namely Brute Force Search, and a population based optimization algorithm, Differential Evolution. The idea behind the Brute Force Search is that each and every possible parameter combinations in the defined search space are tested for a given objective function. The advantage of the method is that one can understand the behavior of the objective function by interpreting the trend of the results since every possibility is searched one by one. However, if the number of parameters to be optimized is high, the search space (upper and lower bounds of the values of the parameters) becomes wide, and the Brute Force Search can be very time consuming. If the evaluation of the function also takes a long

time, the computational time for the determination of optimal set of parameters becomes even longer. Evolutionary algorithms such as Differential Evolution [36, 41], on the other hand, do not search all the parameter possibilities in order to find the optimal set. Thus, this method is more favorable since it is much faster than the Brute Force Search. For this reason, the main optimization algorithm is selected as the Differential Evolution because of its speed. However, the Brute Force Search method will still be employed for benchmarking. The results of Brute Force Search will be analyzed for interpreting the effects of the wave form geometrical parameters on milling forces.

Using these methods, geometrical parameters of sinusoidal, circular and trapezoidal serration wave forms will be optimized for given milling conditions. Objective function is selected to be the maximum value of the resulting force in the X-Y process plane occurring in one tool revolution. Found optimal sets will to be compared with the parameters of some of the commercially available serrated end mills on the market.

In this thesis, Differential Evolution source code by Markus Buehren was adopted. This code is based on the Differential Evolution algorithm of Price et al. [41]

4.1. Differential Evolution

Differential Evolution is a population based algorithm used for finding the global optimum of a given function. The algorithm has 4 main steps namely, initialization, mutation, crossover and selection [41]. . Before going into the steps of the algorithm, some preliminary explanations need to be given. Required inputs for the algorithm can be summarized as follows. Objective function needs to be linked to the main optimization algorithm. In our case the force model presented for serrated end mills in the previous chapter is linked to the algorithm. Parameters to be optimized also need to be defined. For instance, they are wavelength and amplitude in the case of sinusoidal serration wave. In addition, upper and lower bounds for every parameter need to be defined for the construction of the search space. As stated before, Differential Evolution is a population based algorithm. The number of population members needs to be stated since the algorithm samples the search space at multiple, randomly chosen initial parameters, thus the number of sample points which cover the entire search space needs to be known.

83

4.1.1. Initialization

First step of the algorithm is initialization. In this step a vector population, whose elements are the parameters to be optimized, is generated. The number of population members is represented with N_p which is a user defined parameter and needs to be bigger than three. N_p is recommended to be 10*D, where D represents the number of parameters to be optimized. Search space which is restricted with the upper and lower bounds is covered randomly with the generated parameter vectors according to the following equation.

$$x_{j,i,0} = rand_j(0,1)(b_{j,U} - b_{j,L}) + b_{j,L} \tag{4.1}$$

where $b_{j,U}$ and $b_{j,L}$ represents the upper and lower bounds for j^{th} parameter respectively. $rand_j(0,1)$ generates a uniformly distributed random number between 0-1. $x_{j,i,0}$ represents the jth parameter in i^{th} member of the vector population in initialization step which is stated by 0 where

$$j = 1,2, \dots D$$

$$i = 0,1, \dots, N_p\text{-}1$$

In the following figure a two parameter search space is shown with their upper and lower bounds. The points on the figure numbered from 0 to 8 represent the members of the initial population.
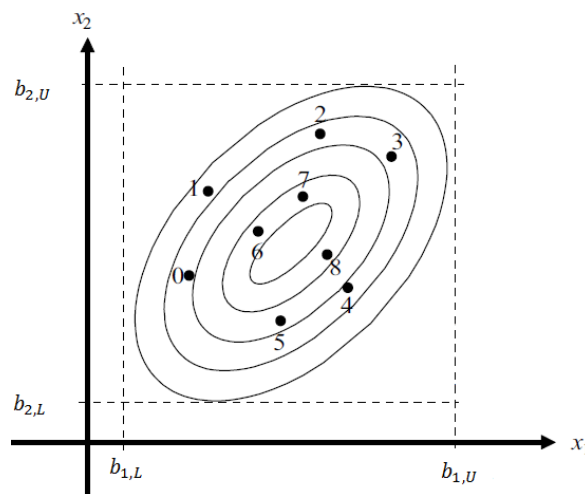
Figure 4.1. Differential evolution initialization step [41]

4.1.2. Mutation

After initialization Differential Evolution produces a trial vector population consisting of N_p trial vectors [41]. Trial vectors are generated with the following procedure:

Two different vectors are selected randomly from the current population. Their scaled difference is added to a third randomly selected vector. Scaling Factor, F which is a positive real number is introduced here. It's suggested to keep this value between 0-1 although there's no upper bound [41].

$$\mathbf{v}_{i,g} = \mathbf{x}_{r0,g} + F(\mathbf{x}_{r1,g} - \mathbf{x}_{r2,g}) \qquad (4.2)$$

The resulting mutant vector is represented with $\mathbf{v}_{i,g}$ where g indicates the generation number.
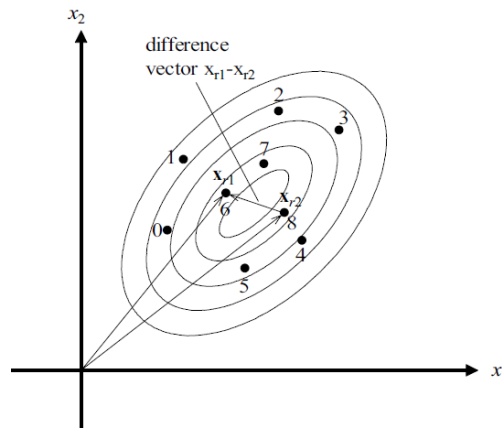
Figure 4.2. Difference vector [41]
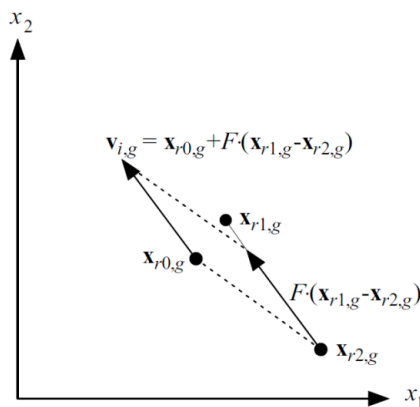
Figure 4.3. Mutant vector [41]

This procedure is done until N_p mutant vectors are created.

4.1.3. Crossover

Differential evolution employs uniform crossover in addition to the mutation process. Each vector $x_{j,i,g}$ at the current population is crossed over with a mutant vector generated in the previous step.

$$\mathbf{u}_{i,g} = u_{j,i,g} = \begin{cases} v_{j,i,g} & if \ (rand_j(0,1) \leq Cr \ or \ j = j_{rand}) \\ x_{j,i,g} & otherwise \end{cases} \qquad (4.3)$$

The crossover probability $Cr \in [0,1]$ is defined by the user. This controls the fraction of parameter values that are copied from the mutant vector. If the number generated by $rand_j(0,1)$ is less than or equal to Cr, the trial parameter is inherited from the mutant $v_{i,g}$, otherwise it's taken from the vector $\mathbf{x}_{i,g}$. Also the trial parameter with randomly chosen index j_{rand}, is taken from the mutant in order not to duplicate $\mathbf{x}_{i,g}$.

4.1.4. Selection

In the selection process, generated trial vector $\mathbf{u}_{i,g}$ is compared to the target vector $\mathbf{x}_{i,g}$. The trial vector inherits some parameters from its target vector in crossover process. If the trial vector has an equal or lower objective function value than its target vector, the trial vector takes the place of its target vector in the next generation. Otherwise, the target stays in the population for at least one more generation.

$$\mathbf{x}_{i,g+1} = \begin{cases} \mathbf{u}_{i,g} & if \ f(\mathbf{u}_{i,g}) \leq f(\mathbf{x}_{i,g}) \\ \mathbf{x}_{i,g} & otherwise \end{cases} \qquad (4.4)$$

The procedure summarized above is repeated until a given termination criteria is met. This termination criteria can be number of generations or a given objective function value.

In the following section, optimization of the serration wave form parameters will be realized.

4.2. Optimization of Serration Parameters

In order to find the optimal serration wave form parameters, some milling cases are considered. Parameters of the cutting tool except serration wave parameters are fixed. The tools have the following fixed parameters.

Table 4.1. Fixed parameters for the cutting tool

R_t	N_t	β
6 mm	4	30°

The optimal serration wave form parameters are sought for various radial immersions and feed per tooth values. Axial depth of cut of the milling operations is fixed as 16mm.

4.2.1. Optimization of Sinusoidal Serration Parameters

In this section, for the given milling scenarios, wave form parameters of a sinusoidal end mill will be optimized with both Brute Force Search and Differential Evolution. The parameters for the Differential Evolution are taken as follows:

Number of parameters to be optimized, D=2 (Wavelength λ, Amplitude A)

Population size, Np=10D=20

Number of generations=250

F,Cr=0.9

Parameters for Differential Evolution are adopted from the literature [35]. Although number of generations is kept higher, the optimization converged at about 100 generations almost always. Search space is restricted for geometrical parameters of the sinusoidal serration form as:

Amplitude, A = [0-2] (mm)

Wavelength, λ = [0-10] (mm)

Force brute force search, parameter search space is kept wider but with higher increments. This way objective function surface is constructed and interpreted. The

parameter ranges where the possible global optimal value can be determined from this result.

Table 4.2. Different milling cases and found optimal serration form parameters

b = 3mm (Quarter Immersion)			b = 12mm (Full Immersion)		
ft = 0.05mm/tooth			ft = 0.05mm/tooth		
A [mm]	λ [mm]	FxyMax [N]	A [mm]	λ [mm]	FxyMax [N]
Regular End Mill		647	Regular End Mill		1493
0.2	2.8	382	0.2	2.8	964
ft = 0.2mm/tooth			ft = 0.2mm/tooth		
A	λ	FxyMax	A	λ	FxyMax
Regular End Mill		1274	Regular End Mill		3446
0.2	2.8	1147	0.3	5.8	3193

In table 4.2., optimal serration form parameters found by Differential Evolution are given for different milling cases. It should be noted that Brute Force search algorithm also found the same optimal values for minimum FxyMax values. In the next figure result of the Brute Force Search can be seen. It's observed that the wavelength has a bigger influence on the maximum force values than the amplitude does. It can also be said that even though there is an optimal vector of parameters, some regions in the search space has close performance to the optimal value.
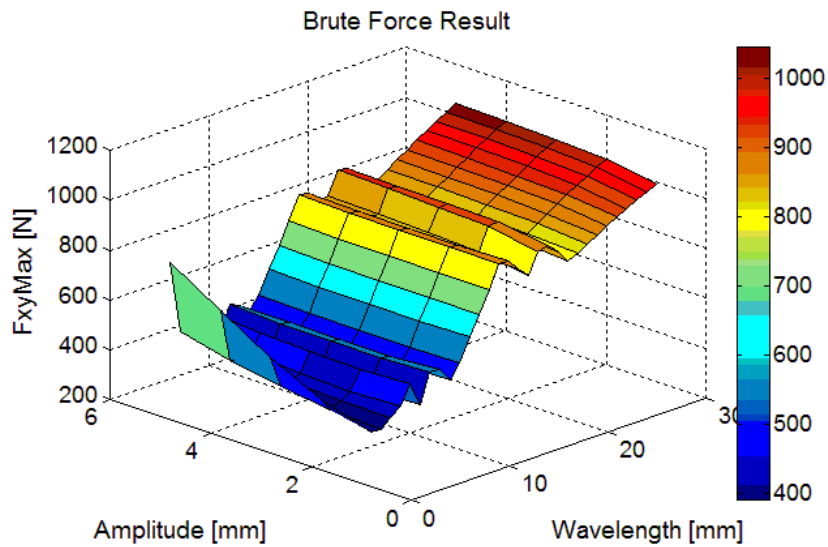
Figure 4.4. Brute force result for **b**=3mm, **ft**=0.05mm/tooth
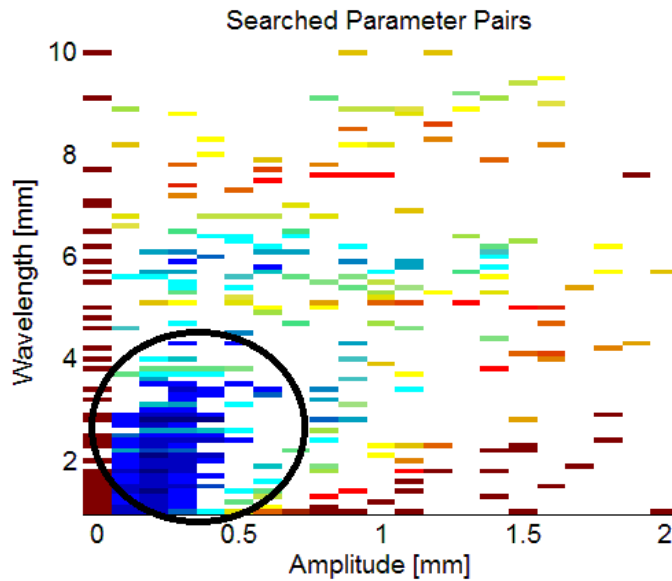
Figure 4.5. Searched parameter pairs with Differential Evolution for case b=3mm, ft=0.05mm/tooth

In figure 4.5, wavelength and amplitude pairs which the Differential Evolution evaluated are illustrated. The Differential Evolution procedure successfully found the global optimum without searching each parameter pair. Because of this reason, global optimum is found much faster than the Brute Force search. This figure also justifies the effectiveness of the Differential Evolution parameters adopted from the literature. As can be seen from both figures 4.4 and 4.5, the Differential Evolution concentrated on the search space where the parameters have lower resultant maximum forces.

The results given in table 4.2 need further discussion. It's seen that for higher feed per tooth values, the reduction in forces is not as drastic as it is for lower feed per tooth values. This originates from the fact that as feed per tooth increases, a bigger portion of the serrated edge immerse in the material. Consequently the total contact length increases, or in another saying total contact length does not decrease as much as it does with lower feed rates. This explains the difference between 0.05 mm/tooth and 0.2 mm/tooth cases.

Another explanation is needed for the cases which have the same feed per tooth value but different radial immersions. Radial immersion affects the maximum uncut chip thickness for a given process. For half immersion or higher radial immersions maximum uncut chip thickness becomes equal to the feed per tooth for regular end mills. However, for serrated end mills maximum uncut chip thickness can increase up to feed

per tooth times N_t. Thus, as the radial immersion increases up to at least half immersion, maximum uncut chip thickness is obtained. As the maximum uncut chip thickness increases the same phenomena occurs, i.e. a bigger portion of the serrated edge immerses into the material which increases the total contact length, and thus the edge force contributions. This is valid for all types of serration wave types. Therefore, the same behavior is observed in optimization of other serration wave types as will be illustrated in the following parts of this chapter.

An interesting result is seen table 4.2 for the milling case with ft=0.2 mm/tooth and full radial immersion. The optimal wavelength is much higher than the ones found for smaller feed rates and smaller radial immersions. Brute Force Search results can be seen in the following figure for this milling case.
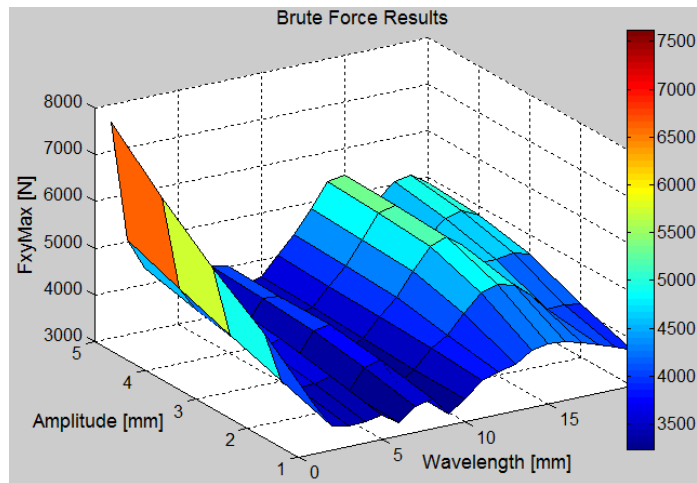
Figure 4.6. Brute Force Search results for **b**=12mm, **ft**=0.2mm/tooth
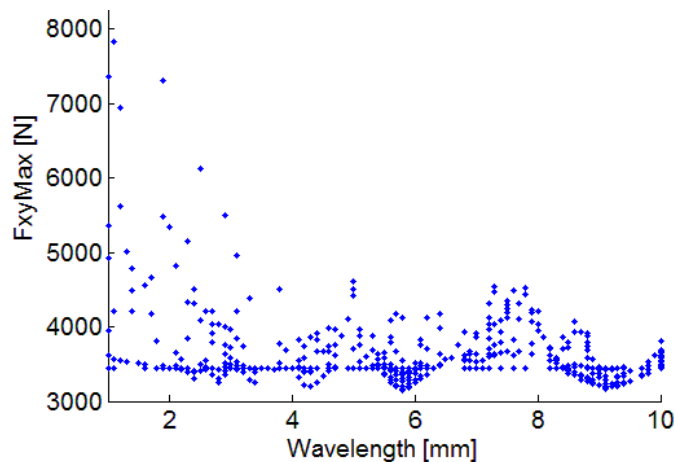
Figure 4.7. Differential Evolution wavelength and FxyMax values for searched pairs
b=12mm, **ft**=0.2mm/tooth

The reason behind the optimal wavelength for the high feed rates being higher than the optimal wavelengths determined for the lower feed rates is the fact that the serrated cutting edge indents less in order to compensate the effect of higher feed rates. This means that if the wavelength is increased the curvature of the serrated edge becomes lower. In order to illustrate this, a very small wavelength of 1mm and a much higher wavelength of 6mm are compared in the next figure. The serration amplitudes and the feed rates are the same for the two cases.
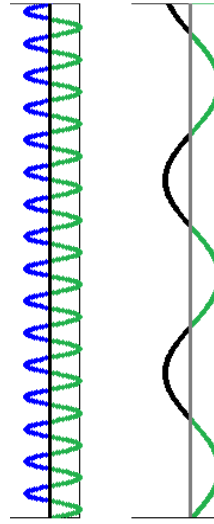
Figure 4.8. Effect of wavelength on contact length for high and low feed rates

In figure 4.8, the green portions of the serrated edges are the immersed parts of the cutting edge into the workpiece. It's obvious that for higher feed rates, higher wavelengths are more effective in reducing the total contact. It should be noted that sinusoidal wave is defined with only two parameters and the wavelength has a direct effect on the curvature of the edge. For example, this kind of effect can be obtained with higher radii on outer arc for circular serration wave easier and with more control. If a circular serration wave is designed for high feed rates, one can increase the radius of the outer arc while keeping amplitude or the radius of the inner arc small. This way it's easier to control the curvature of the edge and wavelength separately. This will be revisited in the following sections.

4.2.2. Optimization of Circular Serration Parameters

Circular serration parameters are optimized for the same milling scenarios with the same scaling factor F, crossover rate C_r and number of generations. Circular serration wave is defined with three parameters, namely, r_1 radius of the outer arc, r_2 radius of the inner arc and A, the amplitude of the wave. Since there are three different parameters, number of population members is chosen as 10*D=30. Circular serration wave consists of two arcs which are tangent to each other. A geometrical constraint needs to be introduced in order to ensure the arcs remain tangent to each other. This constraint is given in (4.5). Also, the amplitude of the serration wave cannot exceed the sum of radius of the outer arc and radius of the inner arcs:

$$A \leq r_1 + r_2 \qquad\qquad (4.5)$$

The Differential Evolution algorithm needs the upper and the lower bounds for every parameter to be optimized. These upper and lower bounds define a continuous parameter space, however with the introduction of the constraint (4.5) this continuity of the parameter space is interrupted.

Upper and lower bounds for r_1, r_2 and A are given as the same fashion as it was done for the sinusoidal serration form. The constraint is included into the optimization problem with an approach called "Brick Wall Penalty". This situation is handled inside the objective function, which is the force code for serrated end mills modeled in the previous chapter. If a member of the current generation is violating the constraint (4.5) its objective function value is not calculated, instead a very big number (i.e. 1e6) is assigned to it. This way it is made sure that the violating member does not survive to the next generation. Upper and lower bounds for the parameters are as follows:

$$r_1 \ [0.1\text{- }3] \ (\text{mm})$$
$$r_2 \ [0.1\text{- }3] \ (\text{mm})$$
$$A \ [0.1\text{-}3] \ (\text{mm})$$

Circular serration waveform parameters are optimized for the same milling cases and the results are presented in the following table.

Table 4.3. Different milling cases and found optimal serration form parameters for the circular serration waveform

b = 3mm (Radial Depth of Cut)				b = 12mm (Radial Depth of Cut)			
ft = 0.05mm/tooth				ft = 0.05mm/tooth			
r_1 [mm]	r_2 [mm]	A [mm]	FxyMax [N]	r_1 [mm]	r_2 [mm]	A [mm]	FxyMax [N]
Regular End Mill			647	Regular End Mill			1493
0.5	0.5	0.6	376	1.8	2.1	1.3	915
ft = 0.2mm/tooth				ft = 0.2mm/tooth			
r_1 [mm]	r_2 [mm]	A [mm]	FxyMax [N]	r_1 [mm]	r_2 [mm]	A [mm]	FxyMax [N]
Regular End Mill			1274	Regular End Mill			3446
1.8	0.1	0.6	1146	2.8	0.8	0.7	3165

The results from table 4.3 show the same trend as the optimal sinusoidal serration wave form. Also, the effects of feed per tooth values and radial immersion on the optimal circular serration wave parameters are the same.
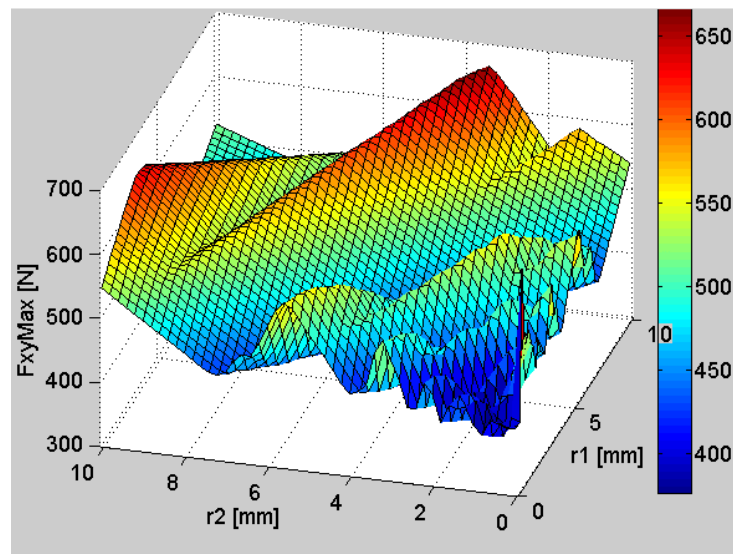
Figure 4.9. Brute force results for b=3mm, ft=0.05mm/tooth, where amplitude is 0.6mm

In figure 4.9 Brute Force Search results can be seen. Since we have three parameters to optimize, the results are kept in a three-dimensional matrix. In order to represent the results, amplitude value is kept constant as the optimal one 0.6mm. The effect of r_1 and r_2 on maximum resultant forces in X-Y plane is illustrated.
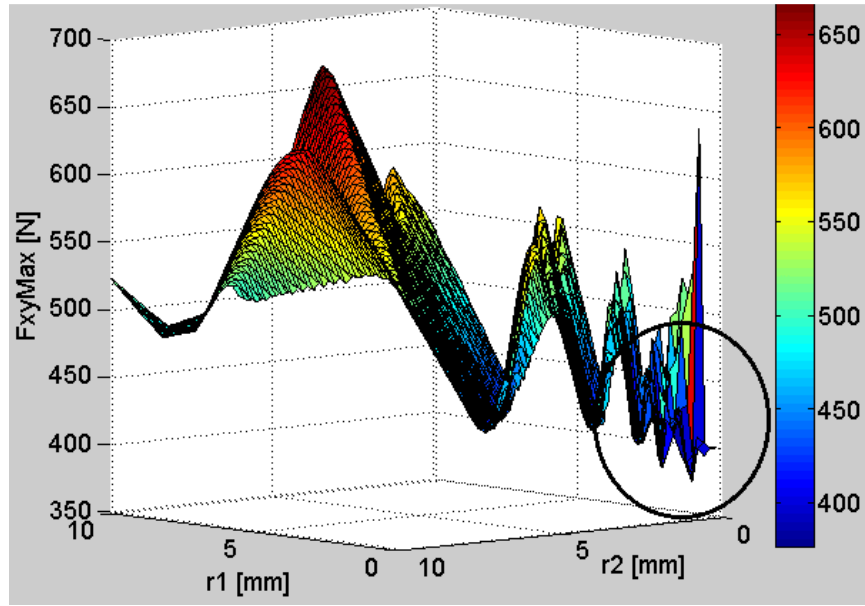
Figure 4.10. Alternative view for figure 4.9

In figure 4.10 the parameters which have the smaller FxyMax values can be seen inside the circle.

4.2.3. Optimization of Trapezoidal Serration Parameters

In this part, optimization of trapezoidal serration wave form parameters will be presented. Optimization of trapezoidal serration wave form needs extra attention since the parameter number is increased to seven. The defining parameters of this wave form are; $r_1, r_2, w_1, w_2, t_1, t_2, A$.

Instead of running the optimization algorithm for seven of these parameters some of them will be kept constant in order to understand the effects of these parameters on milling forces individually.

4.2.3.1. Optimization Attempt 1

In this part, t_1, t_2, $w_1=w_2$, A_1 parameters are optimized while keeping $r1 = r2$=0.2mm. Upper and lower bounds are given in the following:

$$t_1 \ [15°-85°], \ t_2 \ [15°-85°], \ w_1=w_2 \ [0-6] \ (mm) \ , \ A \ [0-3] \ (mm)$$

In table 4.4 results obtained by Differential Evolution can be seen. From the results it can be interpreted that t_1 and t_2 angles do not have a direct effect on optimal geometry. However they affect the overall geometry by changing the wavelength. Because of this

94

reason, these angles will be kept equal to each other and constant, while optimizing other important parameters affecting the wavelength and amplitude.

The parameters to be optimized in the next attempt are w_1, w_2 and A.

Table 4.4. Optimal parameters found by Differential Evolution

b=3mm (Radial Depth of Cut)					**b=12mm (Radial Depth of Cut)**				
ft = 0.05 mm/tooth					**ft = 0.05 mm/tooth**				
t_1 (°)	t_2 (°)	w_1 w_2 [mm]	A [mm]	Fxy Max [N]	t_1 (°)	t_2 (°)	w_1 w_2 [mm]	A [mm]	Fxy Max [N]
Regular End Mill				647	Regular End Mill				1493
52.5	85	0.2	0.6	373	60	50	2.2	3	900
b=3mm (Radial Depth of Cut)					**b=12mm (Radial Depth of Cut)**				
ft = 0.2 mm/tooth					**ft = 0.2 mm/tooth**				
t_1 (°)	t_2 (°)	w_1 w_2 [mm]	A [mm]	Fxy Max [N]	t_1 (°)	t_2 (°)	w_1 w_2 [mm]	A [mm]	Fxy Max [N]
Regular End Mill				1274	Regular End Mill				3446
22.5	40	0.6	0.2	1144	15	42	1.4	0.4	3128

4.2.3.2. Optimization Attempt 2

In this part, r_1 and r_2 values are kept constant at 0.2mm. t_1 and t_2 values kept constant and equal to each other at 15°,30°,45°,60°,75°.

The upper and lower bounds for the parameters to be optimized are as follows:

$$w_1 \ [0\text{-}6] \ (mm)$$

$$w_2 \ [0\text{-}6] \ (mm)$$

$$A \ [0\text{-}3] \ (mm)$$

According to the results, optimal parameters are found and given in the following table:

Table 4.5. Optimal parameters found by Differential Evolution, axial depth of cut 16mm

b = 3mm (Radial Depth of Cut)				b = 12mm (Radial Depth of Cut)			
ft = 0.05mm/tooth				ft = 0.05mm/tooth			
w_1 [mm]	w_2 [mm]	A [mm]	FxyMax [N]	w_1 [mm]	w_2 [mm]	A [mm]	FxyMax [N]
Regular End Mill			647	Regular End Mill			1493
0.2	0.3	0.5	376	2.1	5.5	0.5	900
ft = 0.2mm/tooth				ft = 0.2mm/tooth			
w_1 [mm]	w_2 [mm]	A [mm]	FxyMax [N]	w_1 [mm]	w_2 [mm]	A [mm]	FxyMax [N]
Regular End Mill			1274	Regular End Mill			3446
0.5	0	0.5	1178	4.3	3.5	0.5	3203

where optimal $t_1 = t_2$ are 45°

4.3. Discussions

In this chapter the geometrical parameters of three different serration waveforms, namely, sinusoidal, circular and trapezoidal are optimized in order to lower milling forces. Optimization process is handled with both Brute Force Search and a population based evolutionary algorithm, Differential Evolution. Both methods found the same geometrical parameters for optimal geometries. Although heuristic methods like Genetic Algorithm and Differential Evolution do not guarantee that the global optimal is found, in this case it is verified as Brute Force Search and Differential Evolution gave the same results. However, as expected, the Differential Evolution method took much less time to find the global optimum because it does not search each and every parameter combinations within the given search space.

In order to give an example about the computational times required for both methods, they are compared for a case involving sinusoidal serration waveform. The optimization parameters are the same as given in 4.2.1. Example milling case is a quarter immersion (b=3 for 12mm diameter), 16mm axial depth of cut and ft=0.05mm/tooth operation. Brute Force Search Method takes 266 minutes on a laptop having 2GB RAM and 2.3 GHz Dual-Core CPU while Differential Evolution takes only 26 minutes.

If the results for different serration types are compared, it is seen that every one of the geometries converges to nearly the same objective function value, FxyMax. Thus we can say regardless of the serration type, the same amount of reduction can be obtained if the parameters of the wave types are optimized.

Also another important observation is that optimal circular and trapezoidal serrations have the same exact wavelengths and similar amplitudes, as illustrated in the next figure.
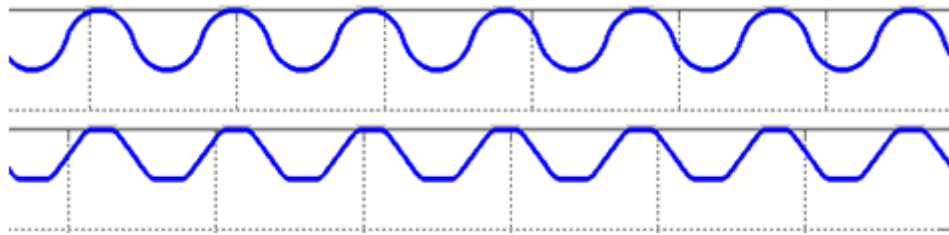
Figure 4.11. Optimal circular and trapezoidal geometries

Obtained optimal serration geometries are compared with some of the available serrated end mills in the market in the following table.

Table 4.6. Comparison of optimized waveforms with standard serrated end mills available in the market.

Standard Serrated Tool 1 r_1=0.78mm r_2=0.58mm A=0.25mm	b = 3mm ft = 0.05mm/tooth down milling	b =12mm ft =0.05mm/tooth, down milling
	FxyMax = 427N Optimal Form = 376N	FxyMax =1098N Optimal Form =900N
Standard Serrated Tool 2 r_1=1.49mm r_2=0.975mm A=0.21mm	b = 3mm ft = 0.05mm/tooth	b =12mm ft =0.05mm/tooth
	FxyMax = 419N Optimal Form = 376N	FxyMax = 1112N Optimal Form = 900N
Standard Serrated Tool 3 r_1=1.44mm r_2=1.035mm A=0.72mm	b = 3mm ft = 0.05mm/tooth	b =12mm, down milling ft =0.05mm/tooth
	FxyMax = 412N Optimal Form = 376N	FxyMax = 972N Optimal Form = 900N

Optimal form parameters are taken from Table 4.5. It can be seen that at least %10 improvement in terms of cutting forces is achieved with optimized end mills comparing to standard serrated end mills available in the market.

In the following, a comparison will be given between optimized serrated end mills for a given milling operation. Also regular end mill performance is going to be included into the comparison. The process parameters for the milling operation are as follows:

Axial depth of cut, a =16mm, Radial depth of cut, b = 3mm, Feed per tooth, ft=0.05mm/tooth.

In the following figures, it's shown that resulting optimized serrated end mills lower milling forces down to half in comparison to their non-serrated regular counterparts.
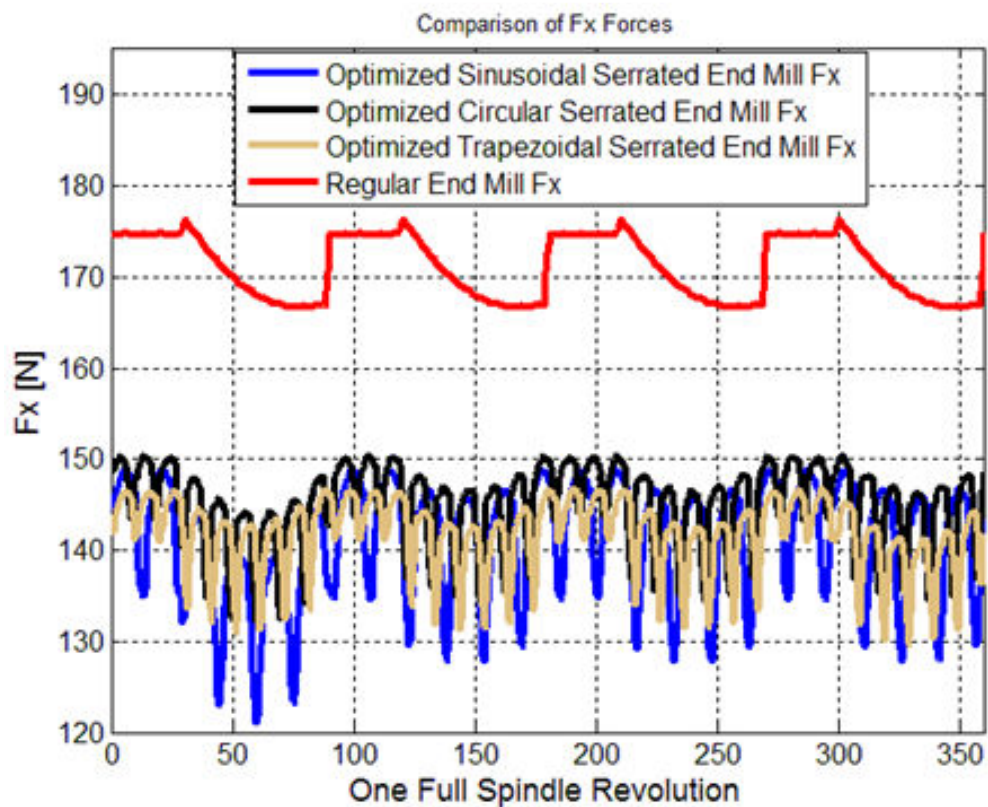
a)
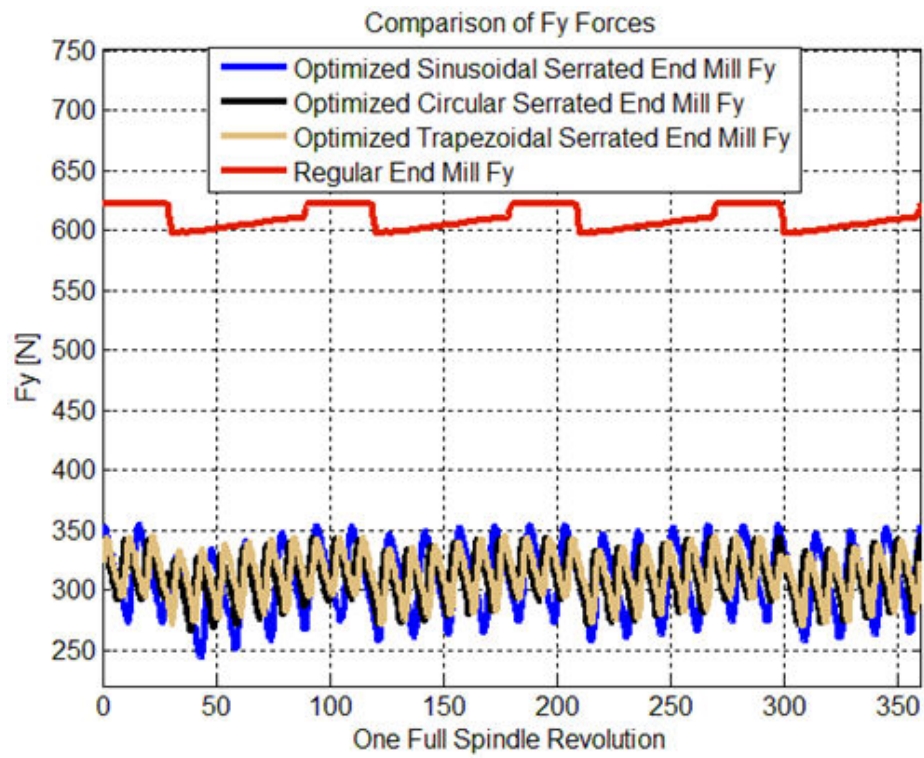
b)
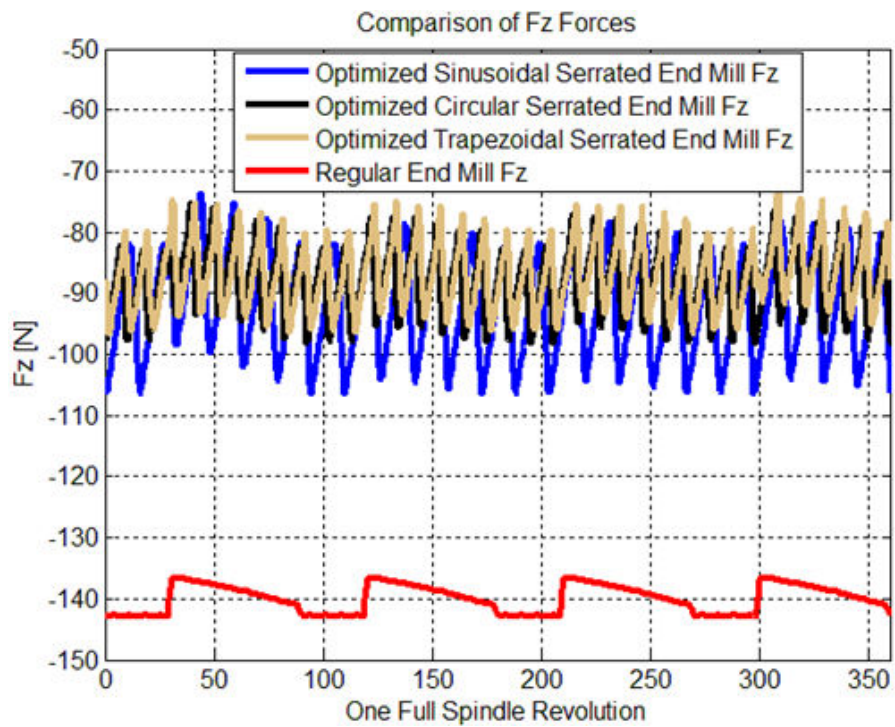
c)

Figure 4.12. Comparison of optimized serrated end mills with each other and with regular end mill

In the following figures, results of both optimized and standard serrated tools are presented for the given milling scenario.
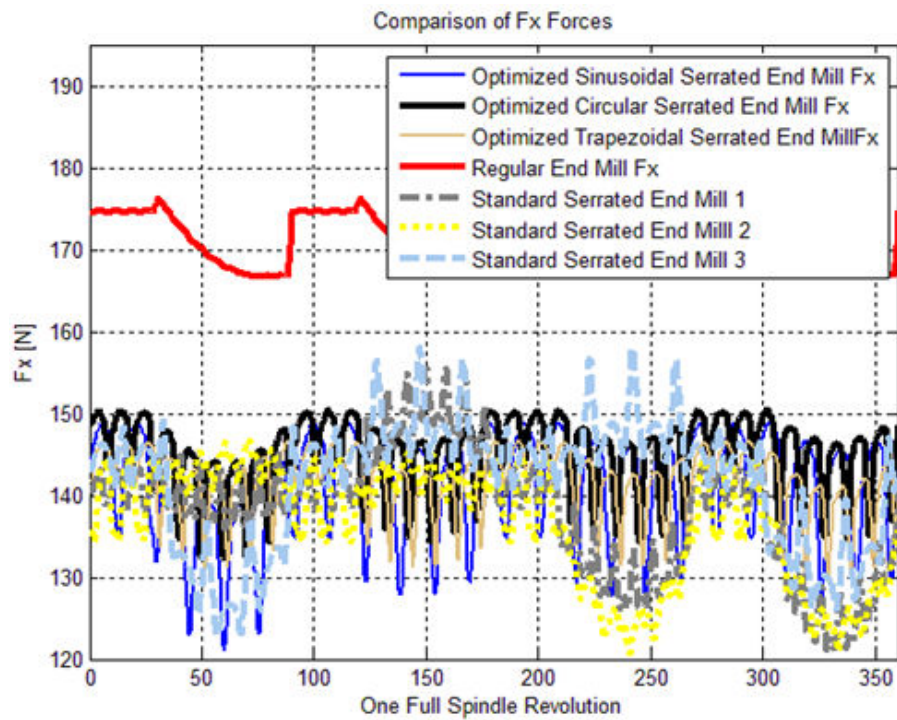
a)
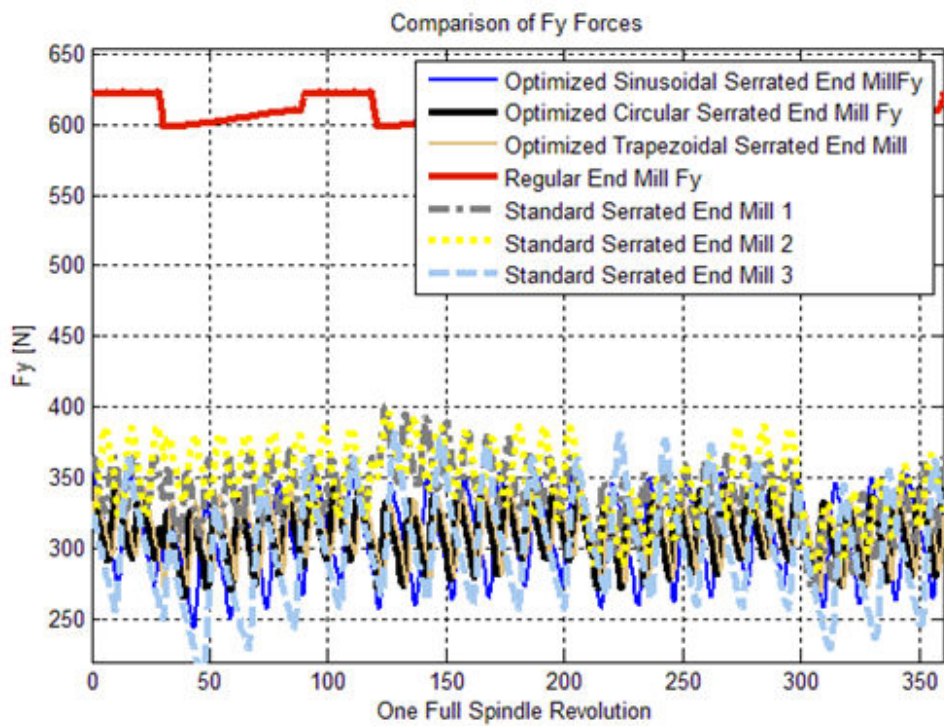
b)
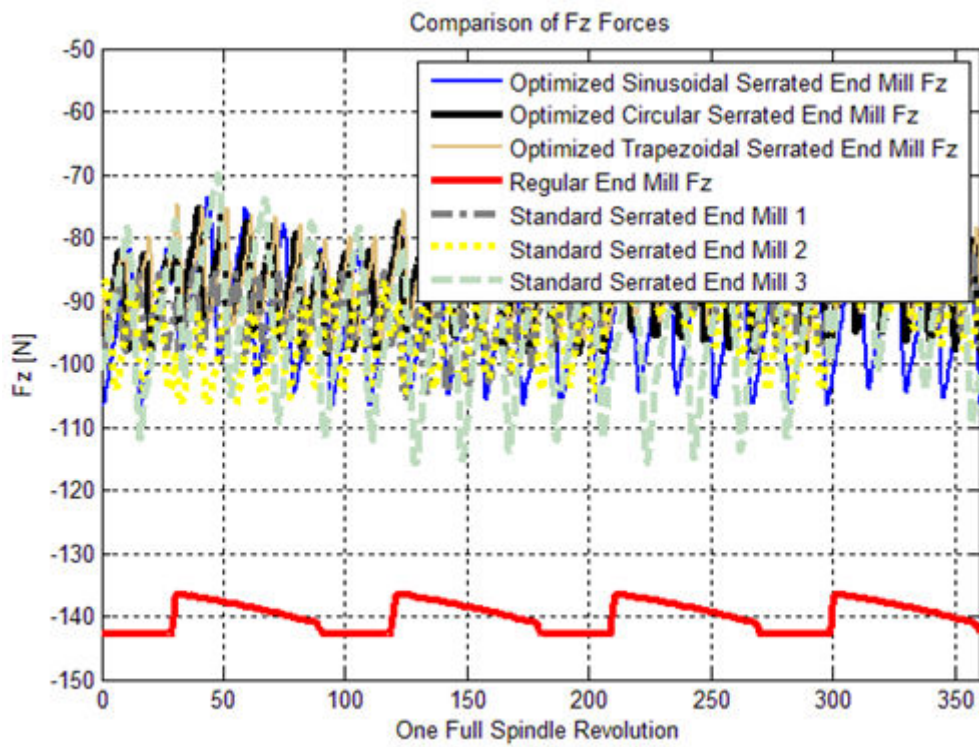
c)

Figure 4.13 Comparison of optimized serrated end mills with each other, with regular end mill and standard serrated end mills

CHAPTER 5

DYNAMICS OF MILLING WITH SERRATED END MILLS

In this chapter, dynamics of milling with serrated end mills will be investigated. Differences between stability models of regular, variable pitch and serrated end mills will be given. The stability model presented in Chapter 2 will be applied to serrated end mills with necessary changes. Presented stability model will be verified with chatter experiments using the optimized custom made serrated end mills in Chapter 4. In addition, chatter stability of commercially available serrated end mills will be compared with that of the optimized serrated end mills. Moreover, serrated end mills with variable pitch angles will be analyzed and their effect on both mechanics and dynamics will be explained.

5.1. Stability Model for Serrated End Mills
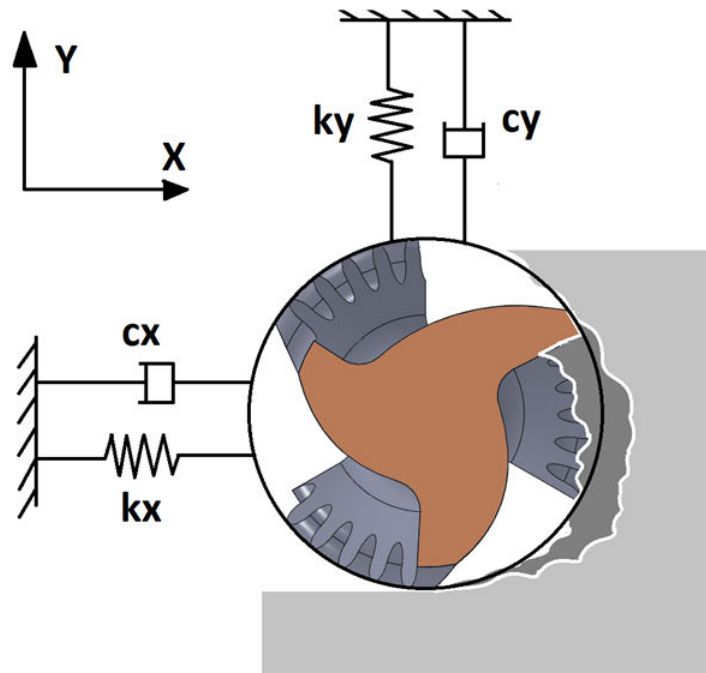
Figure 5.1 Dynamic chip thickness and two orthogonal degrees of freedom

The chatter stability of serrated end mills will be analyzed using time-averaged First Order Semi-Discretization Method including multiple delays which was presented in Chapter 2. However, some necessary changes should be made in order to implement the method for serrated end mills. These necessary changes will be given but the Semi-Discretization formulation will not be repeated here. In Figure 5.1 cross-section of a serrated end mill removing material is shown. As can be seen from the figure, because of the serration form on the cutting teeth, the local radii of the end mill change among cutting teeth. If a serrated end mill is designed and employed properly, only one cutting tooth removes material at a certain axial height. Because of this the effective axial depth of cut decreases substantially. Another result originating from this effect is that the majority of the delays in the system become equal to one spindle period instead of one tooth passing period. However, as the feed per tooth increases, the delays in the system become multiple such as $T, (3T/4), (T/4)$ in case of a regular pitch serratted end mill where T is the spindle period. If the feed per tooth is increased further, all of the cutting edge is immersed into the workpiece. This causes the serrated end mill to behave like a regular end mill in terms of chatter stability, meaning that a substantial stability increase over regular end mills cannot be achieved.

In the following an example milling process with a serrated end mill will be considered and the resulting chip distribution will be discussed in terms of delays.

Table 5.1 Process and tool parameters

R_t	N_t	β	Serration Type	r_1	r_2	A
6mm	4	30°	Circular	0.5 mm	0.5 mm	0.6 mm
Axial DOC (a)			Radial Immersion (b)	ft		
8mm			3mm	0.05 mm/tooth		

In the following figure, isometric view of the chip distribution for the given milling case is illustrated. The axial depth of cut is divided into 800 disk elements. The maximum chip thickness is never equal to 0.2mm/tooth, which is $(Nt * ft)$, because the radial immersion is less than half. The tool has equal pitch angles.
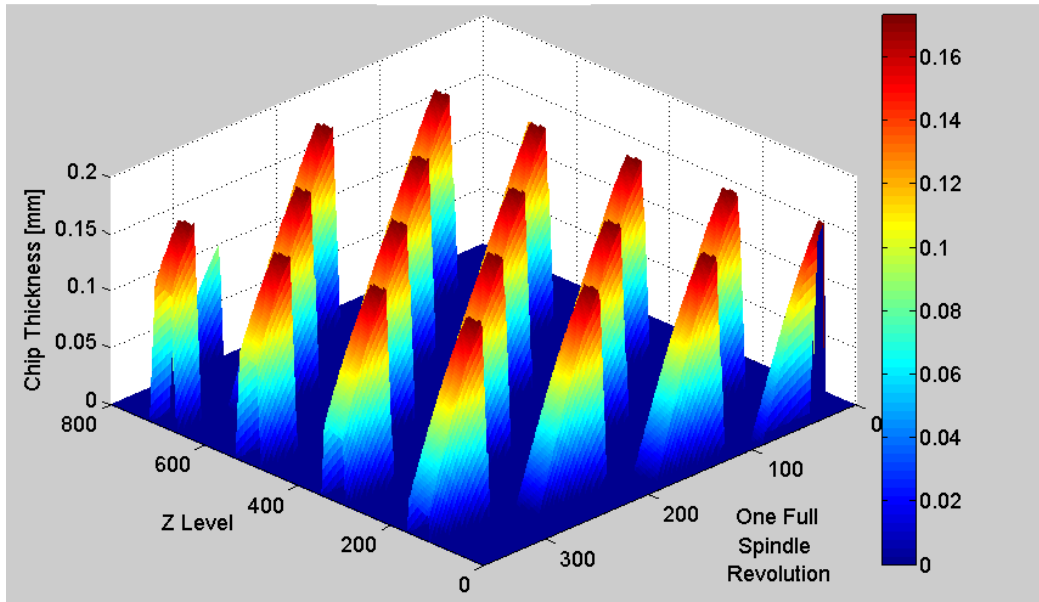
Figure 5.2 Chip thickness distribution for the milling case given in Table 5.1
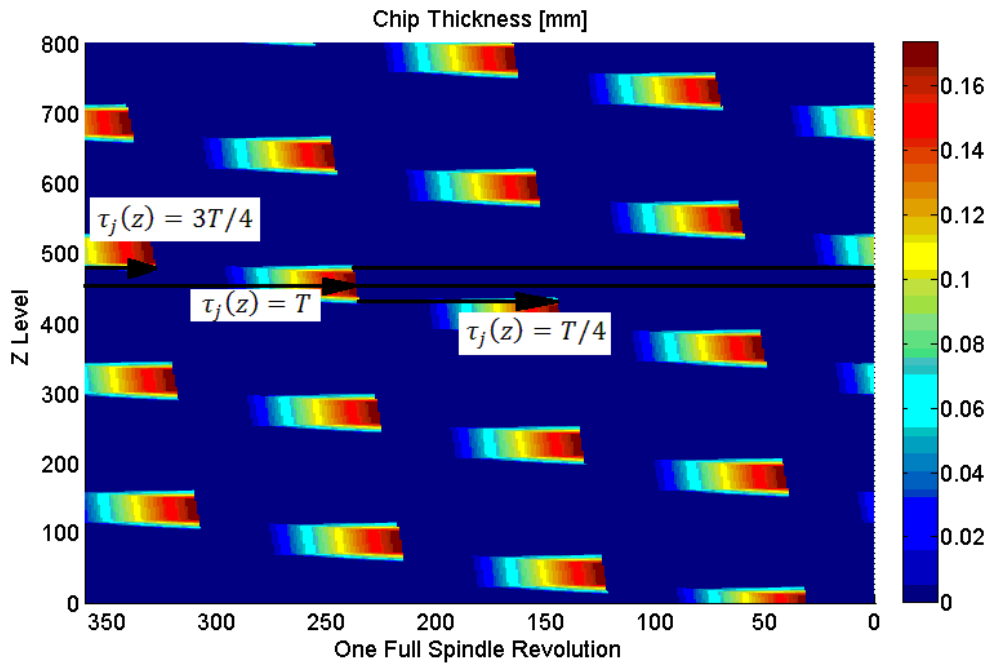
Figure 5.3 The delays and top view of the resulting chip thickness distribution

In Figure 5.3, the top view of the resulting chip thickness distribution is shown. As can be seen, there are multiple delays in the system. However, the majority of the delays in the system are equal to the spindle period.

The delay for a given z level and cutting tooth is calculated with the help of chip thickness $h_j(\emptyset, z)$ and separation angle $\delta\emptyset(j, z)$. A new variable, for determining whether a cutting tooth at a given z level ever removes material or not, is introduced. $h_{01}(j, z)$ is constructed as follows:

$$h_{01}(j, z) = \begin{cases} 0, & if \;\; h_{sum}(j, z) = 0 \\ 1, & if \;\; h_{sum}(j, z) > 0 \end{cases} \tag{5.1}$$

where

$$h_{sum}(j, z) = \sum_{\emptyset=0}^{\emptyset=2\pi} h_j(\emptyset, z)$$

$$j = 1, 2, \dots, N_t \tag{5.2}$$

In above equations, j, $\emptyset$, z, $h_{sum}(j, z)$, N_t, $h_j(\emptyset, z)$ represents the cutting tooth number, rotation angle, axial height, total chip thickness removed by the jth tooth at axial height z in one full revolution, number of cutting teeth on the end mill, chip thickness for j^{th} tooth at axial height z at the rotation angle $\emptyset$, respectively

After constructing the h_{01} matrix, Effective Separation angle $Eff\delta\emptyset(j, z)$ is calculated. According to the h_{01} matrix, if j^{th} tooth at axial height z ever removes material $h_{01}(j, z)$ value for that tooth at that axial height is 1, otherwise it is 0. The delay for the jth tooth at axial height z, $\tau_j(z)$ is calculated as follows:

$$\tau_j(z) = \frac{Eff\delta\emptyset_j(z)\, T}{2\pi}$$

$$T = \frac{60}{\Omega} \tag{5.3}$$

where, Ω and T are the spindle speed and the spindle period, respectively. $Eff\delta\emptyset_j(z)$ is calculated by consequtively checking the h_{01} values for cutting teeth at a given axial height, z. For j^{th} tooth, h_{01} values of the previously in cut $N_t - 1$ teeth are checked. If $(j + 1)^{th}$ tooth does not remove any material in one tool revolution, the separation angle between the jth and the $(j + 1)^{th}$ is added to the $Eff\delta\emptyset_j(z)$. This addition is

carried out until one chip removing cutting teeth is found. This process can be summarized as finding the skipping, i.e. not material removing cutting teeth at a given z level. If only one cutting tooth removes material at a given z level then, the $Eff\delta\emptyset_j(z)$ becomes 2π and $\tau_j(z)$ becomes T. By introducing the $Eff\delta\emptyset_j(z)$ in to the calculations, variable pitch and helix end mills can be handled as well.

As stated earlier, serrated end mills have undulations on the flank faces of the cutting teeth. These undulations change the directions of differential milling forces as explained in Chapter 3. Because of this reason, directional coefficients in dynamics of milling equations are different than the ones for straight edged end mills given in Chapter 2. In the following directional coefficients for serrated end mills are given.

$$a_{xx} = g(\emptyset_j)(sin\emptyset_j(-\sin(\kappa)sin\emptyset_j K_{rc} - \cos(\kappa) sin\emptyset_j K_{ac} - cos\emptyset_j K_{tc}))db$$
$$a_{xy} = g(\emptyset_j)(cos\emptyset_j(-\sin(\kappa)sin\emptyset_j K_{rc} - \cos(\kappa) sin\emptyset_j K_{ac} - cos\emptyset_j K_{tc}))db$$
$$a_{yx} = g(\emptyset_j)(sin\emptyset_j(-\sin(\kappa)cos\emptyset_j K_{rc} - \cos(\kappa) cos\emptyset_j K_{ac} - sin\emptyset_j K_{tc}))db \quad (5.4)$$
$$a_{yy} = g(\emptyset_j)(cos\emptyset_j(-\sin(\kappa)cos\emptyset_j K_{rc} - \cos(\kappa) cos\emptyset_j K_{ac} - sin\emptyset_j K_{tc}))db$$

$$db = \frac{dz}{\sin(\kappa)}$$

Directional coefficients are derived from Fx and Fy formulations. For serrated end mills, κ and K_{ac} affect the Fx and Fy calculations thus their effect is included in the directional coefficients. With the above necessary changes to the dynamics of milling with multiple delays formulation given in Chapter 2, stability of milling with serrated end mills can be analyzed.

5.2. Comparison of Optimized and Standard Serrated End Mills

In this section, time-averaged First Order Semi-Discretization method with multiple delays for serrated end mills will be used in order to compare the optimized serrated waveforms and the standard waveforms available in the market in terms of chatter stability.

Table 5.2 Modal parameters of the milling system

ω_{nx} (rad/sec)	m_x (kg)	ζ_x	ω_{ny} (rad/sec)	m_y (kg)	ζ_y
693*2π	0.8409	%2.503	689*2 π	0.9372	%2.947

In Table 5.2 modal parameters of the 2 degrees-of-freedom milling system is given. These parameters are obtained by impact tests. The details of how impact tests are carried out will be given in Section 5.4, Experimental Verification. In the following table process parameters of the example milling operation are given.

Table 5.3 Process parameters

b (mm)	ft (mm/tooth)	Milling Mode	Workpiece Material
3	0.05	Down Milling	Al7075-T6

In the following table the parameters of the cutting tools used in the simulations are given.

Table 5.4 Properties of the tools

Tool Type	R_t (mm)	N_t	Serration Type	r_1 (mm)	r_2 (mm)	A (mm)	β (°)
Optimized Serrated End Mill	6	4	Circular	0.5	0.5	0.6	30
Standard Serrated End Mill	6	4	Circular	0.78	0.58	0.25	30

Chatter stability behavior of these tools will be illustrated in the following figures. In addition to the serrated tools whose properties are given in Table 5.4, stability diagram of a regular end mill having 6mm radius, 4 cutting teeth and 30° helix angle is also shown in the figures.
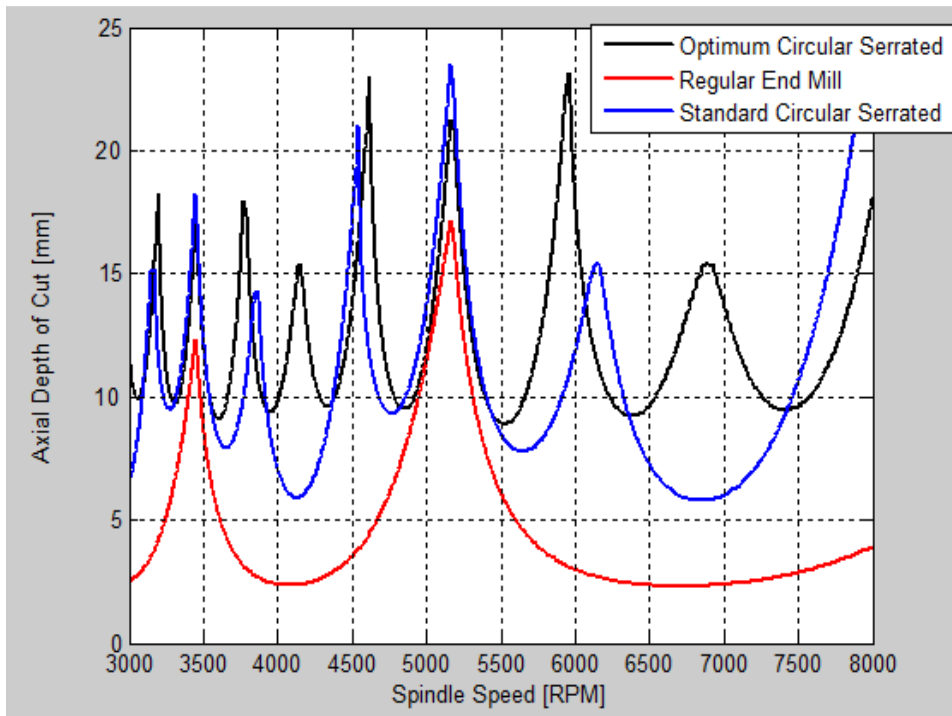
Figure 5.4 Stability comparisons, 3000-8000 RPM
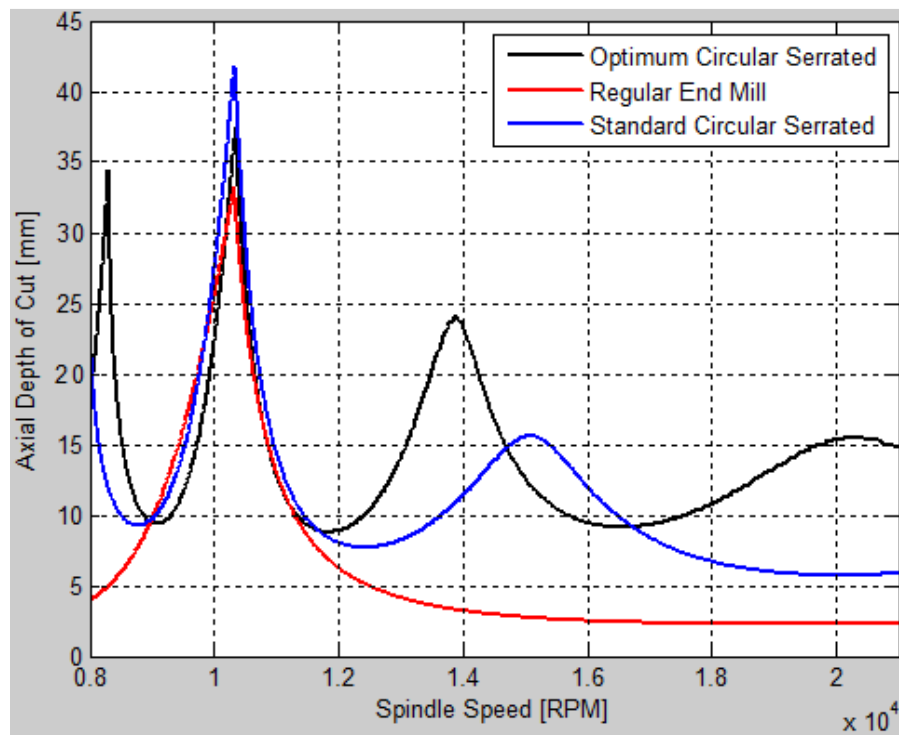
Figure 5.5 Stability comparisons, 8000-21000 RPM

In Figures 5.4 and 5.5 stability diagrams of three different end mills for the given milling operation and the modal parameters are illustrated. As can be seen from the figures, the optimized serrated end mill shows superior chatter stability in comparison to both regular and standard serrated end mills. This can be attributed to the fact that

optimized serrated end mills reduce the effective depth of cut in comparison to standard serrated end mills. Another reason for this stability increase is the reduced cutting force coefficients due higher rake angle parts of the cutting edges and increased chip thickness. As explained earlier in this chapter, with optimized serration waveforms and smaller ft values the serrated end mill tends to behave like a one toothed regular end mill. This is due to the fact that majority of the delays in the system become the spindle period instead of tooth passing period. Because of this behavior added lobes can be seen in Figure 5.4. Furthermore in Figure 5.5, around 14000 RPM and 20000RPM spindle speeds, added lobes can be seen where regular end mills do not have stability pockets. This phenomenon can be exploited for High Speed Machining operations. The addition of reduced cutting force coefficients caused by higher rake angles and higher chip thickness to these effects also increases the chatter stability. These are the reasons for stability increase achieved with serrated end mills and with the optimized serration waveforms.

Another example is given in the following figures. In this example everything (modal, process and tool properties) are kept the same as the previous one except the feed per tooth, ft. Here ft is increased to 0.15mm/tooth.
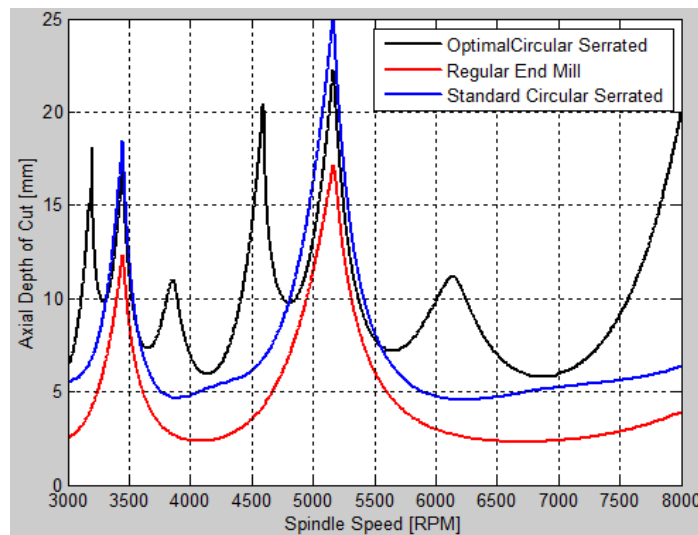
Figure 5.6 Stability comparisons, 3000-8000 RPM
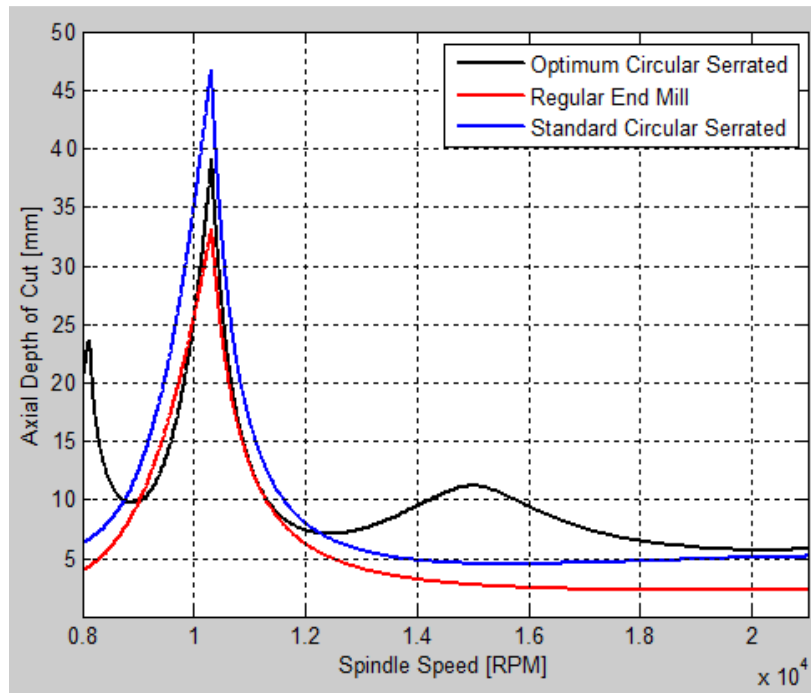
Figure 5.7 Stability comparisons, 8000-21000 RPM

As can be seen from the figures 5.6 and 5.7, optimized serrated end mill still has a better chatter stability comparing to the standard serrated end mill. The effect of increased ft is visible for both optimized and standard serrated end mills. In Figure 5.6 stability limits of both end mills are decreased for ft =0.15mm/tooth comparing to ft=0.05mm/tooth. However the decrease in the stability of the standard serrated end mill is bigger than the optimized serrated end mill. Added lobes almost diminish for standard serrated end mill and the tool starts to behave more like a regular end mill in terms of chatter stability. The same trend would be seen for optimized serrated end mill if ft is increased further.

In the following, chatter stability performances of optimized serrated end mills in Chapter 4 are compared on stability diagrams for the milling operation whose parameters are given in Table 5.2 and 5.3.

Table 5.5 Properties of optimized serrated end mills

Tool No	R_t (mm)	N_t	β (°)	Serration Type	$r_1 = r_2$ (mm)	W_1 (mm)	W_2 (mm)	$t_1 = t_2$ (°)	A (mm)
1	6	4	30	Trapezoidal	0.2	0.3	0.2	45	0.5
2	6	4	30	Circular	r_1 (mm)	r_2 (mm)		A (mm)	
					0.5	0.5		0.6	
3	6	4	30	Sinusoidal	A (mm)			λ (mm)	
					0.2			2.8	

In Table 5.5, properties of the optimized serrated end mills with different waveforms for lower milling forces determined in Chapter 4 are given.
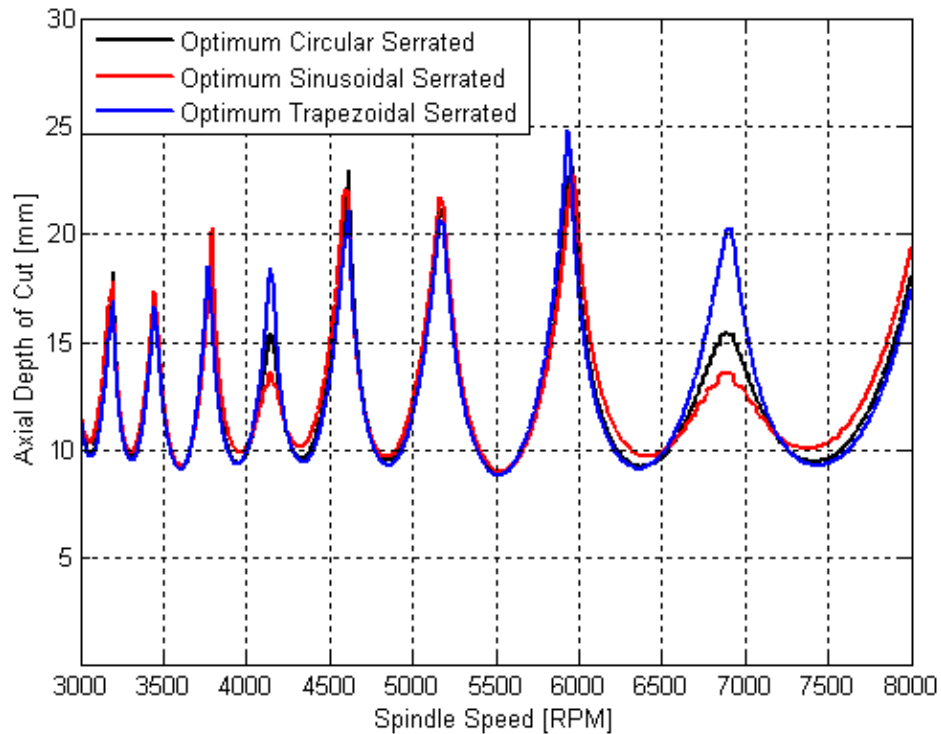
Figure 5.8 Stability comparisons

In Figure 5.8, it can be observed that each optimized serrated end mill achieved almost the same stability performance.

**5.3 Effect of Variable Pitch Angles on Chatter Stability of Serrated End Mills**

In this section, the effect of variable pitch angles on chatter stability of serrated end mills is investigated. Presented stability model in this chapter is able to predict the stability of serrated end mills with variable pitch and helix angles.

As explained and shown by examples in Chapter 2, variable pitch end mills can increase chatter stability significantly if they are designed properly. They alter the phase difference by engaging with the workpiece with a desired delay. In this section, variable pitch angles will be combined with serrated cutting edges in order to see the cumulative effect of these two phenomena on chatter stability. In order to make sure that the effect of variable pitch angles is visible, an optimum variable pitch pattern will be used for a given example milling system. Modal parameters of the example milling system are given in the following table.

Table 5.6 Modal parameters of the milling system

ω_{nx} (rad/sec)	m_x (kg)	ζ_x	ω_{ny} (rad/sec)	m_y (kg)	ζ_y
600*2π	0.12464	%2.503	600*2π	0.12464	%2.503

The properties of the serrated end mill are given in the following table.

Table 5.7 Properties of the serrated end mill

Tool Type	R_t (mm)	N_t	Serration Type	r_1 (mm)	r_2 (mm)	A (mm)	β (°)
Optimized Serrated End Mill	6	4	Circular	0.5	0.5	0.6	30

Desired spindle speed is chosen as 6000 RPM. Variable pitch angles are calculated using the analytical design method presented in [19]. The examples of this method are given in Chapter 2.

Linear pitch variation for the given modal parameters and the desired spindle speed is calculated as 45°, 75°, 105°, 135° with the analytical design method presented in [19].

The stability diagram for the serrated end mill, which has both optimized pitch angles and serration form, is constructed for a quarter immersion milling operation with the feed per tooth of ft=0.05mm/tooth. The workpiece material is chosen as Al7075.
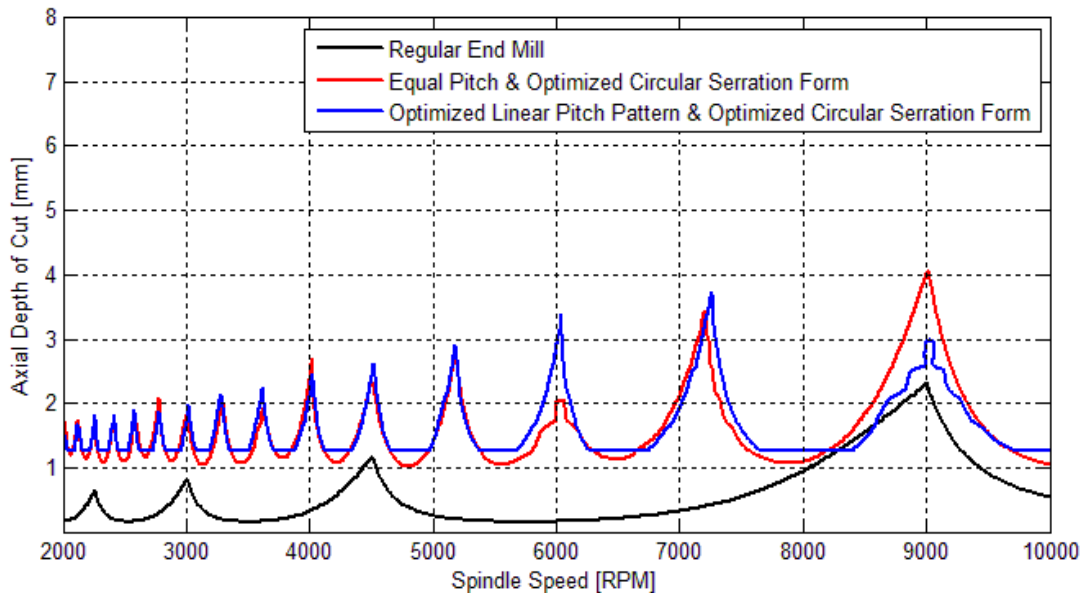

Figure 5.9 Comparison of variable, regular pitch serrated end mills and regular end mill

As can be seen from the stability chart given in Figure 5.9, variable pitch and optimized serrated end mill increased the stability for the desired spindle speed. However it is difficult to say that the reason for stability increase is the change in delays of the system. As stated earlier, for a certain axial height only one cutting tooth removes material with properly designed and employed serrated end mills. Regardless of the variation in pitch angles, the majority of the delays in the system become spindle period instead of tooth passing period because of this reason. Thus variable pitch angles are not expected to be effective when combined with serrated cutting edges. However, in this example variable pitch angles resulted in a higher stability limit than equal pitch serrated end mill. This can be attributed to the different distribution of chip load. This situation might result in a better engagement with the workpiece, allowing the tool to behave more like a one toothed end mill. Further investigation is needed in terms of delays and engagement conditions of variable pitch serrated end mills.

Another important issue of using variable pitch angles with serrated cutting edges is that the chip load distribution changes drastically. The resulting chip load for a quarter immersion operation with the given variable pitch serrated end mill is illustrated in the following figure. Axial depth of cut is chosen as 8 mm.

113
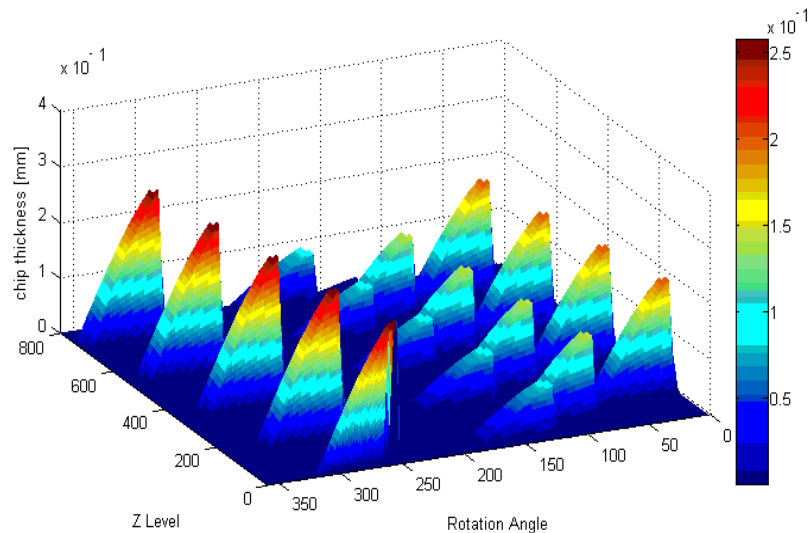
Figure 5.10 Chip load distribution

As can be seen from Figure 5.10, chip load distribution changes dramatically which would cause the maximum milling forces to increase. Excessive chip thickness may result premature cutting edge failure and tool breakage. These effects need to be considered carefully before deciding to combine variable pitch angles with serrated cutting edges.

5.4 Experimental Verification

In this section, presented stability model will be experimentally verified with chatter tests. A photograph of the test set-up is given in the following figure.
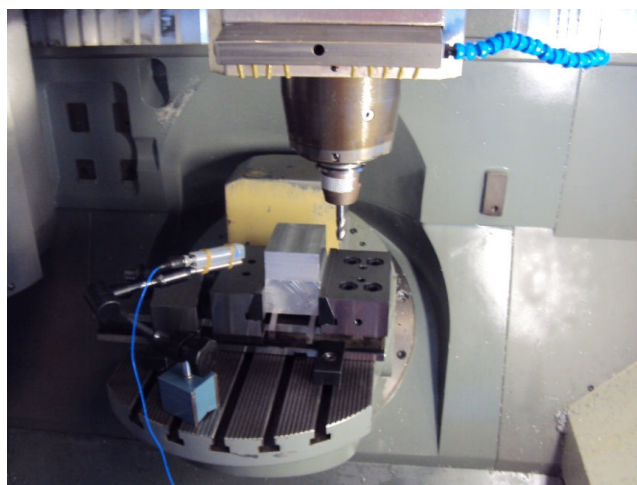
Figure 5.11 Test set-up for chatter experiments

114

As can be seen from the Figure 5.11, an Al7075-T6 prismatic block is mounted on the table of DMG 5-axis machining center rigidly. In order to capture the sound spectrum of the chatter experiments, a directional microphone is mounted as close as possible to end mill-workpiece contact area. Captured sound data is analyzed with LabVIEW software.

Before cutting experiments, modal parameters of the cutter-holder-spindle-machine tool assembly at the tool tip are identified by impact tests using instrumented hammer.
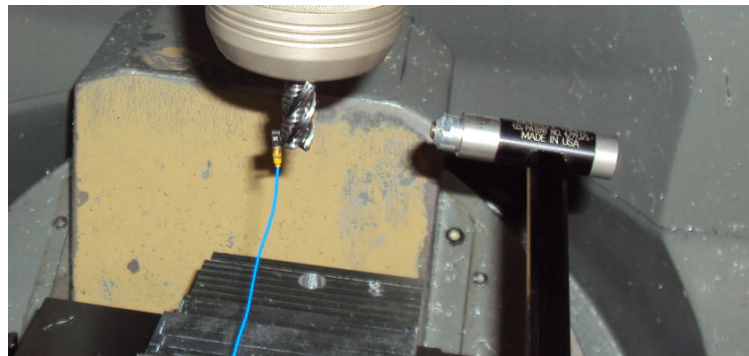

Figure 5.12 Set-up for impact test

Machine tools consist of many different parts, and thus they are complex assemblies. Consequently they have many vibration modes with different natural frequencies. It is difficult and impractical to excite every frequency with a shaker and capture the response. However, with a proper impact test modal parameters of the system can be obtained in a shorter time and with a practical test set-up. If a perfect impulse (very small impact duration) can be applied to the tool tip, all of the important natural frequencies can be exited.

In order to obtain modal parameters of the system at the tool tip, an impact is applied to the tool tip and the response of the system is captured with an accelerometer. Frequency Response Functions of both X, Y directions are analyzed with CUTPRO software.
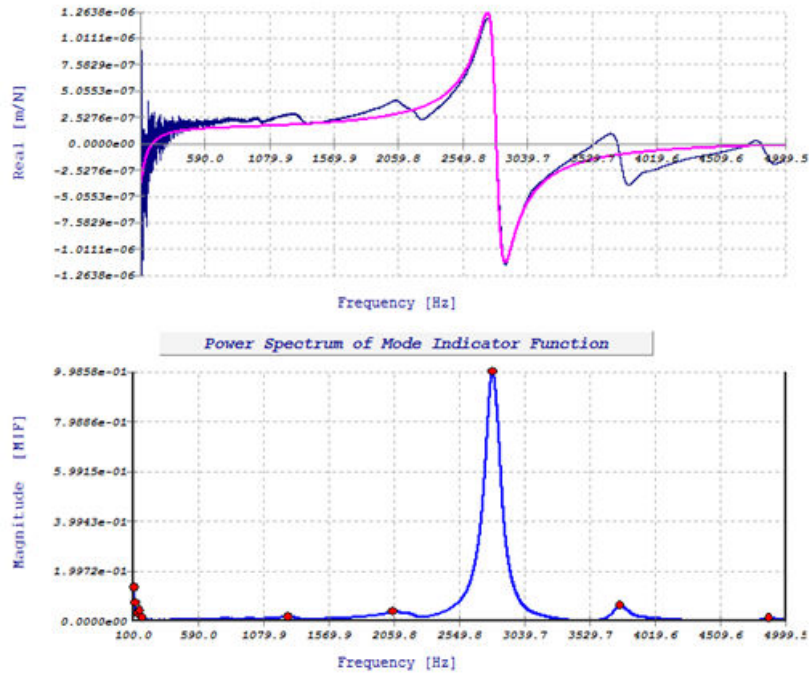
Figure 5.13 X Direction, real part and magnitude of the FRF

In Figure 5.13 real part and magnitude of the FRF in X direction is given. As can be seen, the system has a dominant mode at the tool tip. Same impact test is done in Y direction and resulting FRF is illustrated in the following figure.
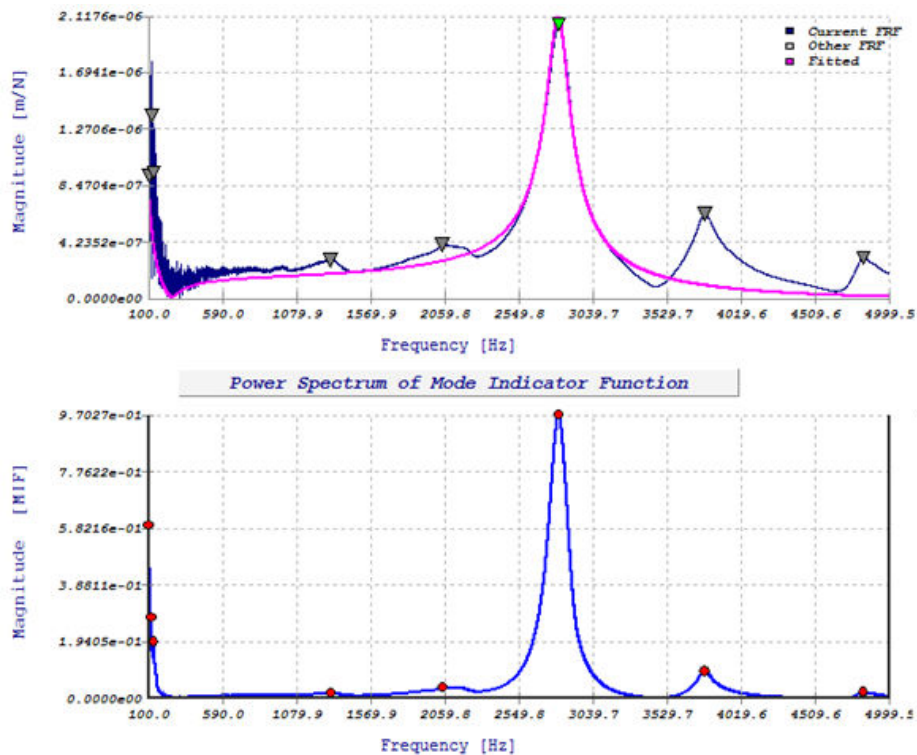
Figure 5.14 Y Direction, real part and magnitude of the FRF

116

In Figure 5.14 real part and magnitude of the FRF in Y direction is given. As can be seen the system has a dominant mode at the tool tip. Comparing Figures 5.13 and 5.14 one can conclude that the system has one dominant vibration mode in X and Y directions. The magnitudes of the dominant modes are way bigger than the other modes, thus other modes will be neglected in the stability analyses. In the following table experimentally obtained modal parameters of the system at the tool tip are given.

Table 5.8 Modal parameters of the system

ω_{nx} (rad/sec)	m_x (kg)	ζ_x	ω_{ny} (rad/sec)	m_y (kg)	ζ_y
2807.3643*2π	0.028	%2.394	2817.1773*2π	0.0286	%2.664

The properties of the serrated end mill to be used in the chatter experiments are given in the following table.

Table 5.9 Properties of the serrated end mill to be used in the chatter experiments

Tool Type	R_t (mm)	N_t	Serration Type	r_1 (mm)	r_2 (mm)	A (mm)	β (°)
Optimized Serrated End Mill	6	4	Circular	0.5	0.5	0.6	30

Chatter experiments are done for a quarter immersion (b=3mm) and feed per tooth, ft =0.05mm/tooth. Workpiece material is chosen as Al7075-T6 alloy whose orthogonal database is given in the following table.

Table 5.10 Material data base for Al7075-T6 alloy [42]

$$\tau_s = 297.1 + 1.1\alpha_r \text{ [MPa]}$$
$$\beta_f = 18.8 + 6.7h + 0.0076V_c + 0.26\alpha_r$$
$$\emptyset_c = 24.2 + 36.7h + 0.005V_c + 0.3\alpha_r$$
$$K_{te} = 23.4N/mm$$
$$K_{re} = 35.2N/mm$$
$$K_{ae} = 5 N/mm$$
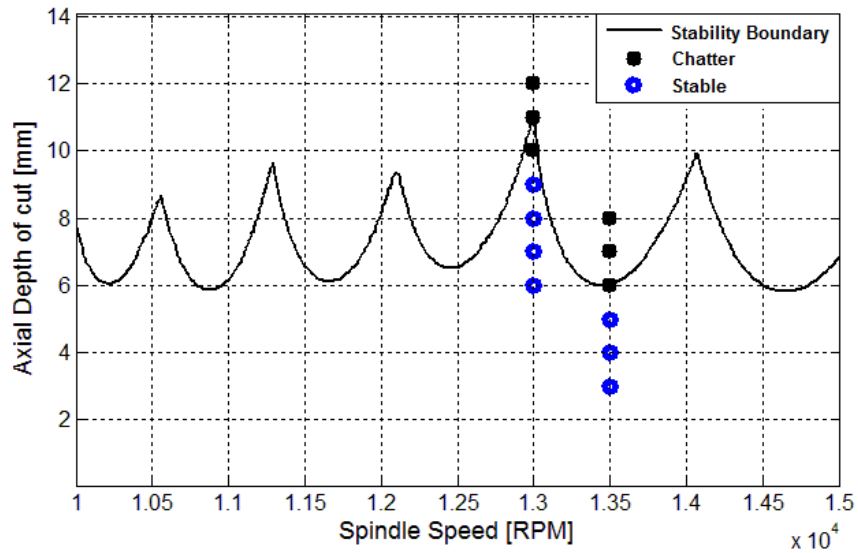
Figure 5.15 Stability chart for the given parameters and the results of chatter tests

In Figure 5.15, the results of the chatter tests are given on the stability diagram. In the following, detailed data and discussion for the chatter experiments will be presented.

For 12mm axial depth of cut with 13000RPM, sound spectrum and surface photograph are shown in Figure 5.16 and 5.17.
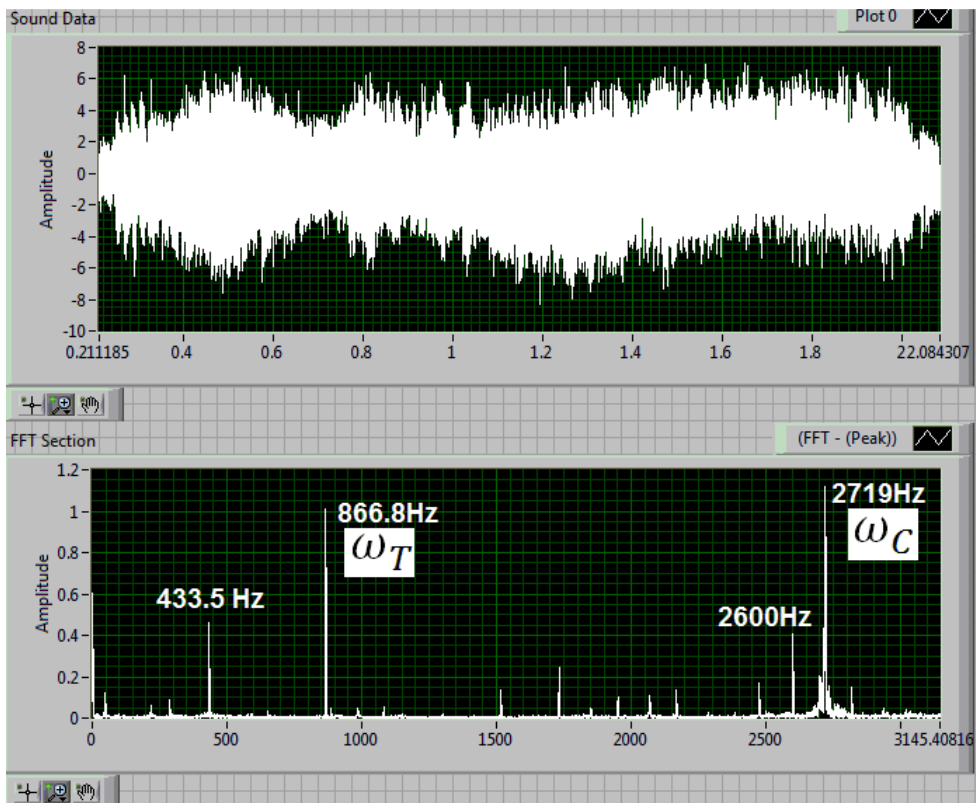
Figure 5.16 Sound spectrum of the 12mm axial depth of cut, 13000RPM

As can be seen from the figure above, system is not stable for 12mm axial depth of cut and 13000 RPM spindle speed. Here ω_T is the tooth passing frequency, ω_C is the chatter frequency. The photograph of the machined surface is given in the following.

Figure 5.17 Resultant surface of the 12mm axial depth of cut, 13000 RPM

As can be seen on Figure 5.17 chatter marks are visible on the surface. However it should be noted that serrated end mills leave bigger feed marks. Thus it becomes difficult to detect chatter only by visual inspection of the cut surface. One needs to be very careful in order to distinguish chatter marks from the feed marks. Thus sound spectrum analysis must also be performed.
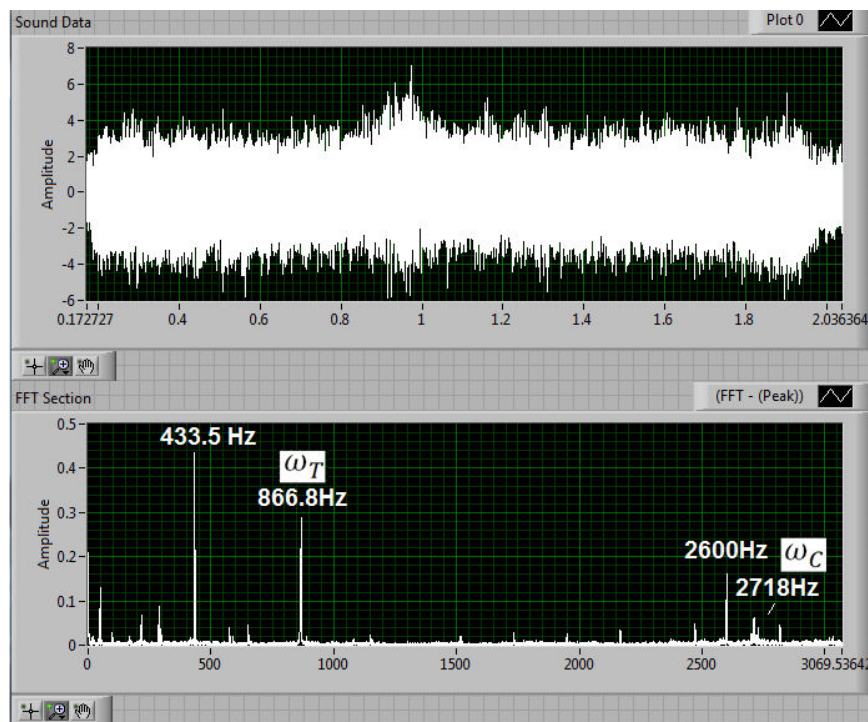
Figure 5.18 Sound spectrum of the 9mm axial depth of cut, 13000RPM

As can be seen from Figure 5.18, system is stable for 9 mm axial depth of cut and 13000 RPM spindle speed.
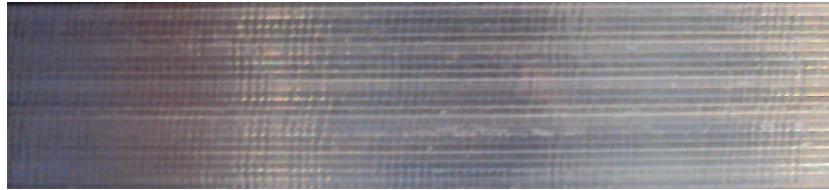
Figure 5.19 Resultant surface of the 9mm axial depth of cut, 13000 RPM

In Figure 5.19, chatter marks vanish from the surface and only feed marks are seen as expected.
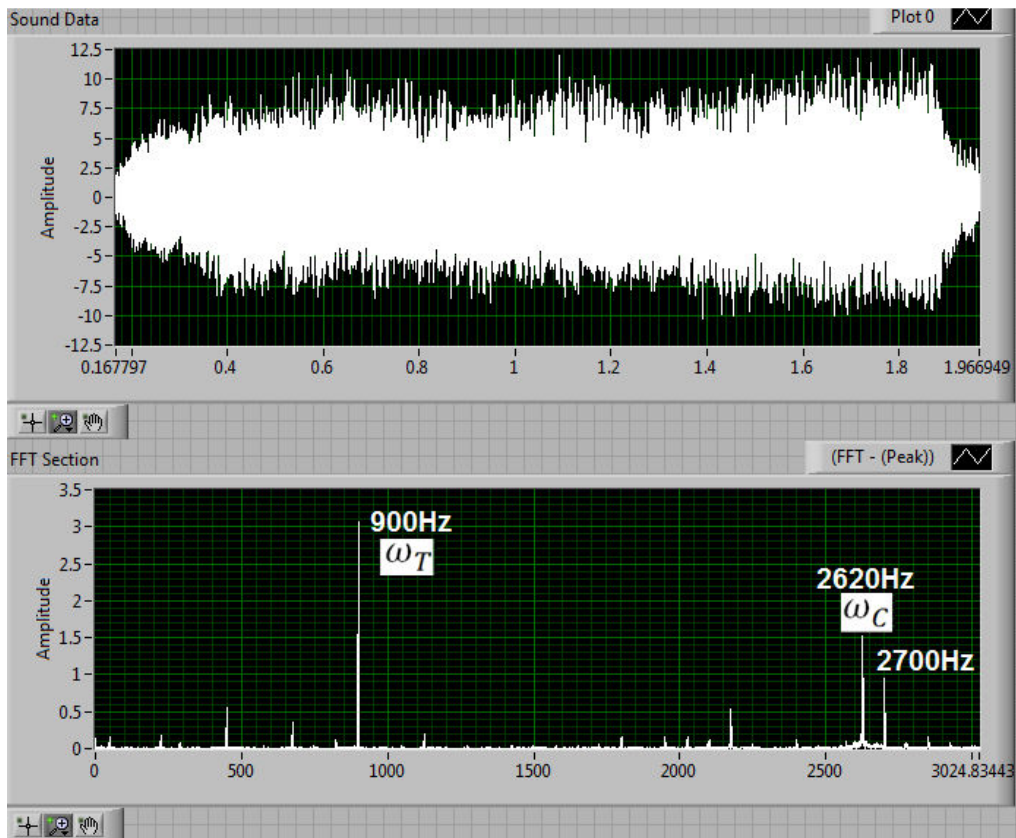
Figure 5.20 Sound spectrum of the 7mm axial depth of cut, 13500RPM

As can be seen from the figure above, system is not stable for 7mm axial depth of cut and 13500 RPM spindle speed. However it is not obvious as in Figure 5.16 because the amplitude of the chatter frequency is smaller than the tooth passing frequency.
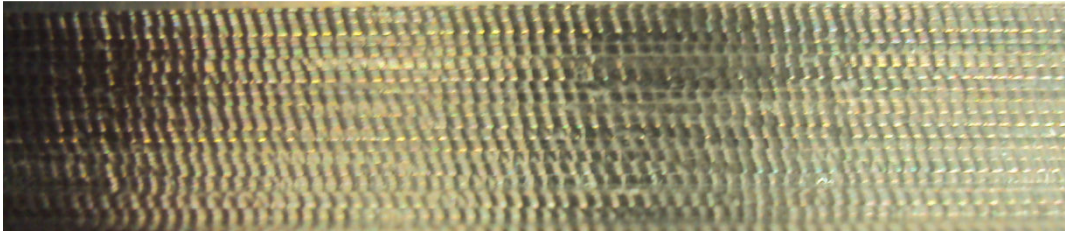
Figure 5.21 Resultant surface of the 7mm axial depth of cut, 13500 RPM

It is observed from both sound spectrum and surface photograph that the system is not stable for the given axial depth of cut and spindle speed pair. In the following the stability of 5 mm axial depth of cut and 13500 RPM spindle speed pair is analyzed.
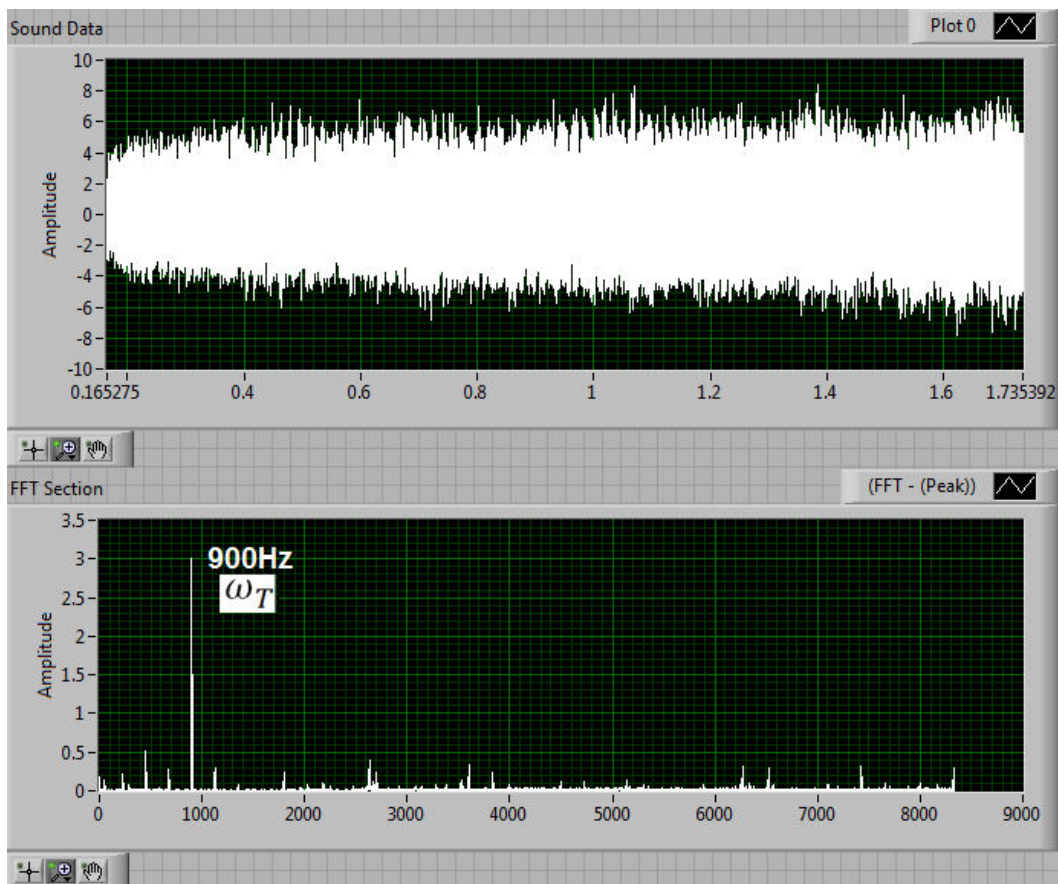
Figure 5.22 Sound spectrum of the 5mm axial depth of cut, 13500RPM

As can be seen from Figure 5.22 chatter frequency is almost diminished from the sound spectrum.

In this chapter, dynamics of milling with serrated end mills is investigated. The differences between variable pitch, variable helix and serrated end mills are explained.

121

Chatter stability model presented in Chapter 2 is used for stability analysis of serrated end mills with necessary changes. Time-averaged First Order Semi-Discretization Method including multiple delays which was explained in detail earlier is applied for chatter stability prediction. Stability performances of standard and optimized serrated end mills are compared and it is shown that optimized serrated end mills have superior stability performance. Furthermore, it is shown that regardless of the serration wave type, optimized serrated end mills show similar, almost the same stability performance. Moreover variable pitch and helix angles are combined with serrated cutting edges and their stability performance is analyzed. Presented stability model is verified with chatter tests.

CHAPTER 6

CONCLUSION

Mechanics, dynamics and optmization of special end mills are investigated in this study. Dynamics of variable pitch and variable helix end mills are modeled with First Order Semi-Discretization Method including multiple delays. An analytical design method for variable pitch end mills for higher milling stability, proposed by Budak [19, 20] was adopted and applied to example cases. Although the effectiveness of the analytical design method was experimentally verified in [20], the overall stability behavior of the optimized variable pitch tools in a wider range of spindle speeds has not been investigated so far. In this study it is shown that optimized variable pitch tools are not only effective for the spindle speed they are designed for, but a wider range. With this result, optimized pitch tools now can be employed more flexibly in milling operations and their application area can be extended. Different variable pitch patterns are analyzed and it is shown that different variable pitch patterns can yield similar amount of performance increase.

Serrated edge geometries are modeled parametrically for commonly used serration forms such as sinusoidal, circular and trapezoidal. Although these parametric forms do not include every wave type in the market, they represent a big majority. They are very practical compared to B-Spline representations which are used in most of the literature on serrated tools.

Mechanics of milling with serrated end mills is investigated in detail. Milling forces are modeled for these tools and the model is verified experimentally for circular and trapezoidal serration forms. It is shown that phase shift direction has an important effect on the milling mechanics of serrated end mills. The effect of phase shift has never been mentioned in the literature before. It is shown that by simply reversing the direction of the phase shift among the cutting teeth, higher performance increase can be achieved. This reverse phase shift enables the portions of the serrated cutting edge where rake

angles are higher to remove material. It is suprising that the serrated end mills available in the market do not have this geometry. Thus, a design improvement is proposed which does not require any additional technological background in terms of equipment nor introduce a complexity in end mill manufacturing.

Defined serrated waveform parameters are optimized in order to reduce milling forces as much as possible. It is found out that with the optimization of serration waveforms, milling forces can further be decreased comparing to serrated end mills availabe in the market. About %10 reduction is achieved in maximum milling forces compared to standard serrated tools. Each of the optimized waveforms achieved the same amount of decrease in milling forces which is another important result. With the help of the optimization results, the effects of process parameters on milling forces with serrated end mills are explained in detail. It shown that the maximum uncut chip thickness has a great influence on the milling forces as it directly affects the portion of the serrated edge that is in contact with the material. Thus, radial depth of cut and feed per tooth have great importance in milling with serrated end mills. As a future work, with the help of the findings in this thesis, an analytical design method for serrated end mills could be developed.

The stability of serrated end mills is also investigated in this thesis. It is found out that optimized serrated end mills can increase the stability limits further compared to standard serrated end mills. The aim of chapter 4 was to optimize serration forms for decreased milling forces. However, optimized serration forms showed a better performance than the standard serrated tools in the market in terms of chatter stability, too. This is very practical since without any analytical expression, it is very difficult to optimize serrated geometries for maximized stability due to long computational times of chatter simulations even with evolutionary algorithms.

The results obtained from this study improve the knowledge on both mechanics and stability of special milling tools. In the literature, there is no work on design and optimization of serrated end mills. With the help of these findings tool manufacturers and users can design or select serrated end mills with higher performance.

Optimized serrated end mills will enable manufacturing engineers to use higher depths of cut while decreasing the milling forces. Thus, shorter lead times can be obtained while improved dimensional tolerances can be achieved as a result of the decreased

milling forces. Decreased power and torque requirements, thus reduced energy consumption, are also important benefits of these tools. In addition, with the findings on optimized variable pitch tools, these tools can be employed more flexibly in a wider range of spindle speeds which eliminates the need for custom tools for each application. As a result, it can be concluded that the findings in this study have positive implications on production quality, leadtime and cost of milling operations.

Bibliography

[1] Budak, E., Altintas, E., "Analytical prediction of stability lobes in milling", Annals of CIRP Vol. 44/1/1995

[2] Insperger, T., Stépán, G., "Semi-discretization method for delayed systems", International Journal of Numerical Methods in Engineering 2002; 55:503–518 (DOI: 10.1002/nme.505)

[3] Altıntas, Y., Shamoto, E., Lee, P., Budak, E., "Analytical prediction of stability lobes in ball-end milling", Transactions of the ASME, Journal of Manufacturing Science and Engineering, 1999, 121(4):586-592

[4] Altıntas, Y., "Analytical prediction of three-dimensional chatter stability in milling", Japan Society of Mechanical Engineers, International Journal Series: Mechanical Systems, Machine Elements and Manufacturing, 2001, 44(3):717-723

[5] Altıntas, Y., Engin, S., Budak, E., "Analytical stability prediction and design of variable pitch cutters", Transactions of the ASME, Journal of Manufacturing Science and Engineering, 1999, 121:173-178

[6] Mann, B.P., Insperger, T., Bayly, P.V., Stépán, G., "Stability of up-milling and down-milling, Part 1: Alternative analytical method", International Journal of Machine Tools and Manufacture, 2003, 43(1), pp.25-34

[7] Mann, B.P., Insperger, T., Bayly, P.V., Stépán, G., "Stability of up-milling and down-milling, Part 2: Experimental Verification", International Journal of Machine Tools and Manufacture, 2003, 43(1), pp.35-40

[8] Insperger, T., Stépán, G., Bayly, P.V., Mann, B.P., "Multiple chatter frequencies in milling processes", Journal of Sound and Vibration, 2003, 262(2):333-345

[9] Gradišek, J., Kalveram, M., Insperger, T., Weinert, K., Stépán, G., Govekar, E., Grabec, I., "On stability prediction for milling", International Journal of Machine Tools & Manufacture, 2005, 45:769-781

[10] Insperger, T., Stépán, G., Turi, J., "On the higher-order semi-discretizations for periodic delayed systems", Journal of Sound and Vibration, 2003, 313:334-341

[11] Insperger, T., Mann, B.P., Surman, T., Stépán, G., "On the chatter frequencies of milling process with run-out", International Journal of Machine Tools & Manufacture, 2008, 48:1081-1089

[12] Insperger, T., "Full discretization and semi-discretization for milling stability prediction: Some comments", International Journal of Machine Tools and Manufacture, 2010, 50(7):658-662

[13] Henninger, C., Eberhard, P.,"Improving the computational efficiency and accuracy of the semi-discretization method for periodic delay differential equations", European Journal of Mechanics – A/ Solids, 2008, Vol.27, Issue 6: 975-985

[14] Slavicek, J., "The effect of irregular tooth pitch on stability of milling", 6th MTDR Conference, Manchester, 1965

[15] Vanherch, P., "Increasing milling machine productivity by use of cutters with non-constant cutting-edge pitch", 8th MTDR Conference, Manchester, 1967

[16] Opitz, H., Dregger, E. U., Roese, H., "Improvement of the dynamic stability of the milling process by irregular tooth pitch", Proceedings of the Adv. MTDR Conference, 1966, No. 7: 213–227.

[17] Doolan, P., Phadke, M. S., Wu, S. M., "Computer design of a vibration-free face-milling cutter", Journal of Engineering for Industry, 1975,

[18] Tlusty, J., Ismail, F., Zaton, W., "Use of special milling cutters against chatter", Technical Report, NAMRC 11, SME, University of Wisconsin, 1983, 408-415

[19] Budak, E., "An analytical design method for milling cutters with nonconstant pitch to increase stability, Part I: Theory", Journal of Manufacturing Science and Engineering, 2003, Vol. 125, pg. 29-34

[20] Budak, E., "An analytical design method for milling cutters with nonconstant pitch to increase stability, Part II: Application", Journal of Manufacturing Science and Engineering, 2003, Vol. 125, pg. 35-38

[21] Turner, S., Merdol, D., Altıntas, Y., Ridgway, K., "Modelling of the stability of variable helix end mills", International Journal of Machine Tools & Manufacture 47 (2007) 1410–1416

[22] Zatarain, M., Muñoa, J., Peigné, G., Insperger, T., "Analysis of the influence of mill helix angle on chatter stability", Annals of the CIRP Vol. 55/1/2006

[23] Budak, E., Altıntas, Y., "Analytical prediction of chatter stability conditions for multi-degree of freedom systems in milling, Part 1: General formulation", 1998, Transactions of ASME, vol. 120:22-30

[24] Budak, E., Altıntas, E., "Analytical prediction of chatter stability conditions for multi-degree of freedom systems in milling: Part 2: Application of the general formulation to common milling systems", 1998, Transactions of ASME, vol. 120 :31-36

[25] Sims, N. D., Mann, B., Huyanan, S., "Analytical prediction of chatter stability for variable pitch and variable helix milling tools", 2008, Journal of Sound and Vibration 317: 664–686

[26] Wan, M., Zhang, W., Dang, J., Yang, Y., "A unified stability prediction method for milling processes with multiple delays", 2010, International Journal of Machine Tools & Manufacture, vol.50: 29–41

[27] Insperger, T., Stépán, G., "Updated semi-discretization method for periodic delay-differential equations with discrete delay", 2004, International Journal of Numerical Methods in Engineering, 61(1): pp. 117-141

[28] Campomanes, M., L., "Kinematics and dynamics of milling with roughing endmills", 2002, Metal Cutting and High Speed Machining, Kluwer Academic/Plenum Publishers

[29] Budak, E., Altintas, Y., Armarego, E., J., "Prediction of milling force coefficients from orthogonal cutting data", 1996, ASME J. Eng. Ind. 118: 216-224

[30] Wang, J.,J.,J., Yang, C.S., "Angle and frequency domain force models for a roughing end mill with a sinusoidal edge profile", 2003, International Journal of Machine Tools & Manufacturing, 43: 1509-1520

[31] Merdol, S. D., Altıntas, Y., "Mechanics and dynamics of serrated cylindrical and tapered end mills", 2004, Journal of Manufacturing Science and Engineering, vol.126: 317-326

[32] Dombovari, Z., Altintas, Y., Stepan, G., "The effect of serration on mechanics and stability of milling cutters", 2010, International Journal of Machine Tools and Manufacture vol.50:511–520.

[33] Dombovari, Z., Stépán, G., "DRAFT: The effect of harmonic helix angle variation on milling stability", 2011, Proceedings of the ASME, International Design Engineering Technical Conferences & Computers and Information in Engineering Conference, Washington, DC, USA

[34] Otto, A., Radons, G., "Frequency domain stability analysis of milling processes with variable helix tools", 2012, Ninth International Conference on High Speed Machining

[35] Yusoff, A., Sims, N. D., "Optimization of variable helix end milling tools by minimizing self-excited vibration", 2009, Journal of Physics : Conference Series on 7th International Conference on Modern Practice in Stress and Vibration Analysis 181:012026.

[36] Storn, R., Price, K., "Differential Evolution: A simple and efficient adaptive scheme for global optimization over continuous spaces", 1995, Technical Report, Berkeley

[37] Compeán, F. I., Olvera, D., Campa, F. J., López de Lacalle, L. N., Elías-Zúníga, A., Rodríguez, C. A., "Characterization and stability analysis of multivariable milling tool by the enhanced multistage homotopy perturbation method", 2012, International Journal of Machine Tools & Manufacture 57:27–33

[38] Song, Q., Ai, X., Zhao, J., "Design for variable pitch end mills with high milling stability", 2011, Int. J. Adv. Manuf. Technol. 55:891–903

[39] Insperger, T., Stépán, G., "Semi-Discretization for Time-Delay Systems Stability and Engineering Applications", Applied Mathematical Sciences, 178, 2011

[40] Altintas, Y., Engin, S., Budak, E., "Analytical prediction of chatter stability and design for variable pitch cutters", Journal of Manufacturing Science and Engineering, 1999, 121:173-178

[41]Price, V.K., Storn, R. M., Lampinen, J.A., "Differential Evolution, A Practical Approach to Global Optimization", Natural Computing Series, Springer, 2005

[42] Ozlu, E., Budak, E., and Molinari, A., "Analytical and Experimental Investigation of Rake Contact and Friction Behaviour in Metal Cutting", International Journal of Machine Tools and Manufacture, Vol. 49/11, 865-875,2009

[43] Ozkirimli, Ö.M., "Mechanical and Dynamical Process Model For General Milling Tools in Multi-Axis Machining, MSc Thesis, 2011, Sabanci University.